

5 RESEARCH ACTIVITIES

5.1 NUCLEAR PHYSICS

S. Muralithar, N. Madhavan and P. Sugathan

The nuclear structure studies at high spin were conducted with the gamma arrays of IUAC. The user experiments, carried out earlier, resulted in several international journal publications in 2022 – 2023. These studies focussed on the following topics: prolate-oblate shape coexistence, single-particle configurations of the excited states of ^{203}Po , chiral-like doublet band structure and octupole correlations in ^{104}Ag , experimental investigation of high-spin states in ^{90}Zr , evolution of nuclear structure through isomerism in ^{216}Fr , level structure in the transitional nucleus ^{215}Fr , effects of entrance channels on breakup-fusion induced by ^{19}F projectiles and shape coexistence and octupole correlations in ^{72}Se . The charged particle detector array (CsI) was first tested in a facility test and later used in an in-beam experiment in conjunction with the Indian National Gamma Array. The nuclear structure and reaction studies undertaken with the gamma arrays in the past year included study of K-Isomers, nuclear structure studies in $A \sim 85$ region, nuclear electromagnetic moment measurements in transitional nuclei, static electromagnetic moment measurements in neutron deficient iodine nuclei, study of transitional nuclei in $A \sim 100$ region, gamma ray spectroscopy of some nuclei of astrophysical importance towards the end-point of nova nucleosynthesis, study of heavy-ion induced incomplete fusion reaction dynamics and high spin states and lifetime measurements in $A \sim 100$ nuclei.

In the Heavy Ion Reaction Analyzer (HIRA), transfer measurements around the Coulomb barrier were carried out for the $^{28}\text{Si}+^{116,120,124}\text{Sn}$ systems to look for enhanced correlated pair transfer of neutrons and to understand the role of neutron transfer on sub-barrier fusion cross sections. The HYbrid Recoil mass Analyzer (HYRA) was used in gas-filled mode to measure evaporation residue (ER) cross sections around Coulomb barrier for $^{30}\text{Si}+^{140}\text{Ce}$, $^{32}\text{S}+^{138}\text{Ba}$ and $^{30}\text{Si}+^{142}\text{Ce}$ systems to probe the effect of positive Q-value neutron transfer channels on sub-barrier fusion cross sections. SC-LINAC campaign is awaited to collect higher energy data for $^{32}\text{S}+^{138}\text{Ba}$ and to carry out measurements for $^{48}\text{Ti}+^{124}\text{Sn}$ to complete the study. These experiments form part of thesis work of three research scholars. Several publications resulted last year based on the experiments carried out in HIRA and HYRA in the recent past. Barrier distributions using fusion cross sections and quasi-elastic scattering cross sections, effects of entrance channel, positive Q-value transfer channels, target deformation and multi-phonon inelastic channel coupling in sub-barrier fusion dynamics were reported for newly studied systems. VME-based Data Acquisition Systems (DAS) were commissioned, with the help and support of the Data Support Group of IUAC, in both HYRA and HIRA. The newly installed systems were tested offline (with pulser and a-particle source) and with beam, prior to carrying out user experiments.

An experiment, to investigate role of nuclear deformation and orientation on multi-nucleon transfer reaction and neutron-proton correlation, was performed in the General-Purpose Scattering Chamber (GPSC) facility. Four charged particle detector telescopes were used to identify the transfer products from reactions involving $^{10,11}\text{B}$ projectiles and ^{40}Ca , ^{154}Sm targets. A new VME-based Data Acquisition System was installed in GDA/GPSC electronics cabin which allowed to collect list-mode data in ROOT format. The new system consisted of home-made VME crate controller and commercial ADCs and TDCs. The existing signal cables from GPSC were re-routed to reach the new DAS. A 16-channel VME QDC was also integrated into the system and thoroughly tested with a time-of-flight setup using two BaF_2 detectors. Measurement of energy of neutrons, emitted from an Am/Be source, using gamma-tagged time-of-flight method was reported recently. The measurement extended the neutron energy down to 0.3 MeV. The new data showed good agreement with that of ISO 8529-2 standard reference neutron spectrum in the energy range 0.3 to 6.0 MeV. Other developmental activities included the initiation of Micro Channel Plate (MCP) -based time-of-flight detector system for GPSC experiments and CsI-based charged particle array for particle-gamma coincidence experiments. The group also conducted two workshops, namely, “Detectors and Allied Instruments” and “Experiments with NAND Facility: Present Status and Future Developments”.

A review article on nuclear physics research, carried out at IUAC in the past three decades, was published in The European Physical Journal A (EPJA) in December 2022. Mr. Chandra Kumar (IUAC, New Delhi) and Ms. Madhu (IIT Roorkee, Roorkee) won two of the best poster presentation awards in the DAE Symposium on Nuclear Physics (SNP-2022) held at Cotton University, Guwahati, Assam in December 2022 based on research work carried out with the HIRA and the INGA, respectively. Mr. Chandra Kumar also won the first prize for presenting a poster in the DAE-BRNS Symposium, Nuclear Reaction and Structure up to Intermediate Energy Collisions (NRSIC-23), held at VECC, Kolkata in January 2023.

5.1.1 Study of multi-nucleon transfer reaction for $^{10,11}\text{B}+^{40}\text{Ca}$ and $^{11}\text{B}+^{154}\text{Sm}$ systems using GPSC facility

Harun Al Rashid,¹ K. Kalita¹, P. Sugathan², A. Jinghan², K. S. Golda², N. Saneesh², Mohit Kumar², B. J. Roy³, J. J Das⁴, Lakhyajit Sarma¹, Amar Das¹, Nabendu K. Deb¹, Honey Arora², Anamika Parihari⁵ and M. Bhuiyan⁶

¹Department of Physics, Gauhati University, Guwahati, Assam 781014, India

²Inter-University Accelerator Centre, New Delhi 110067, India

³Nuclear Physics Division, Bhabha Atomic Research Centre, Mumbai 400085, India

⁴Department of Physics, Cotton University, Guwahati, Assam 781001, India

⁵Department of Physics and Astrophysics, Delhi University, Delhi 110007, India

⁶Department of Physics, Rangia College, Rangia, Assam 781354, India

In order to study multi-nucleon transfer (MNT) reactions and neutron-proton correlation at energy 50 MeV and 75 MeV, we used General Purpose Scattering Chamber (GPSC) of IUAC. Pairing between nucleons of the same isospin (p-p and n-n) are the most important correlations affecting the MNT. However, 1p-1n, 2p-2n pair transfers may enhance the transfer cross section [1,2]. With this motivation, CaF_2 target of thickness $272 \mu\text{g}/\text{cm}^2$ was used to study transfer reactions $^{10,11}\text{B}+^{40}\text{Ca}$. And to study the effect of target deformation, ^{154}Sm target of thickness $170 \mu\text{g}/\text{cm}^2$ for $^{11}\text{B}+^{154}\text{Sm}$ reaction was borrowed from Target laboratory of IUAC [3,4]. For this purpose, four ΔE -E Silicon Surface Barrier (SSB) detectors of thickness ranging from (15-40) μm for ΔE type and (300-2000) μm for E type were mounted on the two movable arms of the chamber. The detector set-up covered angular range of 18° - 62° . Two monitor detectors were also placed at 10° on either side of the beam direction. Signals from telescopic detectors were fetched into pre-amplifiers and then to 16 channel spectroscopic amplifiers (SAs) via differential driver. Then the signals from SA were fed into an Analog to Digital Converter. The data were collected using NIAS-MARS (Multi-parameter Acquisition with Root-based Storage) software. We carried out measurements around the grazing angle for the three systems. Well separated transfer bands along with elastic peaks were observed for $^{10,11}\text{B}+^{40}\text{Ca}$ and $^{11}\text{B}+^{154}\text{Sm}$ reactions. We could identify multi-nucleon transfer channels - stripping channels in case $^{10}\text{B}+^{40}\text{Ca}$ and both pickup and stripping channels in case of $^{11}\text{B}+^{40}\text{Ca}$ and $^{11}\text{B}+^{154}\text{Sm}$. Further analysis of data is going on. Spectra observed for $^{11}\text{B}+^{154}\text{Sm}$ at 75 MeV and for $^{11}\text{B}+^{40}\text{Ca}$ at 50 MeV are shown in Fig. 5.1.1.1.

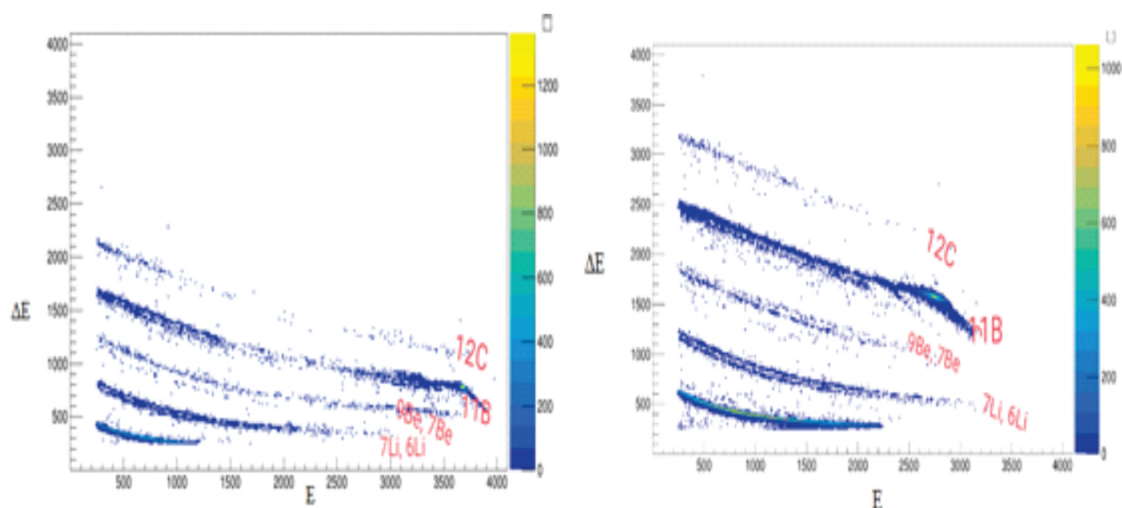


Fig. 5.1.1.1: Typical spectrum observed for $^{11}\text{B}+^{154}\text{Sm}$ (left) at 75 MeV and $^{11}\text{B}+^{40}\text{Ca}$ (right) at 50 MeV.

REFERENCES:

- [1] W. J. Kernan C. Y. Wu, X. T. Liu, X. L. Han *et al.*, Nucl. Phys. A 524, 344 (1991).
- [2] J. A. Lay, L. Fortunato and A. Vitturi, Phys. Rev. C **89**, 034618 (2014).
- [3] H. A. Rashid, M. Bhuiyan, N. K. Deb, Amar Das *et al.*, Proc. DAE Symp. Nucl. Phys. **66**, 1202 (2022).
- [4] Kavita Rani, Abhilash S. R., G. R. Umopathy, D. Kabiraj and B. R. Behera, Nucl. Instrum. Methods A **963**, 163736 (2020).

5.1.2 Investigation of transfer reaction dynamics in the vicinity of the Coulomb barrier for $^{28}\text{Si} + ^{116, 120, 124}\text{Sn}$ systems

Anjali Rani¹, S. Mandal¹, S. Nath², N. Madhavan², J. Gehlot², Gonika², K. Chakraborty¹, Shoaib Noor³, A. Parihari¹, Rohan Biswas², D. Vishwakarma¹, P. Khandelwal¹, Chandra Kumar², P. S. Rawat¹, P. Sherpa¹ and S. Kumar¹

¹Department of Physics and Astrophysics, University of Delhi, Delhi 110007, India

²Inter-University Accelerator Centre, Aruna Asaf Ali Marg, New Delhi 110067, India

³Thapar Institute of Engineering and Technology, Patiala 147004, India

Transfer reactions have always been important to understand the interplay between nuclear structure and reaction dynamics [1]. Single nucleon transfer is a selective and direct probe of single particle shell structure, while two-nucleon transfer serves as a promising tool to investigate the pairing correlations amongst nuclei. Further, transfer channels coupled with inelastic excitations influence the fusion cross-sections at sub-barrier energies [2,3]. The fusion excitation function measurements around the Coulomb barrier with $^{28}\text{Si}+^{116,120,124}\text{Sn}$ systems have also been performed recently. The lucid role of multi-nucleon transfer channels in the sub-barrier fusion enhancement has been reflected in these measurements [4]. The different positive Q-value transfer channels make Sn systems a potential choice for transfer measurements. Sn isotopes possess extra neutrons outside their closed sub-shell, (4 in case of ^{124}Sn and, 2 in ^{116}Sn) resulting in the flow of neutrons between the colliding partners. This might take place either sequentially or simultaneously in the form of a cluster which can aid in the investigation of pairing correlation and superfluidity effects among the interacting nuclei. Therefore, to explore the aforementioned aspects of heavy-ion collision, we have performed transfer measurements for $^{28}\text{Si}+^{116,120,124}\text{Sn}$ systems at energies around the Coulomb barrier using the Heavy Ion Reaction Analyzer (HIRA) at IUAC [5]. The experiment has been performed using ^{28}Si pulsed beam with a pulse separation of 1 μs from the Pelletron. The targets used were isotopically enriched and of thicknesses $\sim 230 \mu\text{g}/\text{cm}^2$ with C backing of $\sim 20 \mu\text{g}/\text{cm}^2$. The spectrometer was rotated to 9° for better primary beam rejection. The forward-moving target-like recoils were detected using a $150 \times 50 \text{ mm}^2$ Multi-Wire -Proportional Counter (MWPC) at the focal plane of the HIRA. A kinematic coincidence between the forward-moving recoils and back-scattered projectile-like particles was employed using a 150 mm^2 silicon detector in the target chamber at a back angle of $\theta_{\text{lab}} = 158^\circ$. This kinematic coincidence (obtained by setting up a Time to Amplitude Converter (TAC) between the two timing signals), coupled with the Time of Flight (TOF) setup between MWPC timing and delayed Radio Frequency (RF), enabled unambiguous identification of the reaction products. The transfer measurements were performed at laboratory beam energies in the range of 97 - 108 MeV in steps of 3 MeV around and below the barrier. Two silicon detectors were mounted inside the target chamber at $\theta_{\text{lab}} = 15.5^\circ$ with respect to the beam direction for beam intensity monitoring. The HIRA was operated with acceptance of 5 mSr during the measurements. Reaction products were dispersed at the focal plane of the HIRA in accordance with their mass (A) to charge (q) ratio. A 2-D spectrum between MWPC position (X) and TOF of the recoils, gated with the TAC signal, was used for identification of reaction products. Preliminary analysis of data shows that neutron transfer probability of $2n$ channel is greater than theoretical predictions *i.e.*, $P^{2n} > (P^{1n})^2$. Further data analysis to apprehend the underlying reaction dynamics is in progress.

REFERENCES:

- [1] L. Corradi, G. Pollarolo and S. Szilner, J. Phys. G **36**, 113101 (2009).
- [2] Vandana Tripathi *et al.*, Pramana – J. Phys. **53**, 535 (1999).
- [3] S. Kalkal *et al.*, Phys. Rev. C **83**, 054607 (2011).
- [4] Anjali Rani, S. Mandal, K. Chakraborty *et al.*, Phys. Rev. C **106**, 064606 (2022).
- [5] A. K. Sinha *et al.*, Nucl. Instrum. Methods A **339**, 543 (1994).

5.1.3 Exploring breakup fusion reactions in the proximity of barrier energies: A thorough investigation

B. P. Singh¹, M. Shariq Asnain¹, Mohd. Shuaib¹, Ishfaq M. Bhatt¹, Manoj Kumar Sharma², Vijay R. Sharma³, Abhishek Yadav⁴, Pushpendra P. Singh⁵, Devendra P. Singh⁶, Unnati⁷, R. Kumar⁸ and R. Prasad¹

¹Aligarh Muslim University, Aligarh 202002, UP, India

²University of Lucknow, Lucknow 226007, UP, India

³University of Maryland School of Medicine, Baltimore, USA

⁴Jamia Millia Islamia, New Delhi 110025, India

⁵IIT Ropar 140001, Punjab, India

⁶UPES, Dehradun 248007, Uttarakhand, India

⁷Amity University, Noida 201301, UP, India

⁸Inter-University Accelerator Centre, Aruna Asaf Ali Marg, New Delhi 110067, India

In recent years, nuclear physicists have taken an interest in examining the breakup of projectiles in heavy-ion (HI) reactions. At projectile energies of approximately 4-7 MeV/nucleon, the prevalent reactions are complete fusion (CF) and incomplete fusion (ICF) processes. Recent measurements have revealed that these processes begin to compete at energies slightly above the Coulomb barrier [1-3]. During ICF reactions, the projectile undergoes partial fusion or breakup, resulting in a fractional linear momentum transfer from the projectile to the target nucleus. As a result, the composite nucleus generated during ICF reactions is expected to have a shorter range in the stopping medium compared to the one created during CF reactions. As such, the measurement of forward recoil range distributions (FRRDs) may be used as one of the most direct and irrefutable methods to distinguish the various CF and ICF components. In FRRD measurements, the residues populated via CF and ICF processes will correspond to different characteristic velocity distribution.

Therefore, the distribution of experimentally measured yields of different reaction residues as a function of velocity and/or range in stopping medium, may give a better insight into the reaction mechanism involved in such reactions. Further, the FRRD measurements has been capable of deciphering the relative contributions of compound and pre-compound components and hence may be used as a promising method to study the reaction dynamics involved in case of heavy-ion (HI) reactions. With this motivation, an attempt has been made to have a detailed investigation on ICF reaction dynamics from the analysis of forward recoil range distribution (FRRD) of heavy residues populated via CF and/or ICF routes. In the present work, the FRRDs of different reaction residues populated in the interaction of ^{19}F with ^{159}Tb , have been measured at two distinct beam energies 82.8 and 94.3 MeV [4].

The experiments for the measurement of FRRDs for $^{19}\text{F}+^{159}\text{Tb}$ system have been performed at IUAC. The $^{19}\text{F}^{8+}$ ion beam was delivered using the 15UD Pelletron accelerator facility. Two different stacks, each consisting of ^{159}Tb target (abundance = 100%) followed by a series of thin Al-catcher foils were irradiated separately at ≈ 83 and ≈ 94 MeV beam energy. The ^{159}Tb target (thickness $\approx 350 \mu\text{g}/\text{cm}^2$) was deposited by the vacuum evaporation technique on Al foil (thickness $\approx 2.03 \text{ mg}/\text{cm}^2$). The ^{159}Tb was mounted in such a way that the ^{19}F beam first faces Al foil so that after the energy loss in Al foil, the beam of required energy may fall on the target. To capture the recoiling residues generated through complete fusion (CF) and/or incomplete fusion (ICF) processes at their corresponding ranges in thin Al-catcher foils, a stack of such foils was placed after the target. The thickness of the foils was adequate to trap the composite nucleus formed through full momentum transfer. In order to have better resolution in recoil ranges of the residues, the thicknesses of Al catchers were kept $\approx 15\text{--}100 \mu\text{g}/\text{cm}^2$. From the kinematics, it was estimated that the heavy recoiling residues are mainly focused within a forward narrow cone of maximum 10° . As a representative case, the angular distribution of ^{174}W and ^{173}W residues populated via $4n$ and $5n$ evaporation, respectively, at ≈ 83 MeV obtained from PACE [5] calculations indicate that most of the residues are emitted in the forward cone of angle up to 7° , which clearly indicates that the emission of residues is forward peaked. The size of the catcher foils of 10 mm diameter was more than sufficient to trap the recoiling heavy residues at these angles. The thickness of the target and individual Al-catcher foils were determined using α -transmission method. Each irradiation was conducted for approximately 12 hours in the General-Purpose Scattering Chamber (GPSC). Following the irradiation, the sample-catcher assembly was removed from the chamber, and the induced activity in each catcher foil was recorded individually using a pre-calibrated high-resolution HPGe γ -spectrometer (100 cc active volume) connected to CANDLER software based on the CAMAC system. The HPGe detector (resolution ≈ 2 keV for 1.33 MeV γ -ray of ^{60}Co) was calibrated both for energy and efficiency. The efficiency of the HPGe detector at various source-detector distances was determined using standard ^{152}Eu γ -source of known strength. Also, corrections for the dead time were also employed during the analysis.

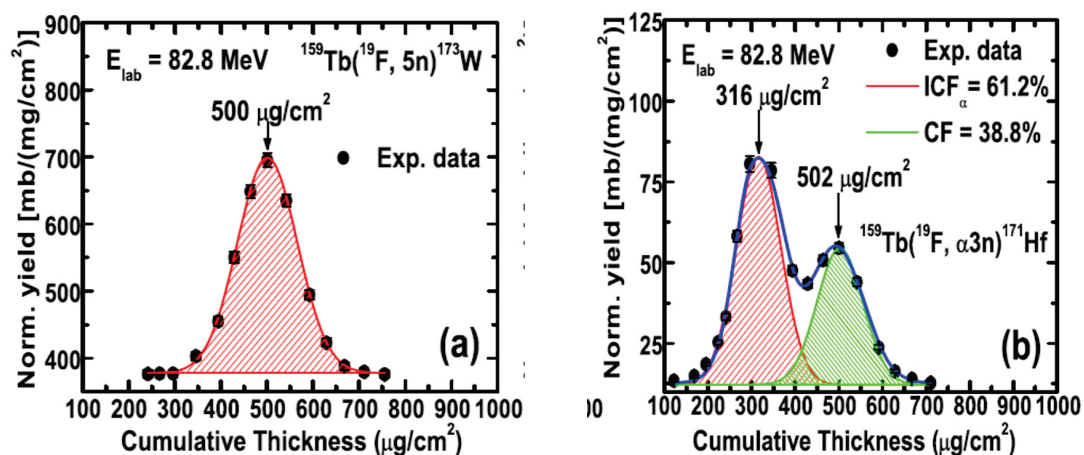


Fig. 5.1.3.1: The experimentally measured FRRD for various residues populated via CF and/or ICF processes at 82.8 MeV.

This study involves examining FRRDs of various evaporation residues (ERs) generated through CF and/or ICF processes. The standard formulation was used to calculate the production cross-section of the different reaction residues that were identified. To obtain normalized yields, the cross-section of residues in each Al-catcher foil was divided by its thickness. The resulting normalized yields were plotted as a function of cumulative catcher depth in order to obtain the range distribution of identified reaction residues. As a representative case, the measured FRRDs for the reaction residues $^{173}\text{W}(5n)$ and $^{171}\text{Hf}(\alpha 3n)$ is shown in Fig. 5.1.3.1 at ≈ 83 MeV beam energy. As can be seen from this figure, the measured FRRDs for $^{173}\text{W}(5n)$ residue shows only a single Gaussian peak indicating the involvement of only one linear momentum transfer (LMT) component in the production of this residue. Therefore, the ^{173}W residues are populated via full linear momentum transfer due to CF process only. The observed FRRDs for $^{171}\text{Hf}(\alpha 3n)$ were resolved into two Gaussian peaks. The Gaussian peak observed at a lower cumulative depth is indicative of partial linear momentum transfer (LMT) from the projectile to the target nucleus. This suggests that the residues detected may have been generated through a combination of both CF and ICF processes.

The findings reveal a notable contribution from ICF reactions in the production of different residues. Recent studies have indicated a transfer of both partial and full momentum from the projectile to the target in α -emitting channels during ICF reactions. The different partial LMT components corresponds to the break up and fusion of ^{19}F into ^{15}N and ^{11}B with the target nucleus. Further, the relative contribution of CF and/or ICF components have also been obtained. The critical angular momentum l_{crit} for the present system at which the pocket in the entrance-channel potential nearly vanishes has been calculated and is found to be 79. The values of l_{max} at two respective energies (82.8 and 94.3 MeV) in the present work are $\approx 22 \hbar$ and $40 \hbar$, respectively, which are less than the l_{crit} for fusion to occur in the present system. The observation of ICF for energies where $l_{\text{max}} < l_{\text{crit}}$ suggests that a significant number of l-waves below l_{crit} may contribute to ICF reactions. To obtain a more comprehensive understanding of the dynamics involved in ICF reactions, additional experimental data encompassing a wider range of nuclei are necessary. Moreover, supplementary experiments involving particle- γ coincidence, particularly for both loosely and strongly bound projectiles may provide a more detailed insight into the ICF dynamics. The new experimental findings could assist in improving the accuracy of existing theoretical models and in establishing systematics for energies approximately equal to 4-7 MeV/nucleon.

REFERENCES:

- [1] E. Holub, D. Hilscher, G. Ingold, U. Jahnke, H. Orf, and H. Rossner, Phys. Rev. C **28**, 252 (1983).
- [2] D. J. Parker, J. J. Hogan, and J. Asher, Phys. Rev. C **35**, 161 (1987).
- [3] M. Shariq Asnain, Mohd. Shuaib, Ishfaq Majeed, Manoj Kumar Sharma, Abhishek Yadav, Devendra P. Singh, Pushpendra P. Singh, R. Kumar, B. P. Singh and R. Prasad, Phys. Rev. C **104**, 034616 (2021).
- [4] M. Shariq Asnain, Mohd. Shuaib, Ishfaq Majeed, Manoj Kumar Sharma, Abhishek Yadav, Devendra P. Singh, Pushpendra P. Singh, R. Kumar, B. P. Singh and R. Prasad, Phys. Rev. C **106**, 064607 (2022).
- [5] A. Gavron, Phys. Rev. C **21**, 230 (1980).

5.1.4 Investigating channel coupling effects in the sub-barrier fusion of $^{30}\text{Si}+^{140}\text{Ce}$ and $^{32}\text{S}+^{138}\text{Ba}$

Malvika Sagwal¹, Moumita Maiti¹, Rishabh Kumar¹, Pavneet Kaur¹, Ankur Singh¹, Gonika², Chandra Kumar², Himanshu Sharma¹, Yasir Arafat¹, S. Nath², J. Gehlot² and N. Madhavan²

¹Department of Physics, Indian Institute of Technology Roorkee, Roorkee 247667, Uttarakhand, India

²Nuclear Physics Group, Inter-University Accelerator Centre, New Delhi 110067, India

The discovery of the quantum-tunneling effect has aided in understanding the fusion phenomenon in nuclei below the Coulomb barrier. However, multiple orders of enhancement in the sub-barrier energy region have been noticed for heavy-ion fusion reactions compared to the tunneling-based one-dimensional barrier penetration model (1DBPM) [for details, see Rep. Prog. Phys. **51** (1988) 1047, Annu. Rev. Nucl. Part. Sci., **48** (1998) 401]. Explanations based on the role of couplings to various degrees of freedom of the participating nuclei, such as static and dynamical deformations, nucleon transfer, etc., have shown substantial success [for details, see Phys. Rev. C, **73** (2006) 034606, Phys. Rev. C **102** (2020) 024615]. However, the extent of their contribution and mutual interplay in deciding the fusion dynamics is still being understood. We aim to measure the fusion excitation functions of $^{30}\text{Si}+^{140}\text{Ce}$ and $^{32}\text{S}+^{138}\text{Ba}$ reactions forming the compound nucleus $^{170}\text{Hf}^*$. The Q-values of neutron transfer are zero for the former reaction. Contrarily, for the latter, they are positive for up to 6n pickup by the projectile from the target. Looking into the structural effects of the nuclei and couplings to transfer channels can assist the knowledge of sub-barrier fusion phenomenon.

The evaporation residue (ER) cross-section (σ_{ER}) measurement was performed at 15 UD Pelletron accelerator facility of IUAC, using the first stage of the Hybrid Recoil mass Analyzer (HYRA) [for details, see Pramana - J. Phys. **75** (2010) 317]. Targets of ^{140}Ce and ^{138}Ba having 200 $\mu\text{g}/\text{cm}^2$ thickness were bombarded with ^{30}Si and ^{32}S beams, respectively. The beam energy (E_{lab}) range was varied between 132 - 105 MeV for the $^{30}\text{Si}+^{140}\text{Ce}$ reaction spanning 13% above to 11% below the Coulomb barrier. While for the $^{32}\text{S}+^{138}\text{Ba}$ reaction, the energy spanned the 130 - 117 MeV range (11% below to near the Coulomb barrier). Two silicon surface-barrier detectors (SSBDs) were mounted in the target chamber to normalize the ER counts absolutely. The helium gas pressure and the magnetic field settings of the HYRA were optimized through an in-house code to result in the maximum transmission of ERs and rejection of the primary and secondary beam-like particles. The ERs were directed to the focal plane of a multiwire proportional counter (MWPC) of $15.0 \times 5.0 \text{ cm}^2$ area. Two-dimensional energy loss (ΔE) vs. time-of-flight (TOF) spectra were generated to identify and gate the ER counts distinctly. The data were acquired through the IUAC software NIAS-MARS and analyzed using the ROOT framework. The total ER cross-section for the $^{30}\text{Si}+^{140}\text{Ce}$ reaction was calculated [for details, see Phys. Rev. C **84** (2011) 064606] by incorporating the yield of elastically scattered beam-like particles and ERs measured by the monitor detectors (SSBDs) and the MWPC, respectively, transmission efficiency of the recoil separator HYRA, etc. Since the fusion-fission probability is negligible for the reaction, the fusion-evaporation process results in $\sigma_{\text{ER}} \sim \sigma_{\text{fusion}}$.

The fusion excitation function of $^{30}\text{Si}+^{140}\text{Ce}$ has been compared with the coupled-channels code CCFULL [for details, see Comp. Phys. Comm. **123** (1999) 143]. The measured fusion cross-sections were found to have enhanced a few orders of magnitude with respect to 1DBPM predictions deep below the Coulomb barrier. The projectile is a static deformed nucleus with $\beta_2 = 0.315$, and the target exhibits low-lying vibrational states.

The detailed investigation of couplings in the colliding partners' rotational and vibrational degrees of freedom; and the nature of fusion barrier distribution is in progress. The $^{32}\text{S}+^{138}\text{Ba}$ reaction measurement is yet to be carried out for the near and above Coulomb barrier energies. The study can subsequently reveal the additional facets of transfer-channel couplings and their role in the sub-barrier fusion enhancement.

REFERENCES:

- [1] M. Beckerman, Rep. Prog. Phys. **51**, 1047 (1988).
- [2] M. Dasgupta, D. J. Hinde, N. Rowley and A. M. Stefanini, Annu. Rev. Nucl. Part. Sci. **48**, 401 (1998).
- [3] A. M. Stefanini, F. Scarlassara, S. Beghini, G. Montagnoli, R. Silvestri, M. Trotta, B. R. Behera *et al.*, Phys. Rev. C **73**, 034606 (2006).
- [4] R. N. Sahoo, M. Kaushik, A. Sood, A. Sharma, S. Thakur, P. Kumar, Md. Moin Shaikh *et al.*, Phys. Rev. C **102**, 024615 (2020).
- [5] N. Madhavan, S. Nath, T. Varughese, J. Gehlot, A. Jhingan, P. Sugathan, A. K. Sinha *et al.*, Pramana - J. Phys. **75**, 317 (2010).
- [6] E. Prasad, K. M. Varier, N. Madhavan, S. Nath, J. Gehlot, S. Kalkal, J. Sadhukhan *et al.*, Phys. Rev. C **84**, 064606 (2011).
- [7] K. Hagino, N. Rowley and A. T. Kruppa, Comp. Phys. Comm. **123**, 143 (1999).

5.1.5 Measurement of evaporation residue cross-sections for $^{30}\text{Si}+^{142}\text{Ce}$ reaction

Amninderjeet Kaur¹, Ashok Kumar¹, Chetan Sharma¹, Neha Dhanda¹, Raghav¹, N. Madhavan², S. Nath², J. Gehlot², Gonika², Chandra Kumar², P. Sherpa³, A. Parihari³, Jyoti Pandey², A. K. Gupta⁴, H. P. Sharma⁴, and B. R. Behera¹

¹Department of Physics, Panjab University, Chandigarh-160014, India

²Inter University Accelerator Centre, Aruna Asaf Ali Marg, New Delhi-110067, India

³Department of Physics and Astrophysics, University of Delhi, Delhi 110007, India

⁴Department of Physics, Banaras Hindu University, Uttar Pradesh 221005, India

To study the effect of entrance channel mass asymmetry on fusion-fission dynamics, we have selected two projectile target combinations: $^{30}\text{Si}+^{142}\text{Ce}$ and $^{48}\text{Ti}+^{124}\text{Sn}$, both these systems lead to the same compound nucleus (CN) $^{172}\text{Hf}^*$. Energy of the projectile is chosen in such a way that in both the cases the same CN is populated at same excitation energy. Out of these two reactions, we have measured the evaporation residue (ER) cross-sections for $^{30}\text{Si}+^{142}\text{Ce}$ system using the HYRA facility. We have measured the ER cross-sections at 11 energy points in the range of 9% below and 13% above the barrier. ^{30}Si beam is accelerated up to 140 MeV energy using the Pelletron facility and is bombarded on a ^{142}Ce target having thickness $200\ \mu\text{g}/\text{cm}^2$ on a carbon backing of thickness $20\ \mu\text{g}/\text{cm}^2$. In the target chamber, two silicon detectors were placed at a distance of 42 mm from the target, making an angle of 26.1° with respect to the beam direction. These detectors were used for detection of elastically scattered ^{30}Si ions for cross-section normalization and for positioning the beam at the center of the target. ERs formed in the target chamber were detected by a multi-wire proportional counter (MWPC) of dimension $15 \times 5\ \text{cm}^2$.

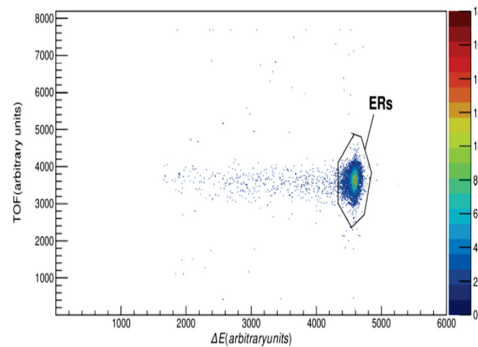


Fig. 5.1.5.1: Two-dimensional plot of energy loss (ΔE) vs. Time of flight (TOF) for $^{30}\text{Si}+^{142}\text{Ce}$ at 133 MeV.

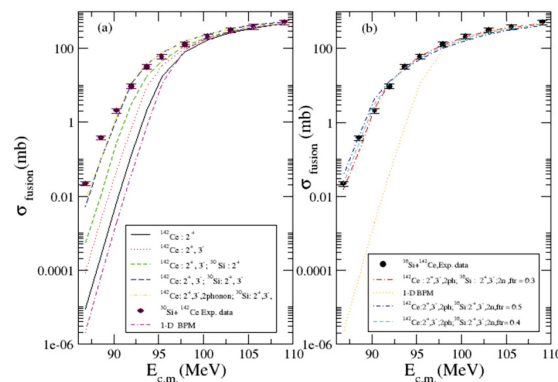


Fig. 5.1.5.2: Coupled-channels calculations using the CCFULL code for $^{30}\text{Si}+^{142}\text{Ce}$ (a) by including various couplings and (b) by coupling with +2n transfer channel.

Fig. 5.1.5.1 shows that ERs are clearly separated from the beam background. To analyse the experimental data, we have performed the coupled-channels calculations using the CCFULL code [1]. Experimental results overpredicts one-dimensional barrier penetration model predictions, as shown in Fig. 5.1.5.2(a), so to explain this enhancement below the barrier, we included couplings both in projectile and target nucleus. We have used the Akyuz-Winther parameterization of nuclear potential in the present calculations [2]. Fig. 5.1.5.2(b) shows that inclusion of transfer coupling, $F_{tr} = 0.3$, gives best fit to the data.

REFERENCES.:

- [1] K. Hagino, N. Rowley and A. T. Kruppa, *Comput. Phys. Commun.* **123**, 143 (1999).
 [2] R. A. Broglia and A. Winther, *Heavy Ion Reactions*, (Benjamin Cummings, San Francisco, 1981).

5.1.6

Investigation of nuclear structure at high spin in neutron deficient nuclei

Diwanshu¹, A. Kumar¹, Bharti Rohila¹, Chetan¹, Subodh¹, Ishika Sharma², H. P. Sharma², P. S. Rawat³, S. Kumar³, Anand Pandey³, S. K. Chamoli³, K. Katre, H. Arora⁴, Uday Ghosh⁴, Yashraj⁴, Indu Bala⁴, R. P. Singh⁴ and S. Muralithar⁴

¹Department of Physics, Panjab University, Chandigarh, India

²Department of Physics, Banaras Hindu University, Varanasi, India

³Department of Physics and Astrophysics, University of Delhi, New Delhi, India

⁴Inter-University Accelerator Centre, Aruna Asaf Ali Marg, New Delhi, India

The transitional nuclei in the mass range $A = 100-120$ has been studied via heavy ion fusion evaporation reaction using the Indian National Gamma Array (INGA) at IUAC. In $A \sim 100$ mass region, evolution of shapes from spherical to deformed and rotational like band structures due to $h_{11/2}, g_{7/2}, d_{5/2}$ neutron orbitals and high- Ω $g_{9/2}$ proton orbitals is a topic of interest since many years. Specific coupling of these low- Ω neutron particles and high- Ω proton holes gives rise to exciting phenomena [1]. On the other hand, in $A \sim 120$ mass region [2], the proton fermi surface lies near lower $h_{11/2}$ subshell. These nuclei are considered to be soft with respect to γ . Gamma spectroscopy and lifetime measurements in this region has been carried out to probe the role of these orbitals in their structure.

To study the nuclear structural phenomena in this mass region, two different systems have been studied (i) $^{16}\text{O}+^{94}\text{Zr}$ and (ii) $^{16}\text{O}+^{107}\text{Ag}$, leading to the population of ^{106}Cd and ^{120}Cs , respectively. Other nuclei were also populated along with ^{120}Cs , like ^{120}Xe , ^{119}Xe , and ^{119}I . The 1.1 mg/cm^2 ^{94}Zr target with 4.7 mg/cm^2 thick Au backing and 1.1 mg/cm^2 ^{107}Ag with 6.09 mg/cm^2 Au backing have been fabricated by cold rolling method at the Target Development Laboratory of IUAC. Both the reactions were induced by 77 MeV ^{16}O beam, provided by the Pelletron at IUAC. The data were taken in both single and double coincidence mode by 11 Clover detectors arranged in the INGA setup [3] at three different angles *i.e.*, $\theta = 148^\circ, 90^\circ$ and 32° . Root-based data acquisition system NiasMARS developed by the IUAC group was used to process and analyze the data. Symmetric and angle-dependent γ - γ matrices were generated by NiasMARS and analyzed by the RADWARE package for further analysis.

From the primary analysis, coincidence γ - γ spectrum with gate on 998 keV transition, showing the peaks belonging to ^{106}Cd [4], is shown in Fig. 5.1.6.1. For the $^{16}\text{O}+^{107}\text{Ag}$ system, all vs all projection spectrum, showing all the populated nuclei marked with their characteristic γ -rays, is shown in Fig. 5.1.6.2. Further analysis for lifetime and excitation function measurements is in progress.

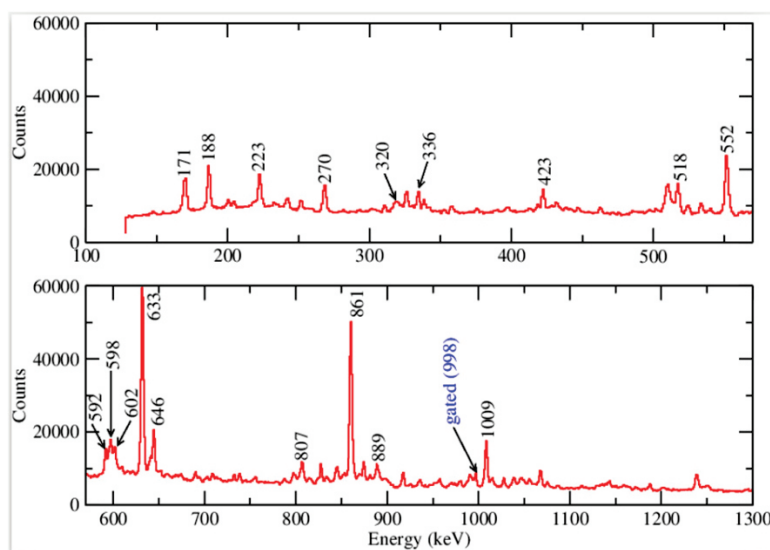


Fig. 5.1.6.1: γ - γ coincidence spectra for ^{106}Cd (from the reaction $^{16}\text{O}+^{94}\text{Zr}$) with gate on 998 keV transition.

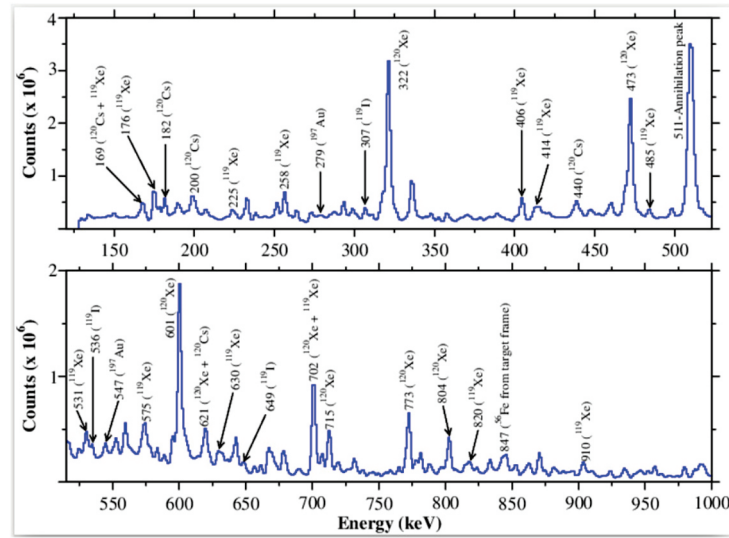


Fig. 5.1.6.2: A typical all vs all projection spectrum showing all the populated nuclei in the $^{16}\text{O}+^{107}\text{Ag}$ system.

REFERENCES:

- [1] D. Chaudhary *et al.*, Phys. Rev. C **91**, 014318 (2015).
- [2] C.-B. Moon *et al.*, Nucl. Phys. A **696**, 45 (2001).
- [3] S. Muralithar, R. P. Singh, K. Rani, R. Kumar *et al.*, Nucl. Instrum. Methods A **622**, 281 (2010).
- [4] P. H. Regan *et al.*, Nucl. Phys. A **586**, 351 (1995).

5.1.7

Lifetime measurement study in nuclei having mass $A \sim 120$

Anand Pandey¹, Ravi Bhushan¹, Prabhat Sharma¹, Suresh Kumar¹, Prerna Singh Rawat¹, Nandini Patel¹, Bharti Rohilla², H. P. Sharma³, Md. Ansar³, R.P. Singh⁴, S. Muralithar⁴, Yashraj⁴, Uday Shankar Ghosh⁴ and S. K. Chamoli¹

¹Department of Physics and Astrophysics, University of Delhi, Delhi 110007, India.

²Department of Physics, Panjab University, Chandigarh 160014, India

³Department of Physics, Banaras Hindu University, Varanasi, India

⁴Inter University Accelerator Centre, Aruna Asaf Ali Marg, New Delhi 110067, India

Nuclei with $A \sim 120$ ($50 \leq Z \leq 56$) are of significant interest because of the competing shape driving tendencies of the orbitals occupied by their neutrons and protons. In recent years, neutron deficient Ba, Cs, and Xe nuclei with mass $A \sim 120$ have gained considerable attention due to the presence of both quadrupole and octupole collectivity. According to theoretical calculations, octupole degree of freedom plays an important role in atomic nuclei after the quadrupole degree of freedom [1]. Octupole correlations arise from the interaction between nucleons of opposite-parity orbitals near the Fermi level, whose angular momenta differ by $3\hbar$. Calculations suggest that nuclei with neutron or proton numbers of 34 ($g_{9/2} \leftrightarrow p_{3/2}$), 56 ($h_{11/2} \leftrightarrow d_{5/2}$), 88 ($i_{13/2} \leftrightarrow f_{7/2}$), and 134 ($j_{15/2} \leftrightarrow g_{9/2}$) [1–3] exhibit softness towards octupole deformation. Moreover, double octupole shell closure nucleus with $Z = 56$ and $N = 88$, ^{144}Ba [4] display enhanced octupole collectivity. Investigations in nuclei with $Z \approx N \approx 56$ indicate that alternate-parity bands in these nuclei are linked by E1 transitions with higher transition rates, $B(E1) \sim 10^{-4}$ W.u., which are similar to those observed in neutron-rich barium ($Z = 56$) nuclei [4]. Furthermore, the shell structure in the $Z \sim 56$ and $N \sim 66$ region exhibits similar features to those of lanthanide and actinide regions where octupole correlations have been observed [5]. While low-energy spectra of deformed nuclei can be explained in terms of rotation of axially symmetric shape, chiral rotation has been observed as one of the preferred modes of excitation in a nucleus with triaxial shape. In a recent study [6], lifetime measurements in ^{124}Cs were extended to higher spin states in the chiral partner bands.

Further experiments are necessary to systematically investigate the prevalence of the octupole phenomenon and chiral bands in the odd-odd nuclei having mass $A \sim 120$ region. In pursuit of this objective, a recent experiment was conducted at IUAC to explore the high spin states in ^{122}Cs nuclei via lifetime measurement using the Doppler Shift Attenuation Method (DSAM). High spin states in ^{122}Cs were achieved by populating them through the $^{107}\text{Ag}(^{19}\text{F}, p3n)^{122}\text{Cs}$ fusion evaporation reaction at a beam energy of 88 MeV. The target used consisted of a ^{107}Ag foil that was nicely rolled to a thickness of approximately 1.1 mg/cm^2 on a 6 mg/cm^2 thick Au backing. The de-exciting γ -rays were detected using the Indian National Gamma Array (INGA) setup [7], which comprised of 11 Compton-suppressed Clover detectors arranged in five rings at angles of 32° , 90° , and 148° relative to the beam direction. Data was collected in γ - γ coincidences mode for 12 shifts, and to optimize the yield of ^{122}Cs , an excitation function was conducted at 86, 88, 90, and 94 MeV of beam energy. Part of the data displaying the clearly-marked γ energy peaks of various nuclei populated in the reaction is illustrated in Figure 5.1.7.1. Detailed analysis of data is currently in progress.

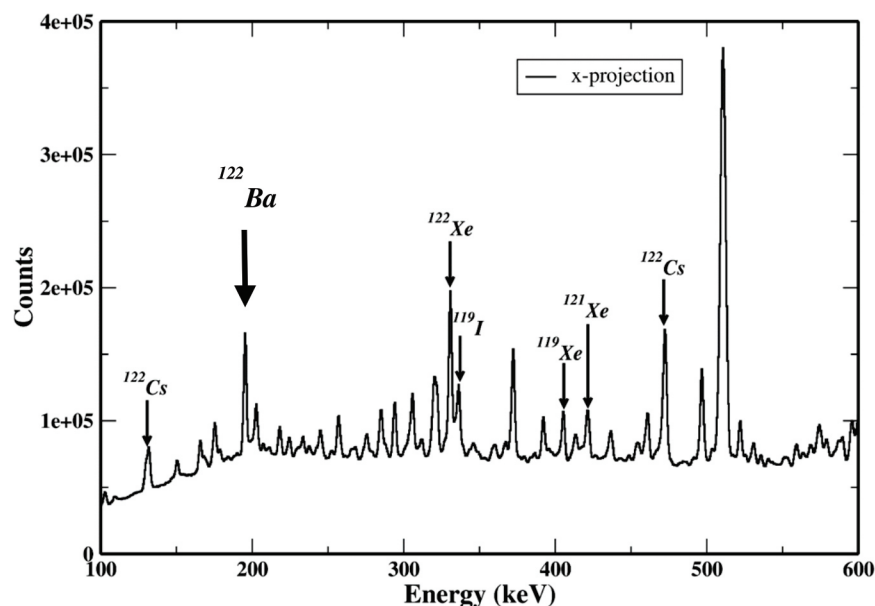


Fig. 5.1.7.1: Energy spectrum showing quality of data taken. Most intense peaks of different nuclei populated in the reaction are clearly marked.

REFERENCES:

- [1] W. Nazarewicz *et al.*, Nucl. Phys. A **429**, 269 (1984).
- [2] J. Skalski, Phys. Lett. B **238**, 6 (1990).
- [3] P.-H. Heenen *et al.*, Phys. Rev. C **50**, 802 (1994).
- [4] W. R. Phillips *et al.*, Phys. Rev. Lett. **57**, 3257 (1986).
- [5] P. D. Cottle *et al.*, Phys. Lett. B **219**, 27 (1989).
- [6] K. Selvakumar *et al.*, Phys. Rev. C **92**, 064307 (2015).
- [7] S. Muralithar *et al.*, Nucl. Instrum. Methods A **622**, 281 (2010).

5.1.8 Spectroscopy of ^{67}Ga

U. S. Ghosh^{1,5}, S. Rai¹, B. Mukherjee¹, A. K. Mondal¹, K. Mandal¹, S. Barman¹, A. Goswami¹, S. Biswas¹, B. Kharpuse¹, A. Chakraborty¹, G. Mukherjee², S. Chakraborty^{2,3}, A. Sharma⁴, I. Bala⁵, S. Muralithar⁵ and R. P. Singh⁵

¹Department of Physics, Visva-Bharati, Santiniketan 731235, India

²Variable Energy Cyclotron centre, 1/AF Bidhannagar, Kolkata 700064, India

³Department of Physics, Banaras Hindu University, Varanasi 221005, India

⁴Department of Physics, Himachal Pradesh University, Shimla 171005, India

⁵Inter-University Accelerator Centre, Aruna Asaf Ali Marg, New Delhi 110067, India

All the nuclear structural phenomena originating out of single-particle and collective modes of excitations are, respectively, due to the occupation of valance nucleons in fp-orbitals and particle-hole excitation to the shape-driving $1g_{9/2}$ orbital. Evolution of shapes and collective structures have been observed in many Zn isotopes [1,2,3] in this mass region.

Moreover, in the study of high spin states in ^{62}Zn super-deformation was found for the first time in this mass region [3]. This phenomenon was expected from calculations predicting large shell gaps in the single particle energies for proton and neutron numbers $N, Z = 30-32$ [4,5]. Various reports in the literature suggest that this kind of exotic phenomena at high spin is due to the significant occupation of $1g_{9/2}$ orbital.

The high spin structures are certainly not explored to that extent for the Ga nuclei in this region. So, our primary motivation is to study the high spin phenomena in Ga and here, we report few preliminary results observed in the in-beam spectroscopy of ^{67}Ga .

The nucleus of interest was populated via fusion-evaporation reaction. In this reaction a beam of ^{18}O at 72.5 MeV was obtained from the 15UD Pelletron accelerator [6] at IUAC. The Indian National Gamma Array (INGA) [7] was used to detect the emitted γ -rays. Multipolarity of a transition was determined from the DCO ratio (R_{DCO}) [8]. The detectors at 90° and 148° were considered for R_{DCO} measurement. Electric or magnetic nature of γ -ray transitions was determined from the linear polarization measurement [9, 10] from the data recorded in the 90° detectors. Details of the experimental set-up and analysis methods are given in Refs. [1,11].

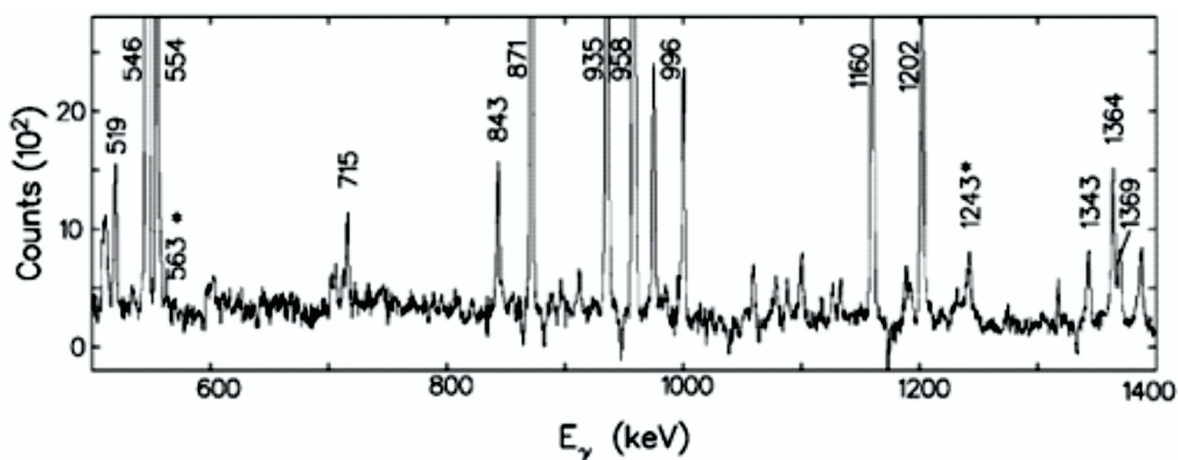


Fig. 5.1.8.1: γ - γ coincidence spectra for ^{67}Ga gated on 713 keV ($19/2^+ \rightarrow 15/2^+$) transition. Here, y-axis represents counts/1.0 keV. New transitions are highlighted with "*" symbol.

Two gated spectra, obtained in the present analysis by γ - γ coincidence spectra for ^{67}Ga gated on 713 keV (Fig. 5.1.8.1, $9/2^+ \rightarrow 15/2^+$) and 888 keV (Fig. 5.1.8.2, $25/2^+ \rightarrow 21/2^+$) transitions, are shown here. Few new transitions which are observed in the present work are also marked in the gated spectra. Spin-parity of the many states are assigned on the basis of DCO and polarization measurement. Many states are assigned with definite spin-parity which were assigned tentatively in previous works. Detail analysis is in progress and the results will be communicated shortly.

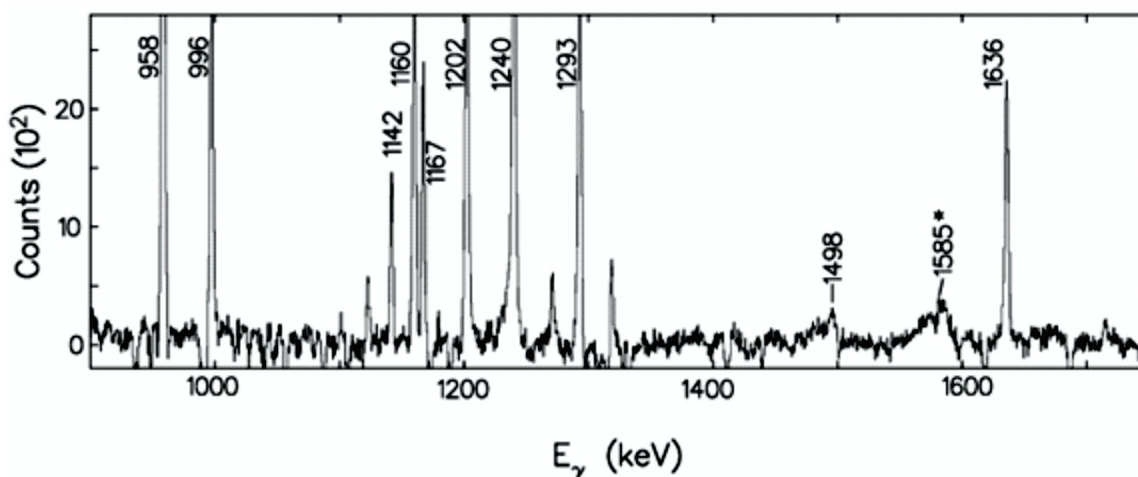


Fig. 5.1.8.2: γ - γ coincidence spectra for ^{67}Ga gated on 888 keV ($25/2^+ \rightarrow 21/2^+$) transition. Here, y-axis represents counts/1.0 keV. New transitions are highlighted with "*" symbol.

The authors thank the operating crew of the Pelletron and the Target Development Laboratory at IUAC, New Delhi for providing excellent support throughout the experiment. We thank S. Nandi (VECC, Kolkata), S.S. Bhattacharjee (IUAC) and R. Garg (IUAC) for their help during the experiment. We acknowledge the financial assistance received from IUAC, New Delhi, via Project No. UFR-49318, UFR-67309 and SERB (India) via Project No. EMR/2015/000891, CRG/2020/000715.

REFERENCES:

1. S. Rai *et al.*, Phys. Rev. C **102**, 064313 (2020).
2. J. Gellanki *et al.*, Phys. Rev. C **86**, 034304 (2012).
3. C. E. Svensson *et al.*, Phys. Rev. Lett. **79**, 1233 (1997).
4. R. K. Sheline, I. Ragnarsson and S. G. Nilsson, Phys. Lett. **41B**, 115 (1972).
5. J. Dudek, W. Nazarewicz, Z. Szymanski and G. A. Leander, Phys. Rev. Lett. **59**, 1405 (1987).
6. G. K. Mehta *et al.*, Nucl. Instrum. Methods A **268**, 334 (1988).
7. S. Muralithar *et al.*, Nucl. Instrum. Methods A **622**, 281 (2010).
8. K. S. Krane *et al.*, Nucl. Data Tables **11**, 351 (1973).
9. G. Duchene *et al.*, Nucl. Instrum. Methods A **432**, 90 (1999).
10. K. Starosta *et al.*, Nucl. Instrum. Methods A **423**, 16 (1999).
11. U. S. Ghosh *et al.*, Phys. Rev. C **100**, 034314 (2019).

5.1.9 Study of ^{100}Rh nucleus

Kaushik Katre¹, Yashraj¹, Sushil Kumar¹, Honey Arora¹, Uday Ghosh¹, Bharti Rohila², Subodh Yadav²,

Diwanshu Sharma², Prerna Rawat³, Dhananjaya Sahoo⁴, Shashi Shekher Tiwary⁴, Indu Bala¹, Rakesh Kumar¹, S. Muralithar¹ and R. P. Singh¹

¹Inter-University Accelerator Centre, New Delhi 110067, India

²Department of Physics, Panjab University, Chandigarh 147002, India

³Department of Physics and Astrophysics, Delhi University, Delhi 110007, India

⁴Department of Physics, Indian Institute of Technology Roorkee, Roorkee 247667, India

The nuclei in $A \approx 100$ region have drawn a lot of attention in the recent times due to the existence of various dynamical symmetries. For example, the collective excitations like wobbling, chirality, magnetic and anti-magnetic rotation have been reported in these nuclei along with non-collective single-particle excitations [1-3].

In order to investigate the level structure of ^{100}Rh [4], the high spin states of ^{100}Rh were populated using $^{89}\text{Y}(^{14}\text{N}, 1p2n\gamma)$ fusion evaporation reaction at a beam energy of 55 MeV. The ^{14}N beam was delivered by the 15UD Pelletron facility of IUAC. The beam impinged on a $400 \mu\text{g}/\text{cm}^2$ thick ^{89}Y target, evaporated on a $10 \text{mg}/\text{cm}^2$ thick gold foil. The de-exciting γ -rays were detected by the Indian National Gamma Array (INGA) [5], having 11 Clover detectors during this experiment. The detectors were mounted at three different angles with respect to the beam direction. The data were collected using a VME-based data acquisition system [6] and sorted into the symmetric γ - γ matrix. The symmetric matrix was used to confirm the previously known level scheme and to place new γ -rays in the level scheme by generating various gated spectra. The energy and efficiency calibration were done by using the standard ^{152}Eu source. Fig. 5.1.9.1 shows the gated spectrum with gate on 397 keV (10^{-9}) transition. The known γ -transitions in ^{100}Rh are marked.

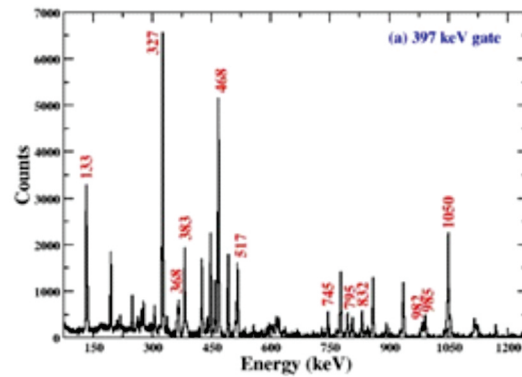


Fig. 5.1.9.1: The spectrum showing γ -rays for ^{100}Rh with gate on 397 keV transition.

In order to identify the new γ -rays and extend the level structure of ^{100}Rh , further data analysis is under process.

REFERENCES:

- [1] P. Datta *et al.*, Phys. Rev. C **69**, 044317 (2004).
- [2] A. Sharma *et al.*, Phys. Rev. C **103**, 044322 (2021).
- [3] J. Timar *et al.*, Phys. Rev. Lett. **122**, 062501 (2019).
- [4] A. Gizon *et al.*, Eur. Phys. J. A **2**, 325 (1998).
- [5] S. Muralithar *et al.*, Nucl. Instrum. Methods A **622**, 281 (2010).
- [6] Mamta Jain *et al.*, Rev. Sci. Instrum. **94**, 013304 (2023).

5.1.10 High spin study and lifetime measurements in mass region $A \sim 120$ nuclei

Bharti Rohila¹, A. Kumar¹, Diwanshu¹, Chetan Sharma¹, Amit¹, Subodh¹, S. S. Tiwary², Mohammad Anser³, H. P. Sharma³, Anand Pandey⁴, S. K. Chamoli⁴, Kaushik Katre⁵, Honey Arora⁵, Yashraj⁵, Indu Bala⁵, R. P. Singh⁵ and S. Muralithar⁵

¹Department of Physics, Panjab University, Chandigarh 160014, India

²Department of Physics, Manipal University, Jaipur 302033, India

³Department of Physics, Banaras Hindu University, Varanasi 221005, India

⁴Department of Physics and Astrophysics, University of Delhi, Delhi 110007, India

⁵Inter-University Accelerator Centre, Aruna Asaf Ali Marg, New Delhi 110067, India

Transitional nuclei between spherical and strongly deformed regions are usually soft with respect to deformation changes. Shape changes, including triaxiality can be induced by the excitation of nucleons into specific deformation-driving orbitals. In particular, attention has been paid to Ba isotopes because of their softness with respect to deformation and of the possible presence of octupole correlations [1,2]. The ^{122}Ba nucleus has been studied by Petrache *et al.* [3] and spin-parity of a few bands have not been assigned. Our aim

was to search for new collective and non-collective bands in this nucleus. In even light Ba nuclei, E1 transitions, linking positive-parity and negative parity structures have been observed. Apart from this we wanted to measure the lifetimes of γ -transitions with the emphasis on linking E1 transitions to establish the role of octuple correlations in the origin of the parity doublets shown by $^{120-125}\text{Ba}$ isotopes. Therefore, it was required to perform an experiment for developing the level scheme as well as lifetime measurements.

To investigate the structure of the nucleus, high spin study and lifetime measurements were done using the Indian National Gamma Array (INGA) [4]. To populate high spin states for the nuclei in mass region $A \sim 120$, a heavy ion fusion evaporation reaction was performed with incident beam of ^{32}S on the targets of thin ^{93}Nb with gold backing and ^{93}Nb self-supporting thick target at 124 MeV and 128 MeV, respectively. The beam was provided by the 15UD Pelletron accelerator at IUAC. The thin ^{93}Nb target of thickness $\sim 550 \mu\text{g}/\text{cm}^2$ with the backing of ^{197}Au of thickness $\sim 9.8 \text{ mg}/\text{cm}^2$ and thick ^{93}Nb target of thickness $\sim 6.8 \text{ mg}/\text{cm}^2$ were fabricated in the Target Development Laboratory of IUAC. The coincidence measurements were done using the array comprised of eleven Compton-suppressed Clover detectors. The data were acquired using the ROOT-based data acquisition system known as NiasMARS. To calibrate the spectra of each crystal, the NiasMARS software was used. Recalibration and matrix formation was done using the programs MarsReCalibrate.C and MarsMatrix.C developed at IUAC. Further analysis of data is going on with RADWARE [5] and lineshape [6].

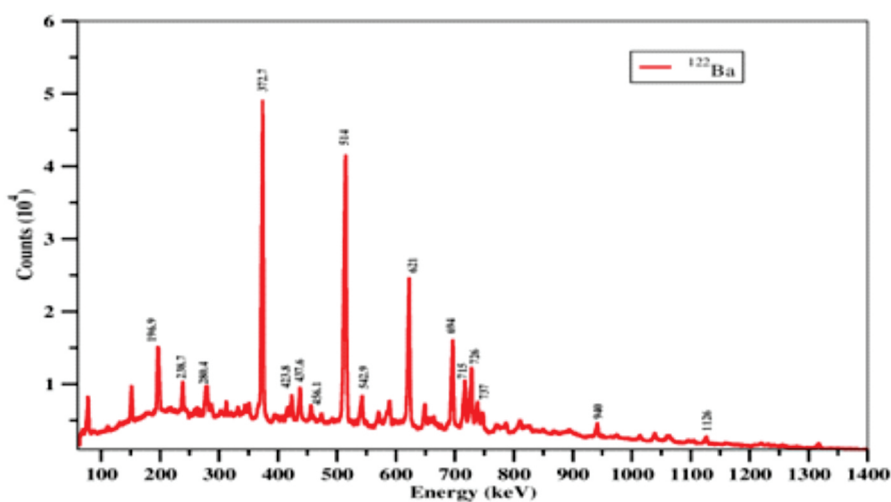


Fig. 5.1.10.1: Gated spectrum of ^{122}Ba (gate on 197 keV transition) populated in the reaction.

REFERENCES:

- [1] W. Wyss *et al.*, Nucl. Phys. A **505**, 337 (1989).
- [2] W. Nazarewicz *et al.*, Nucl. Phys. A **429**, 269 (1984).
- [3] C. M. Petrache *et al.*, Eur. Phys. J. A **12**, 135 (2001).
- [4] S. Muralithar *et al.*, Nucl. Instrum. Methods A **622**, 281 (2010).
- [5] <https://radware.phy.ornl.gov/>
- [6] J. C. Wells *et al.*, Report No. ORNL-6689, 44 (1991).

5.1.11

Gamma ray spectroscopy of some astrophysically important nuclei towards endpoint of nova nucleosynthesis

Subodh¹, Raghav¹, Amit¹, Chetan¹, Bharti Rohilla¹, B. R. Behera¹, P. S. Rawat², Anuj², S. S. Tiwari³, Yashraj⁴, Mohit Kumar⁴, Akhil Jhingan⁴, H. Arora⁴, Indu Bala⁴, S. Muralithar⁴ and R. P. Singh⁴

¹Department of Physics, Panjab University, Chandigarh 160014, India

²Department of Physics and Astrophysics, University of Delhi, New Delhi 11007, India

³Department of Physics, Manipal University, Jaipur 302033, India

⁴Inter-University Accelerator Centre, Aruna Asaf Ali Marg, New Delhi 110067, India

Astronomical observations of classical novae are among the most prolific obtained for any explosive event in our Galaxy. The classical novae occur in semidetached close interacting binary system consisting of a carbon-oxygen rich (CO) or an oxygen-neon rich (ONe) white dwarf and a main sequence star [1]. Relative to solar abundance, the ejecta of classical novae show significant nuclear processing [2]. Both theoretical and the abundance pattern inferred from observations of nova ejecta agree that the nuclear activity in classical novae relates around $A \sim 40$. However, significant discrepancies currently exist between observations *i.e.*, theoretical and experimental data of these nuclei in nova ejecta [3]. From nuclear physics point of view, nuclei in the upper sd shell in this mass region shows interesting phenomena *e.g.*, interplay between collective and single-particle motion, clusterization and its correlation with superdeformed bands [4]. By

comparing high spin states with shell model calculation for improving the effective nucleon-nucleon interactions in *sdf* and *sdfp* space is also an important aspect for nuclei in this mass region. Hence in order to deduce level structure and spin parity assignment for different states of nuclei in mass region $A \sim 40$, a γ -ray spectroscopy experiment was required.

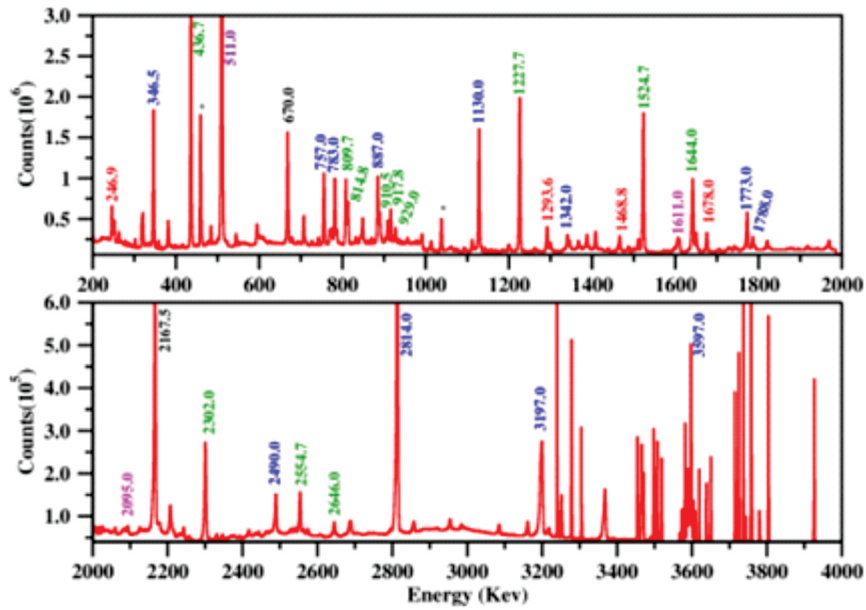


Fig. 5.1.11.1: A typical all vs all projection spectrum is showing the counts of γ -transitions from $A \sim 40$ mass region nuclei.

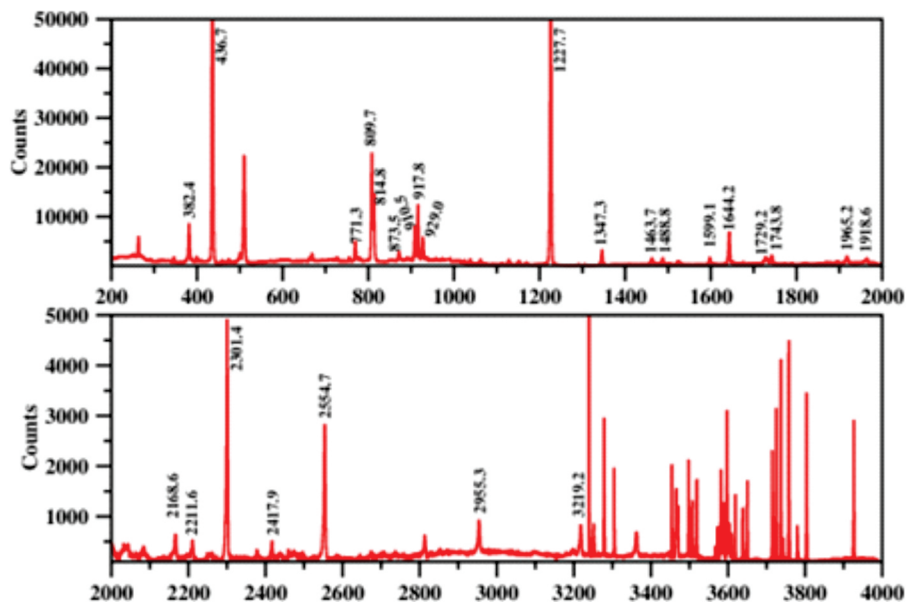


Fig. 5.1.11.2: A typical 1524 keV gated spectrum representing γ -ray transitions from ^{42}Ca nuclei.

To populate high spin states for the nuclei around $A \sim 40$ (*i.e.*, ^{38}Ar , ^{39}Ca , ^{41}K and ^{42}Ca), $\text{Si}(^{16}\text{O}, \alpha\text{pn})$ reaction was employed. The reaction was induced by a 50 MeV beam provided by the 15UD Pelletron at IUAC. The Si target of thickness $\sim 450 \mu\text{g}/\text{cm}^2$ backed with ^{197}Au of thickness $6\text{-}7 \text{ mg}/\text{cm}^2$ was fabricated at the Target Development Laboratory of IUAC. The γ - γ coincidence measurements have been done using a multidetector array of 11 Compton-suppressed Clover detectors (the INGA Setup) [5]. To detect light charged particles from fusion evaporation, Charge Particle Detector Array (CPDA) [6] was employed for the first time with the INGA setup. The acquired data were processed using the newly adopted ROOT-based data acquisition system called NiasMars. To generate two-dimensional E_γ - E_γ matrix, an in-house developed program was used. These matrices were further analyzed using the RADWARE package [7].

From the preliminary analysis, a typical spectrum of all vs all projection is shown in Fig. 5.1.11.1. Different colours represent γ -ray transition from different nuclei: green- ^{42}Ca , black- ^{38}Ar , red- ^{41}K , blue- ^{39}K and magenta- ^{37}Ar . The coinciding γ -ray transition with 1524 KeV (belonging to ^{42}Ca) [8] are shown in Fig. 5.1.11.2.

Further analysis to determine the intensity and DCO values is currently ongoing.

REFERENCES:

- [1] V. Renvoize *et al.*, *Astron. Astrophys.* **389**, 485 (2002).
- [2] J. Jose *et al.*, *Astrophys. J.* **494**, 680 (1998).
- [3] G. Lotay *et al.*, *Phys. Rev. Lett.* **116**, 132701 (2016).
- [4] C. D. O'Leary *et al.*, *Phys. Rev. Lett.* **79**, 4349 (1997).
- [5] S. Muralithar, K. Rani, R. Kumar, R.P. Singh *et al.*, *Nucl. Instrum. Methods* **622**, 281 (2010).
- [6] Akhil Jhingan *et al.*, *Proc. DAE Symp. Nucl. Phys.* **66**, 1100 (2022).
- [7] <https://radware.phy.ornl.gov/>
- [8] M. Lach *et al.*, *Eur. Phys. J. A* **16**, 309 (2003).

5.1.12 Study of intermediate and high spin states in ^{85}Rb nuclei

Anuj¹, P. S. Rawat¹, P. Sherpa¹, P. Khandelwal¹, S. Kumar¹, D. Sahoo², P. Chaudhary², S. S. Tiwary², Ajay Y. Deo², P. C. Srivastava², A. Sharma³, H. P. Sharma⁴, T. Trivedi⁵, K. Katre⁶, U. Ghosh⁶, H. Arora⁶, S. Dutt⁶, Yashraj⁶, Indu Bala⁶, R. Kumar⁶, R. P. Singh⁶ and S. Muralithar⁶

¹Department of Physics and Astrophysics, University of Delhi, Delhi 110007, India

²Indian Institute of Roorkee, Roorkee 247667, India

³Department of Physics, Himachal Pradesh University, Shimla 171005, India

⁴Department of Physics, Banaras Hindu University, Varanasi 221005, India

⁵Department of Physics, Guru Ghasidas Vishwavidyalaya, Bilaspur 495009, India

⁶Inter-University Accelerator Center, Aruna Asaf Ali Marg, New Delhi 110067, India

Experimental investigations have shown that, in nuclei with neutron numbers $N < 50$ and proton numbers $Z > 28$, occurrence of quasi-rotational bands is far away from the shell closure at $N, Z = 50$, while the effects of the shell model are dominant near or at the magic numbers [1-4]. Quasi-rotational bands represent a collective motion in nuclei with well-defined shapes where the nucleus rotates around an axis that is not necessarily aligned with its intrinsic symmetry axis. On the other hand, shell model effects are predominant in nuclei with magic numbers, which are specific values of neutron and proton numbers that make the nuclei stable with closed-shell configurations. The behavior of nuclei with $N < 50$ and $Z > 28$ is complex and can show a combination of quasi-rotational motion and shell model effects [5-7]. Studying the intermediate and high-spin states of the yrast band in the transitional Rb ($Z=37$) isotopes with mass number $A=85$ can provide important information about the interplay between particle-hole excitations, collectivity, and deformation properties associated with unpaired nucleons. In the mass $A = 85$ region, the alignment of a pair of $g_{9/2}$ protons and/or neutrons has been observed at high spin, which is associated with a change in the nuclear shape [8-9]. An experiment was performed to study the intermediate and high spin states of ^{85}Rb .

The $^{82}\text{Se}(^7\text{Li}, 4n)$ reaction was employed to populate the excited states of ^{85}Rb . The reaction was induced by a 33 MeV beam provided by the 15UD Pelletron at IUAC. The target used in the experiment consisted of $710 \mu\text{g}/\text{cm}^2$ ^{82}Se and was backed with $7 \text{mg}/\text{cm}^2$ ^{197}Au . The de-excited γ -rays were detected by means of the Indian National Gamma Array (INGA) [10], which consisted of 11 Compton-suppressed HPGe Clover detectors. The acquired data were processed using a newly adopted data acquisition system called NiasMars, followed by sorting with an in-house program to produce two-dimensional symmetric and asymmetric E_γ - E_γ matrices. These matrices were further analyzed using the RADWARE package [11]. In the initial analysis, a partial level scheme was constructed, as depicted in Fig. 5.1.12.1. A new γ -ray transition was observed with an energy of 726.7 keV, and was added to the level scheme.

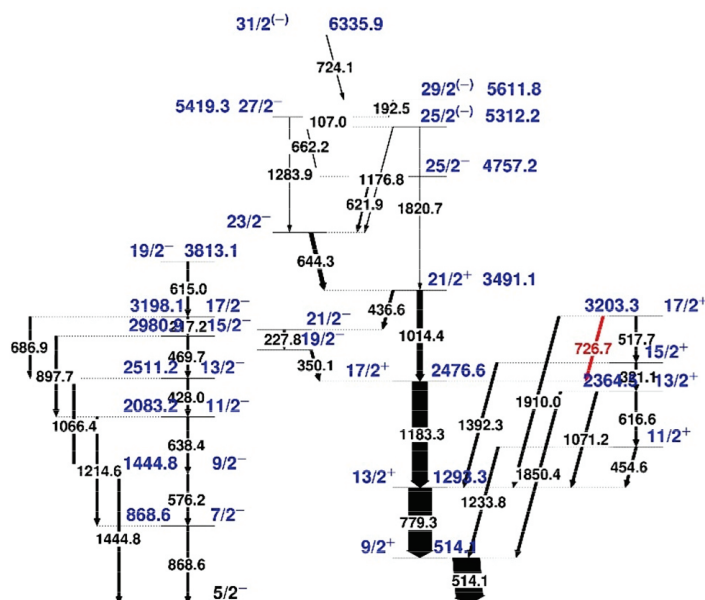


Fig. 5.1.12.1: The partial level scheme obtained in the present work. A newly found γ -ray transition is shown by red color. All the energies are in keV. Intensity values are not included for most of the transitions.

The coinciding γ -rays with the 779.3 keV transition are displayed in Fig. 5.1.12.2, while the dipole and quadrupole characteristics of the transitions in coincidence with the 779.3 keV transition are illustrated in Fig. 5.1.12.3. The analysis to determine the intensity and polarization asymmetry values are currently ongoing.

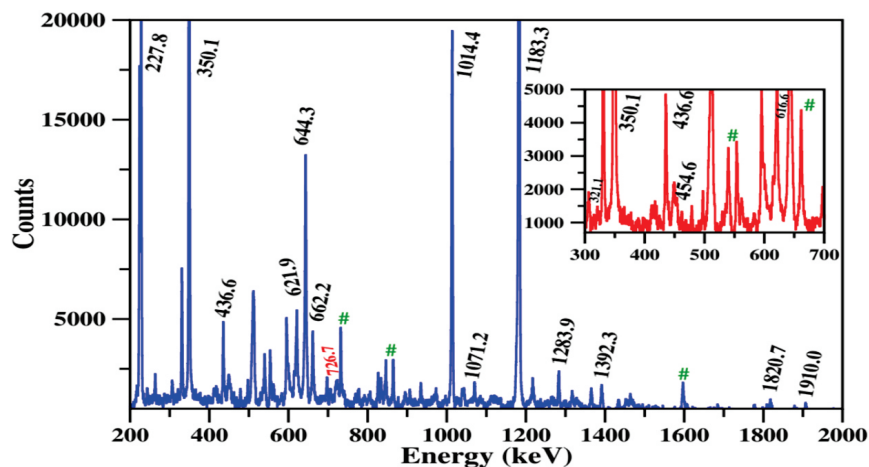


Fig. 5.1.12.2: The displayed spectrum depicts the γ -ray transitions that correspond to ^{85}Rb in coincidence with the 779.3 keV transition. Any transitions that are contaminants from neighboring residual nuclei populated during the reaction are denoted by the symbol #. The newly identified γ -ray transition is highlighted in red.

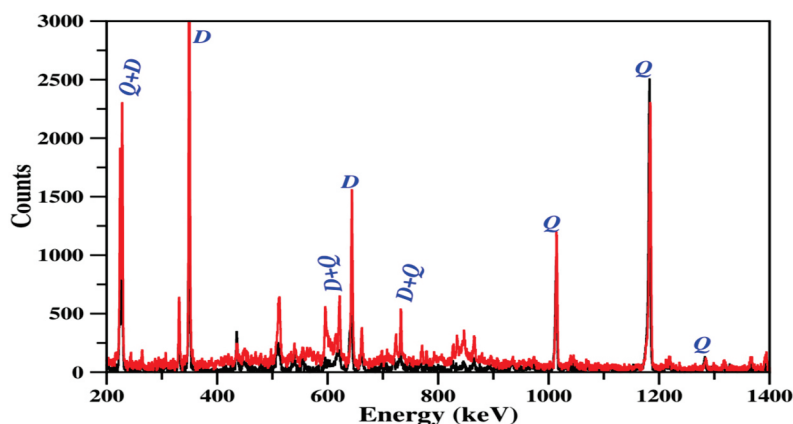


Fig. 5.1.12.3: The spectrum displays γ -ray transitions that were obtained through coincidence with the 779.3 keV stretched quadrupole transition. The spectrum was gated on the asymmetry matrix to obtain the DCO ratio values, which are presented using a red line for 90° and a black line for 148° .

REFERENCES:

- [1] K. O. Zell, H. G. Friederichs, B. Heits, H. W. Schuh and P. von Brentano, *Z. Phys. A* **276**, 371 (1976).
- [2] J. V. Mariscotti, G. G. Bermudez, J. C. Acquadro, A. Lepine *et al.*, *Nucl. Phys. A* **250**, 13 (1975).
- [3] H. G. Friederichs, A. Gelberg, B. Heits, K. O. Zell and P. von Brentano, *Phys. Rev. C* **13**, 2247 (1976).
- [4] R. Broda, A. Z. Hryniewicz, J. Styczen and W. Walus, *Nucl. Phys. A* **216**, 493 (1973).
- [5] R. C. Chopra, *Z. Phys.* **260**, 493 (1973).
- [6] C. Eckstroem, S. Ingelman, G. Wannberg and M. S. Karestad, *Nucl. Phys. A* **311**, 269 (1978).
- [7] L. C. Oelrich, K. Krien, R. L. DelVecchio and R. A. Naumann, *Phys. Rev. C* **14**, 563 (1976).
- [8] J. E. Kitching, P. A. Batay-Csorba, C. A. Fields, R. A. Ristinen and B. L. Smith, *Nucl. Phys. A* **302**, 159 (1978).
- [9] H. Guyer, V. Meyer, H. H. Mueller, W. Reichhart and P. Schobertz, *Rapp. Sess. Aut. Soc. Suisse Phys.* **51**, 97 (1978).
- [10] S. Muralithar, K. Rani, R. Kumar, R. P. Singh *et al.*, *Nucl. Instrum. Methods A* **622**, 281 (2010).
- [11] D. Radford, *Nucl. Instrum. Methods* **361**, 297 (1995).

5.1.13 Study of K-Isomers and high-spin states in A = 180 mass region

A. Sharma¹, S. Muralithar², S. K. Dhiman¹, P. S. Rawat³, S. Kumar³, Yashraj², Umakant Iamani⁴, Sunil Dutt², Uday Shankar Ghosh², Kaushik Katre², Ishtiaq Ahmad², Honey Arora², Subodh⁵, Siddharth⁶, Anuj³, H. P. Sharma⁷ and R. P. Singh²

¹Department of Physics, Himachal Pradesh University, Shimla, Himachal Pradesh 171005, India

²Nuclear Physics Group, Inter-University Accelerator Centre, New Delhi 110067, India

³Department of Physics and Astrophysics, University of Delhi, Delhi 110007, India

⁴Department of Physics, Indian Institute of Technology Bombay, Mumbai 400076, India

⁵Department of Physics, Punjab University, Chandigarh, Punjab 160014, India

¹School of Applied Sciences, Reva University, Bengaluru, Karnataka 560064, India

²Department of Physics, Banaras Hindu University, Varanasi, Uttar Pradesh 221005, India

To investigate level structure of the nucleus ^{185}Ir [1], an experiment is performed with the Indian National Gamma Array (INGA) at IUAC. The target material consists of $620\ \mu\text{g}/\text{cm}^2$ thick ^{179}Hf deposited on a backing of ^{197}Au having thickness $10\ \text{mg}/\text{cm}^2$. The target is irradiated by $65\ \text{MeV}$ ^{11}B beam, provided by the 15UD Pelletron at IUAC. The emitted γ -rays are detected by the INGA array consisting of 11 HPGe Clover detectors at 148° (4 detectors), 90° (4 detectors) and 32° (3 detectors). A Low Energy Photon Spectrometer (LEPS) is also placed in the array to detect the low energy γ -rays. The events are recorded in singles as well as in γ - γ coincidence mode. Fig. 5.1.13.1 shows the projection spectrum from γ - γ coincidence matrix (made with one-fourth of data). The γ -rays corresponding to different nuclei are indicated. It could be seen that the cross sections for $^{203,204}\text{Po}$ [2,3] and ^{204}Pb , produced in reaction with ^{197}Au , are much more enhanced, compared to ^{185}Ir produced in reaction with ^{179}Hf . This could be attributed to the difference in thickness of the target and backing materials. Fig. 5.1.13.2 and Fig. 5.1.13.3 show gated spectra for the most dominant reaction channels *i.e.*, ^{203}Po (gate on 612.9 keV) and ^{204}Po (gate on 684.1 keV) and nuclei of interest ^{185}Ir (sum gate of 152.7 and 413.1 keV). The previously identified γ -rays are indicated. Further analysis of data is under process.

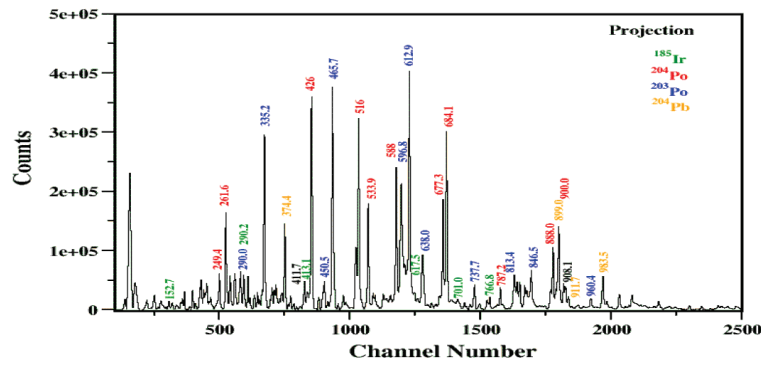


Fig. 5.1.13.1: Projection spectrum indicating the identified γ -rays from various nuclei produced in reactions $^{11}\text{B}+^{179}\text{Hf}$ and $^{11}\text{B}+^{197}\text{Au}$ at 65 MeV beam energy.

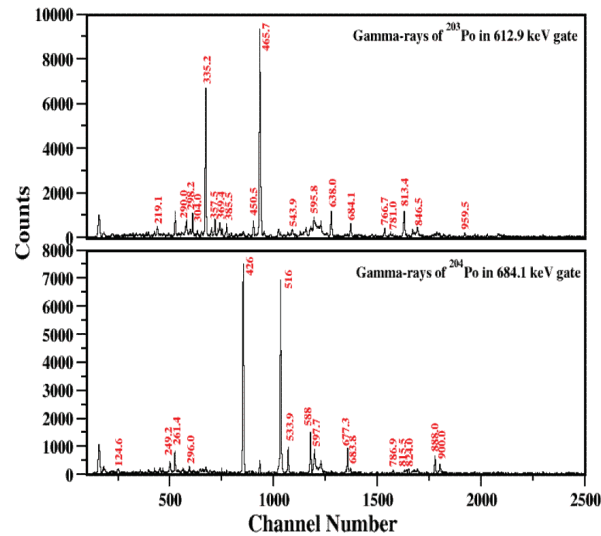


Fig. 5.1.13.2: Spectrum showing γ -rays for (a) ^{203}Po (gate on 612.9 keV transition) and (b) ^{204}Po (gate on 684.1 keV transition).

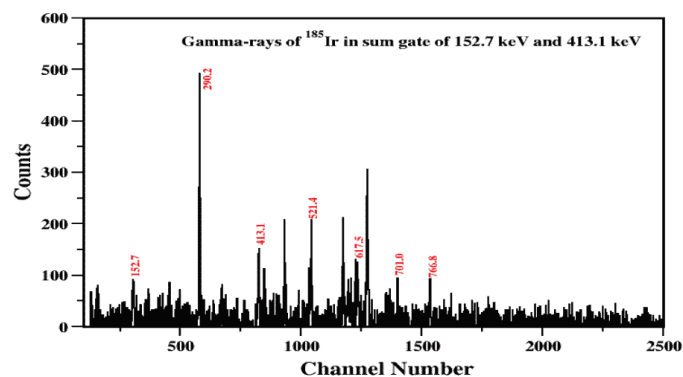


Fig. 5.1.13.3: The spectrum showing γ -rays for ^{185}Ir with sum gate of 152.7 keV and 413.1 keV transitions.

REFERENCES:

- [1] S. André *et al.*, Nucl. Phys. A **325**, 445 (1979).
 [2] B. Fant, T. Weckström, V. Rahkonen, C. J. Herrlander and A. Källberg, Nucl. Phys. A **453**, 77 (1986).
 [3] B. Fant, T. Weckström and A. Källberg, Phys. Scr **41**, 652 (1990).

5.1.14 g-factors and quadrupole moments of the isomeric states in ¹³⁹Pr

Anu Rathi¹, Ritu Rani¹, N. Bansal¹, R. Kumar², Yashraj², I. Ahmed², S. Kumar², U. S. Ghosh², Bharti Rohila¹, Diwanshu¹, P. S. Rawat³, Manpreet Kaur⁴ and A. K. Bhati¹

¹Department of Physics, Panjab University, Chandigarh 160014, India

²Nuclear Physics Group, Inter-University Accelerator Centre, New Delhi 110067, India

³Department of Physics and Astrophysics, University of Delhi, Delhi 110007, India

⁴Department of Physics, University Institute of Sciences, Chandigarh University, Punjab 140413, India

The transitional nuclei in the A~130 mass region with few valence nucleons near shell closure offer to study the rich variety of shapes and structures due to interplay of various multi quasi-particle excitations and the collective behavior of the underlying core. Many experimental studies based on γ -ray spectroscopy with heavy ion-induced reactions evidenced mainly high-spin level structures, an outstanding one being that due to the unique parity orbital $h_{11/2}$ for both protons and neutrons [1]. The different deformation driving forces of the valence protons and neutrons occupying low and high states of the $h_{11/2}$ intruder orbital leads to phenomenon of shape coexistence. The $I = \frac{19^-}{2}$ ($\tau_{1/2} = 9$ ns) and $I = \frac{25^-}{2}$ ($\tau_{1/2} = 12$ ns) isomeric states in ¹³⁹Pr have been considered for the g-factor and quadrupole moment measurements using the time differential perturbed angular distribution (TDPAD) technique at IUAC. The isomeric states were populated using the nuclear reaction ¹³⁰Te(¹⁴N, 5n γ)¹³⁹Pr at 80 MeV. The beam was pulsed with 250 ns pulse separation. Preliminary analysis of the data has shown the half-lives of the states comparable to that of the previous measurements. Further analysis of the data is in progress.

REFERENCES:

- [1] R. F. Casten and P. von Brentano, Phys. Lett. B **152**, 22 (1985).

5.1.15 Systematics of electric field gradients in rare-earth metals

Anu Rathi¹, Ritu Rani¹, N. Bansal¹, R. Kumar², Yashraj², I. Ahmed², S. Kumar², U. S. Ghosh², Bharti Rohila¹, Diwanshu¹, Gobind Ram³, A. K. Rana⁴ and A. K. Bhati¹

¹Department of Physics, Panjab University, Chandigarh 160014, India

²Nuclear Physics Group, Inter-University Accelerator Centre, New Delhi 110067, India

³Department of Physics, Jamia Milia Islamia, New Delhi 110025, India

⁴Department of Applied Physics, Banaras Hindu University, Varanasi 221005, India

The aim of the present measurements is twofold: (1) to understand the source of electric field gradient (*efg*) in rare earth metals; (2) to utilize the information for the nuclear electromagnetic moment measurements of rare earth nuclei. The spectroscopic quadrupole moment measurements in La nuclei, situated in the transitional region between N = 66 to N = 82, are of vital importance. They exhibit γ -softness, moderate deformation and shape co-existence related to the excitation of the specific pairs of proton or neutron. It is interesting to analyze the configuration-dependent quadrupole deformation in this mass region and compare the same with various theoretical predictions. The available theoretical values found in literature are not in good agreement with the corresponding measurements [1,2]. The time differential perturbed angular distribution (TDPAD) set up at IUAC has been used for investigation of the *efg* in La nuclei. The calibration of *efg* will help to determine the quadrupole moment of some of the isomeric states in La nuclei. The $I = \frac{11^-}{2}$ isomeric state in ¹³³La is excited through the nuclear reaction ¹²⁴Sn(¹⁴N, 5n γ)¹³³La using 75 MeV ¹⁴N pulsed beam with 250 ns pulse separation. Preliminary analysis of the data has shown that the half-life of the isomeric state is comparable to that of the previous measurements. Further analysis of the data is ongoing.

REFERENCES:

- [1] L. S. Kisslinger and R. A. Sorensen, Rev. Mod. Phys. **35**, 853 (1963)
 [2] N. Freed and W. Miles, Nuovo Cim. B **60**, 301 (1969).

5.1.16 g-factors and quadrupole moments of isomeric states in ^{175,176}Re

Ritu Rani¹, Anu Rathi¹, N. Bansal¹, R. Kumar², Yashraj², I. Ahmed², S. Kumar², Neha Dhanda¹, Gobind Ram³, U. S. Ghosh², D. Kumar⁴, F. S. Shana⁵ and A. K. Bhati¹

¹Department of Physics, Panjab University, Chandigarh 160014, India

²Inter-University Accelerator Centre, New Delhi 110067, India

³Department of Physics, Jamia Milia Islamia, New Delhi 110025, India

⁴Department of Physics, University of Lucknow, Lucknow 226007, India

⁵Department of Physics, Government Arts and Science College, Calicut 673018, India

There has been much interest in the mass region A~180 to understand the deformation associated with the intruder bands. In this region, proton and neutron Fermi surfaces are well separated and proton and neutron pairing correlations are largely decoupled. For the neutrons, the deformation of the $h_{9/2}$ were predicted to remain stable with increasing spin and to be unaffected by the alignment of $i_{13/2}$ neutrons. The predictions for the proton $i_{13/2}$ bands were much different [1]. It is interesting to measure the deformation associated with high- K isomers elucidating the dependence of pairing correlations and nuclear shapes on the multi-quasiparticle configurations, and the decay mechanisms governing their decay to lower-lying states. The time differential perturbed angular distribution (TDPAD) technique at IUAC has been used for the investigation of electromagnetic moments of the isomeric states in $^{175,176}\text{Re}$ nuclei. The isomeric states $I = 8^-$ and $I = \frac{19}{2}^-$ in ^{176}Re and ^{175}Re , respectively, were populated through the nuclear reaction $^{165}\text{Ho}(^{16}\text{O}, xn\gamma)^{175,176}\text{Re}$ at 95 and 104 MeV ^{16}O pulsed beam with 250 ns pulse separation. Preliminary analysis of the data has shown the half-lives of the states comparable to that of the previous measurements and more detailed analysis is in progress.

REFERENCES:

[1] R. A. Bark, R. Bengtsson and H. Carlsson, Phys. Lett. B **339**, 11 (1994).

5.1.17 g-factors of the $\frac{9}{2}^-$ and $\frac{5}{2}^-$ isomeric states in ^{169}Ta

Ritu Rani¹, Anu Rathi¹, N. Bansal¹, R. Kumar², Yashraj², I. Ahmed², S. Kumar², Neha Dhanda¹, Gobind Ram³, Jagbir Singh¹, Anjali Sharma¹ and A. K. Bhati¹

¹Department of Physics, Panjab University, Chandigarh 160014, India

²Inter-University Accelerator Centre, New Delhi 110067, India

³Department of Physics, Jamia Milia Islamia, New Delhi 110025, India

The ground states in odd-even $^{171,173}\text{Ta}$ nuclei are established as $\frac{5}{2}^-$, $\frac{1}{2}^-$ [541] Nilsson configuration. But in case of neighbouring nuclei $^{167,169}\text{Ta}$, there is ambiguity in the assignment of low-lying proton intrinsic states because of missing inter-band transitions [1,2]. The identification of the band heads and the rotational bands built on them is based on the in-band analysis and the systematics of the transitional energies in neighbouring nuclei. Zhang *et al.* [3] have observed two isomeric band heads $I = \frac{5}{2}^-$ ($E = (169.5 + x)$ keV, $T_{1/2} = 17(4)$ ns) and $I = \frac{9}{2}^-$ ($E = 220$ keV, $T_{1/2} = 28(5)$ ns) in ^{169}Ta , respectively. Transitions to the lower level are still uncertain. Both the rotational bands belong to the high- j proton configurations having different deformation-driving forces, confirmed by the quadrupole moment measurements by our group [4]. Guided by these facts, it was desired to measure the g-factors of the isomeric states using the time differential perturbed angular distribution (TDPAD) technique to confirm the configuration of the isomeric states. The isomeric states in ^{169}Ta were excited through the nuclear reaction $^{159}\text{Tb}(^{16}\text{O}, 6n)^{169}\text{Ta}$ using 104 MeV ^{16}O pulsed beam with 250 ns pulse separation. The excited Ta nuclei were recoiled implanted into lead in the presence of ~ 9 kG external magnetic field. Preliminary analysis of the data has shown that the half-lives of the isomeric states are comparable to that of the previous measurements. Further analysis of the data is ongoing.

REFERENCES:

[1] K. Theine *et al.*, Nucl. Phys. A **536**, 418 (1992).

[2] S. G. Li *et al.*, Nucl. Phys. A **555**, 435 (1993).

[3] Y. H. Zhang *et al.*, Eur. Phys. J. A **1**, 1 (1998).

[4] Vivek Kumar *et al.*, Eur. Phys. J. A. **26**, 311(2005).

5.2 MATERIALS SCIENCE

Ambuj Tripathi

The materials science facilities continue to support various research programmes of users from universities and institutions from all over India, besides providing critical support on priority to programmes of national significance from many organizations and research institutes. This year a total of 54 user experiments spread over 181 shifts took place with no beam time loss due to any major facility break down in the two beamline facilities for materials science experiments. Major efforts were undertaken this year to complete the projects of students in final years of their Ph.D.s and 39 such experiments spanning more than 130 shifts were conducted. Though the swift heavy ion (SHI) irradiation experiments mostly utilize irradiation facilities in materials science beamlines in beamhall-I there were three special runs (from URSC Bangalore, SAC Ahmedabad and BARC Mumbai) spread over 23 shifts performed in the GPSC for low fluence irradiation and a special proton run for IGCAR Kalpakkam in LIBR Proton beamline. High temperature irradiation experiments were done in materials science beamline in Beamhall 2 and two in-situ transport measurements on semiconductor devices took place in BH-I.

Besides irradiation facilities, materials science group is also providing support to users with many materials synthesis and characterization facilities. As the covid related restrictions were relaxed, the users have started visiting IUAC for various characterizations and this year more than seven hundred samples were characterized by users. The materials science research programmes utilize various irradiation facilities in Pelletron beamlines, LEIBF, NIBF, Table top accelerators in a wide range of energies varying from tens of keV to hundreds of MeV. There were more than 120 publications in reputed journals such as Physical Review B, Journal of Applied Physics, Applied Surface Science, Journal of Physical Chemistry C, Radiation Physics and Chemistry, Journal of Alloys and Compounds etc and a list of publications is given in section 6. This year there were many interesting results in the various areas of research including those on RRAM performance, Gas sensing, Radiation stability of devices, Implantation, Strain engineering, Phase transitions, Thermoelectricity, Photocatalytic degradation, Green synthesis, Nanostructuring, Nanocomposites and some of these are highlighted below.

Ion beams from Pelletron accelerator are widely used for user experiments in the two beamhalls. The radiation stability of MOSFETs, which are important for space applications due to their faster switching speeds were studied and the threshold bias of 100 MeV Sulphur ion irradiated MOSFETs, measured up to 30 Mrad of total dose, showed that gate bias during irradiation enhances the device degradation. Similarly, cryogenic temperature effects on NPN transistors irradiated with 80 MeV Nitrogen ion showed that the degradation in electrical parameters is more for the devices irradiated at low temperature than at room temperature. Tuning of charge carriers in Bi₂Te₃ thin films due to 100 MeV Ni ion irradiation was observed and the transition in conductivity suggested the controlling of charge carriers through irradiation. For radiation stability analysis, the RRAM devices have been studied and effects on SrTiO₃ thin films exposed to the Au⁹⁺ ions of 120 MeV energy for a different fluence showed a significant reduction in the switching ratio from 655 (pristine) to 10 (1×10^{13} ions/cm²) with stable data retention capability. Further, the surface morphological and RRAM properties were investigated and the performances of the fabricated devices before and after irradiation were compared and analysed for the various performance parameters of RRAM. Co-doping effect on the thermoluminescence properties of nanocrystalline SrSO₄:Dy,Er and nanophosphor's response to different gamma-radiation doses ranging from 10 Gy to 7 KGy and irradiation with carbon ion beams of two different energies i.e. 65 MeV and 85 MeV at 5 different fluences was studied. 120 MeV Ag⁹⁺ ion irradiation effects on the structural, optical and electrical properties of pristine and Ni doped BiFeO₃ thin films grown by pulsed laser deposition is studied and a decrease in the band gap has been observed with the increase of ion fluence. Tailoring of structural properties of CoYFeO/Polythiophene and ZnYFeO/Polythiophene nanocomposites with 160 MeV Nickel ion irradiation was studied and the annealing of surface defects at higher fluences was observed. The performance of commercial devices such as microcontrollers in high radiation conditions in nuclear plants were studied using proton ion beams. Reaction-Diffusion-Driven Stoichiometric Gradient in Co evaporated Superconducting NiBi₃ Thin Films was studied, and it was shown that the variation of Bi deposition rate in co-deposition technique results in the synthesis of thicker NiBi₃ film with a reduction in impurity Ni and Bi with enhancement in the superconducting transition temperature. A study on damage of Gd₂O₃-CeO₂ composites under electronic energy loss and nuclear energy loss regime was studied to compare bulk-like and nanostructured films using 80MeV Ag and 400 keV Ar ions. The impact of 150MeV Ni ion irradiation on the dielectric properties of K₂Bi₄Ti₄WO₁₈ and observed decrease in dielectric constant attributed to the introduction of defects by irradiation. Luminescence tuning in Cr doped BiFeO₃ thin-films by 100 MeV Au⁹⁺ irradiation showed a decrease in the band gap of the thin film allowing the photovoltaic effect to occur even at low energies. The influence of defect dynamics on the nano-hardness of NiCoCrFePd high entropy alloy under high dose Xe⁻³ irradiation and 120 MeV Au⁻⁷ irradiation of understating the dynamics of defects produced by the ion beams and their evolution with ion fluences was studied, which further will help in designing a radiation resistant alloy. Besides Pelletron accelerator, ion beams from low energy ion beam facilities: LEIBF and NIBF are also widely used. Improvements in electrical and optical properties of TiO₂ by inserting suitable dopants for resistive switching behavior of the anatase TiO₂ thin films was studied by implanting Cu in the fluence range 1×10^{15} - 2×10^{16} ions/cm². Radiation damage effects on nano-crystalline Zirconolite ceramic compositions using 2 MeV Kr⁺ ions for the ion fluence varying from 1×10^{14} to 2×10^{16} ions/cm²

(studied using XRD) showed that zirconolite was not amorphized even on irradiation up to a fluence order of 2×10^{16} ion/cm². In-silico studies are also being initiated and the DFT and DFT+U computational study has been done to understand the biaxial strain effect on electronic band structures, structural, and elastic properties of monolayer MoS₂. Significant changes in the bond distances, bond angles, electronic structures, and effective mass of electron m_e^* (hole m_h^*) are observed under biaxial strain.

As the Covid norms were relaxed, efforts in organizing workshops, schools and conferences on specialized topics in “In-person” mode were restarted this year after approximately two years of on-line activities. 7th International Conference on Ion Beams in Materials Engineering and characterization (7-IBMEC-2022: Nov 16-19, 2022), International School on Ion Beams in Material Science (IBMS-2022: Nov 10-14, 2022) Workshop on In-silico quantum modeling studies (ISQMS: Oct 30- Nov 3, 2022) were organized this year and details are given in section 6.

5.2.1 Tailoring structural properties of CoY_{0.04}Fe_{1.96}O₄/Polythiophene and ZnY_{0.04}Fe_{1.96}O₄/Polythiophene nanocomposites with 160 MeV Nickel ion irradiation

Joshi A.¹, Srivastava R.C.¹, and Meena R.C.²

¹Department of Physics, G.B. Pant University of Agri. & Technology, Pantnagar 263145, Uttarakhand, India

²Material Science Division, Inter University Accelerator Centre, New Delhi, 110067, India

In the present work, Y³⁺ ions doped cobalt ferrite (CP) and zinc ferrite (ZP) nanoparticles were synthesized via sol-gel autocombustion method. The nanocomposites of these nanoparticles with polythiophene (PTh) were synthesized via *in-situ* polymerization method. The samples were irradiated with 160 MeV Ni¹²⁺ ions at fluences of 5×10^{12} ions/cm² and 1×10^{13} ions/cm². The XRD patterns are shown in Figure 1 and Figure 2. ZP pristine, ZP5E12, ZP1E13, CP pristine, CP5E12 and CP1E13 represents unirradiated ZnY_{0.04}Fe₂O₄/polythiophene, ZnY_{0.04}Fe₂O₄/polythiophene irradiated with fluence of 5×10^{12} ions/cm², ZY4/PTh irradiated with fluence of 1×10^{13} ions/cm², unirradiated CY4/PTh, CY4/PTh irradiated with fluence of 5×10^{12} ions/cm², and CY4/PTh irradiated with fluence of 1×10^{13} ions/cm², respectively.

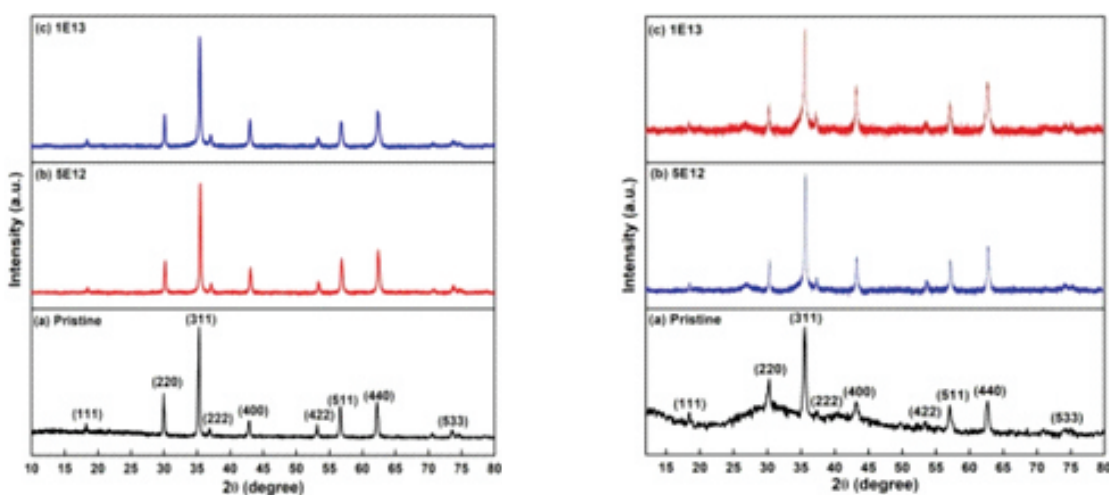


Figure 1: XRD pattern of (a) ZP Pristine, (b) ZP5E12, (c) ZP1E13 Figure 2: XRD pattern of (a) CP Pristine, (b) CP5E12, (c) CP1E13

XRD patterns of samples showed pure cubic phase with Fd3m space group of spinel ferrite present in pristine and irradiated samples. The lattice constants were found to be 8.381 Å, 8.395 Å for ZP5E12 and ZP1E13 samples, respectively. These values are less than 8.429 Å obtained for ZY4/PTh pristine (unirradiated) sample. Thus, irradiation led to shrinkage of unit cell. Singh et al. (2010), observed similar decrease in lattice constant on irradiation[2]. On further increasing fluence to 1×10^{13} ions/cm², crystallite size was decreased which can be attributed to the splitting of crystallites by ion irradiation [3]. Lattice constant and crystallite sizes are presented in Table 1. The XRD pattern of CY4/PTh showed both polycrystalline nature of ferrite and amorphous nature of PTh. On irradiation with 160 MeV Ni¹²⁺ ion beam, low intensity separate peak corresponding to PTh was seen in the XRD patterns. The peak was at $\sim 27^\circ$ in the irradiated samples. CY4/PTh showed similar variation of lattice constant and crystallite size as shown by ZY4/PTh on irradiation.

Table 1. Lattice constant 'a' and crystallite size (D) of pristine and irradiated samples.

Sample Code		a (Å)	D (nm)
ZY4/PTh	Pristine	8.429	28.42
	5E12	8.381	36.72
	1E13	8.395	32.86
CY4/PTh	Pristine	8.365	19.91
	5E12	8.345	31.33
	1E13	8.363	23.29

Raman spectra of the samples are shown in Figure 3. Characteristic Raman bands of PTh are present at ~ 696 , ~ 1043 , ~ 1213 , ~ 1453 which corresponds to C-S-C ring deformation, C-H bending, C-C stretching, and C=C stretching, respectively. Polythiophene in the oxidized state (positively charged polymer chain) shows intense peak at ~ 1420 cm^{-1} . However, in the reduced state (neutral chain) the peak at ~ 1420 cm^{-1} (quinoid) is absent and most intense peak is at ~ 1455 cm^{-1} [4]. Thus, from the obtained spectra it can be inferred that PTh is present in the reduced state in pristine and irradiated samples of ZY4/PTh and CY4/PTh nanocomposites. Cubic spinel ferrites have characteristic Raman bands at ~ 189 , 308, 470, 580, 621, 682 cm^{-1} due to symmetric, antisymmetric stretching and bending of oxygen atoms in Fe-O bond at tetrahedral and octahedral sites. In the pristine and irradiated samples of nanocomposites, low intensity bands corresponding to spinel ferrite were present. It was observed that irradiation led to broadening of most intense peak in the nanocomposites. This is attributed to the stronger local heating effect induced in the ordered ferrite/PTh nanocomposites [5]. In the irradiated nanocomposites an additional peak at ~ 645 cm^{-1} was present. Shemer et al, and Naik et al. also observed this peak in their study of ferrite nanoparticles. It was reported that this peak corresponds to Co^{2+} ions residing at defect sites located probably near the surface of nanoparticles. Thus, the nanocomposites when irradiated with Ni^{12+} ions at higher fluences, the surface defects were annealed and peak at ~ 645 cm^{-1} was observed. With incorporation of PTh in ferrite, slight shift in Raman bands were due to interaction between ferrite and PTh.

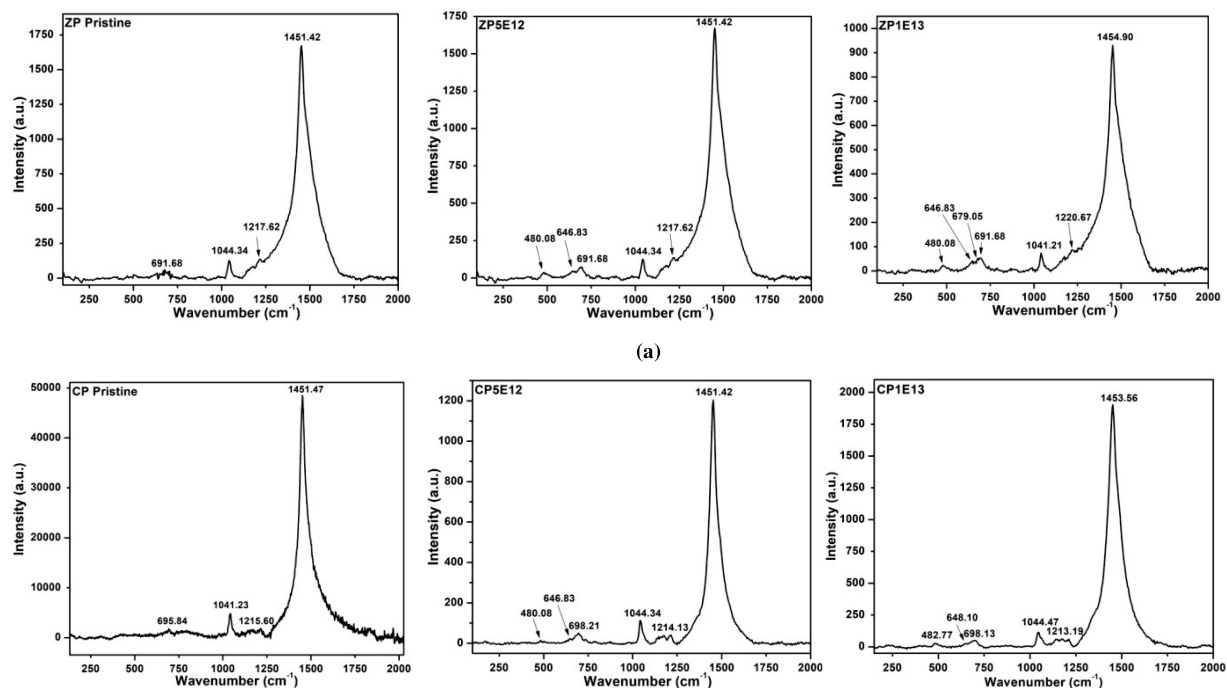


Figure 3: (a) Raman spectra of ZP Pristine, ZP5E12, ZP1E13. (b) Raman spectra of CP Pristine, CP5E12 and CP1E13

References:

- [1] J.P. Singh, R.C. Srivastava, H.M. Agrawal, and R. Kumar, Nucl. Instrum. Methods Phys. Res. B 268(9) (2010), 1422-1426.
- [2] S. Raghuvanshi, P. Tiwari, S.N. Kane, D.K. Avasthi, F. Mazaleyrat, T. Tatarchuk, and I. Mironyuk, J. Magn. Magn. Mater. 471(2018), 521-528
- [3] J.P. Singh, G. Dixit, R.C. Srivastava, H. Kumar, H.M. Agrawal, and R. Kumar, J. Magn. Magn. Mater. 324(20) (2012), 3306-3312
- [4] Q.T. Vu, M. Pavlik, N. Hebestreit, U. Rammelt, W. Plieth, and J. Pfeifer, React. Funct. Polym. 65(1-2) (2005), 69-77
- [5] M. Balaji, P.C. Lekha, and D.P. Padiyan, Vib. Spectrosc. 62(2012), 92-97.
- [6] G. Shemer, E. Tirosh, T. Livneh, and G. Markovich, J. Phys. Chem. C 111(39) (2007), 14334-14338
- [7] S.R. Naik and A.V. Salker, J. Mater. Chem. 22(6) (2012), 2740-2750.

5.2.2

Synthesis, Structural and Microstructural Studies of $\text{Al}_2\text{O}_3/8\text{YSZ}$ (8% Yttria Stabilized Zirconia) composite oxide ceramics

Asha Panghal¹, Indra Sulania³, Sanjay Kedia³, Birendra Singh³, F. Singh³, D. K. Avasthi⁴, Sejal Shah^{1,2*}

¹ITER-India, Institute for Plasma Research, Gandhinagar, Gujarat, India

²Homi Bhabha National Institute, Anushaktinagar, Mumbai, India

³Inter University Accelerator Centre (IUAC), Aruna Asaf Ali Marg, New Delhi, India

⁴Department of Physics, School of Engineering, University of Petroleum and Energy Studies, Dehradun - 248007, Uttarakhand, India

E-mail: sejal.shah@iterindia.in

1.

Introduction

Al_2O_3 , Aluminum oxide, is an important material for use as radiation-resistant shielding in nuclear

applications. Al_2O_3 has demonstrated excellent radiation resistance properties, making it an ideal choice for use in nuclear damage shielding. Al_2O_3 is a brittle material and can suffer from mechanical failure under certain conditions. This can limit its use in applications where high mechanical strength and toughness are required. 8% Ytria Stabilized Zirconia (8YSZ's) high toughness and fracture resistance make it an effective material for resisting radiation-induced damage, preventing micro-cracking, and structural failure. The combination of Al_2O_3 and 8YSZ can provide improved mechanical properties, such as higher toughness and fracture resistance, compared to either material used alone. This is because the two materials have complementary properties that can enhance each other's strengths. This research is dedicated to synthesizing a composite ceramic material and ensuring its improved mechanical strength, toughness, and fracture resistance post ion beam irradiation.

2. Synthesis

The composite ceramic sample of Al_2O_3 and 8YSZ is synthesized via solid state synthesis method in the form of pellets at the Inter-University accelerator centre. The prepared pellets are being characterized and we are waiting for the beam time schedule for performing the ion irradiation of prepared samples. We have also prepared composite samples in the form of a thin film via the Sputtering method at UPES, Dehradun.

3. Results and Discussion

Preliminary characterization like AFM, RBS, and Optical microscopy of the thin film has been performed at IUAC, New Delhi. We are expecting beam time to performed irradiation induced impact study for mentioned compositions in near future. The results obtained so far are in line with the available literature and are being more probed for nuclear application. The study is ongoing and is being compiled in the form of a peer-reviewed paper.

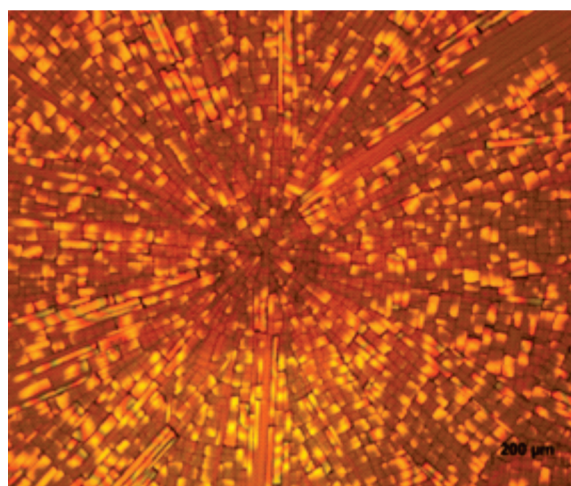
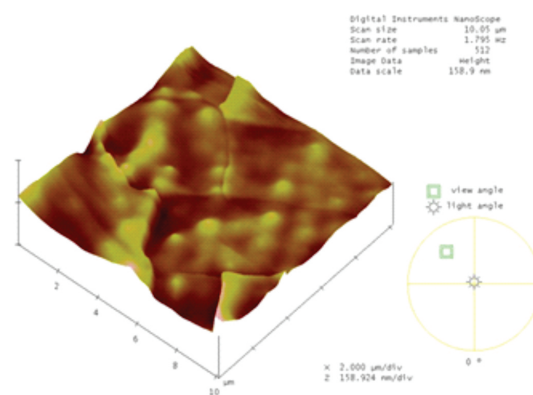


Fig1: Optical image and AFM spectroscopy of one of the thin film samples performed at IUAC.

References:

- [1] Sunil Kumar, Sejal Shah, I. Sulania, F. Singh, A. Chakraborty, Structural investigation of low energy ion irradiated Al_2O_3 , *Ceram. Int.* 45, 20346 (2019), <https://doi.org/10.1016/j.ceramint.2019.07008>.
- [2] Paramita Patra, Sejal Shah, M. Toulemonde, I. Sulania, F Singh, Investigation of radiation damage using thermal spike model for SHI irradiation on Al_2O_3 , *Rad. Eff. Def. Sol.* 177 (5-6), 513-530 (2022), <https://doi.org/10.1080/10420150.2022.2048658>.

5.2.3 Impact of SHI irradiation on the dielectric properties of $\text{K}_2\text{Bi}_2\text{Ti}_4\text{WO}_{18}$

Vipul K. Sharma¹, Ashish K. Kumawat¹, Satyapal S. Rathore², Indra Sulania³, R. C. Meena³, S. K. Kedia³, Rashi Nathawat^{1*}

¹ *Functional Ceramics and Smart Materials Lab, Department of Physics, Manipal University Jaipur, Jaipur, India.*

² *Department of Physics, Cluster University of Jammu, Jammu, India.*

³ *Inter-University Accelerator Centre, New Delhi, India.*

In this work, a new compound from the Aurivillius family $K_2Bi_4Ti_4WO_{18}$ (KBTW) was synthesized, and the impact of swift heavy ion (SHI), Ni^{+11} irradiation on its surface, and dielectric properties has been studied in detail. The phase formation of this complex oxide and the crystallization to the $B2cb$ symmetry have been confirmed by X-ray diffraction. However, post-irradiation the XRD, SEM, and AFM studies show the surface amorphization, in agreement with the theoretical calculations. In addition, the effects of radiation were observed in the bulk-dielectric properties of the system in the phase of a negative-dielectric constant over 350 K in radio frequencies. This transition is in correlation with significant changes in other dielectric parameters such as enhancement in AC conductivity, a helical Nyquist plot, and multiple dielectric relaxations. These conspicuous changes in the dielectric response post-irradiation are attributed to the SHI-induced defect formation, modification of energy barriers, and their consequences on the electronic structure. For the synthesis of polycrystalline $K_2Bi_4Ti_4WO_{18}$ (KBTW), a solid-state reaction technique was used. The sintered pellets were uniformly exposed to Ni^{+11} of 150 MeV energy at a fluence of 5×10^{12} ions/cm². The SHI irradiation was performed at UD Pelletron Accelerator at the Inter-University Accelerator Centre (IUAC), New Delhi. The room temperature XRD measurement of pristine (unirradiated) and irradiated samples was performed using a BRUKER D-8 X-ray diffractometer with Cu – $K\alpha$ radiation of 1.54 Å. The SEM imaging was performed with a JEOL JSM-7610F Plus FESEM. The AFM was performed using Veeco Instruments Inc. made a Multi-Mode SPM system with a Nanoscope IIIa controller. The temperature (100 K–420 K) dependent dielectric measurement was performed using an Agilent LCR meter in a frequency range of 10 Hz–2 MHz. (Model No. E4980A) with Lakeshore temperature controller (Model No. 340). The initial calculation of expected radiation damage was performed using Stopping and Range of Ions in Matter (SRIM) software. The temperature (100K–420K) and frequency (10 Hz–2MHz) dependence of the real part of the dielectric constant (ϵ') for KBTW ceramics before and after irradiation has been studied in detail. The pristine KBTW follows a non-linear modified Debye equation. The dielectric behavior for the irradiated sample can be divided into two parts below and above 350 K. Below the transition temperature, the dielectric constant was observed to show an appreciable decrease in the dielectric constant. This decrease in dielectric constant is attributed to the introduction of defects by irradiation which provides additional inertia to dipole relaxations. In conclusion, ceramic is modified post-irradiation due to the energy of ions both via electronic and nuclear energy losses. These interactions along with the impingement of ions create defects, and charge separation with modified energy barrier configuration. These dipoles, when subjected to an external field result in an unconventional macroscopic dielectric response.

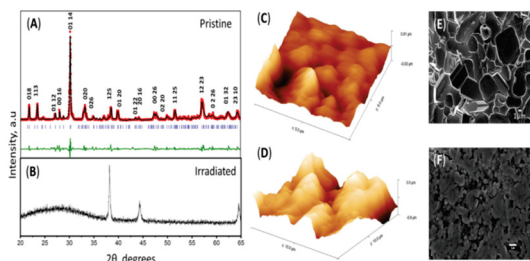


Figure 1

Figure:1 (A) The x-ray diffractogram of polycrystalline $K_2Bi_4Ti_4WO_{18}$. The bottom pattern (B) shows the amorphization post irradiation. The AFM images also depict an expected increase in the surface roughness after irradiation (D), when compared before irradiation (C) (E) The electron micrograph shows a grain distribution typical of bismuth layered structure. (F) The irradiation leads to surface amorphization with no clear crystallites.

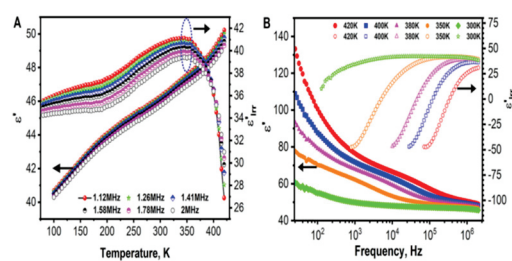


Figure 2

Figure:2 (A)The temperature dependent dielectric response for pristine (left y-axis) and irradiated (right y-axis) $K_2Bi_4Ti_4WO_{18}$. (B) The frequency dispersion of the real part of dielectric constant at various temperatures, shows a transformation to negative values above 350 K.

References:

- [1] Vipul K. Sharma, Ashish K. Kumawat, Satyapal S. Rathore, Indra Sulania, R. C. Meena, S. K. Kedia, Rashi Nathawat*, "The SHI irradiation induced transition to negative dielectric constant phase in $K_2Bi_4Ti_4WO_{18}$," *Frontier in Physics*, vol. 11, no. February, pp. 18, 2023, doi: 10.3389/fphy.2023.1127118.

5.2.4

Effect of Swift heavy ion (SHI) irradiation on Structural and Optical properties of Organic-Inorganic composites

Ashish K. Kumawat¹, Vipul K. Sharma¹, Satyapal S. Rathore², Indra Sulania³, S. K. Kedia³, Rashi Nathawat^{1*}

¹Functional Ceramics and Smart Materials Lab, Department of Physics, Manipal University Jaipur, Jaipur 303007, India

²Inter-University Accelerator Centre, New Delhi-110067, India

³Department of Physics, Cluster University of Jammu, Jammu & Kashmir, 180001, India

The Swift heavy ion (SHI) beam irradiation provides possibilities to tailor the functional properties of materials for various applications. In present work, $(\text{PANI})_x-(\text{V}_2\text{O}_5)_{1-x}$ ($x=0.025, 0.05, 0.1, 0.15$) (Polyaniline-vanadium pentoxide) $[\text{P}_x(\text{VO})_{1-x}]$ composites were synthesized by hydrothermal technique. The effect of 150 MeV Ni^{+11} (fluence $\sim 2.5 \times 10^{11}$ ions/cm²) ion irradiation on the structural and optical properties were studied in detail. The XRD study revealed that pure V_2O_5 is in crystalline phase [1], whereas pure PANI and composite samples have amorphous nature. After irradiation shifting and peak broadening are observed due to expansion and disordering of the lattice. The crystallinity decreased up to 51–69% after the irradiations. The SHI induced surface modification is also evident in the electron micrograph. A significant change in microstructure due to inelastic collision with high energy ions observed in FESEM. The grain size is reduced post irradiation. The appearance of V=O and aromatic C–H in-plane bending vibrations are characteristics of the PANI in FTIR spectra. The peak shifting to lower wavenumber in V–O–V asymmetric stretching vibration found in irradiated samples is attributed to increased molecular mass [2],[3]. After the irradiation, V–O–V symmetric stretching fixed and V–O–V bending of V_2O_5 shows a remarkable signature, the peak shift to a higher wavenumber with a maximum difference value of 21 cm⁻¹. The value of $[\text{P}_x(\text{VO})_{1-x}]$ composites for V–O–V peak are 18, 6, -1, -2 cm⁻¹ of $\text{P}_{2.5}\text{V}$, P_5V , P_{10}V and P_{15}V respectively. The UV-vis spectroscopy shows an increment in absorption and a change in band gap due to insertion of metal ions into composite matrix. Ni^{+11} irradiation, a consistent red shift was observed in the band gap for pure as well as the composites, indicating modification of underlying band structure. The optical bandgap decreased up to 1.21 eV after SHI irradiation for highly doped composite. This result exhibit that the molecules of PANI were more damaged by the bombardment of Ni-ions concerning V_2O_5 .

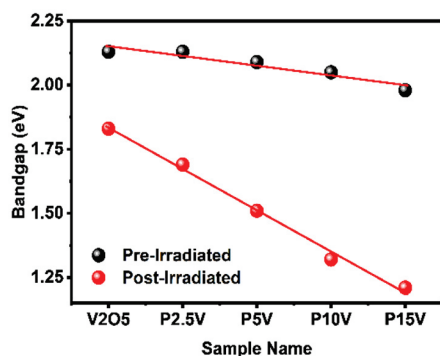


Figure 1

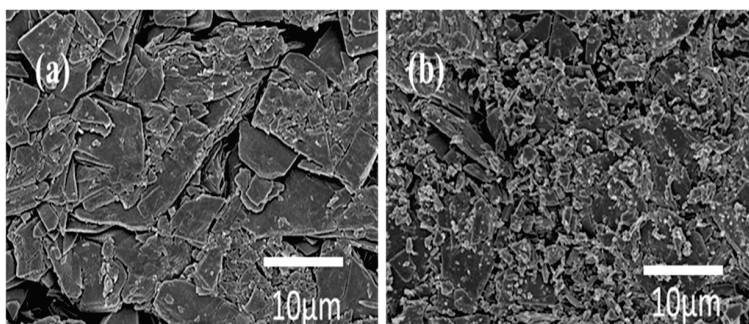


Figure 2

Figure 1: The bandgap of pristine and Ni-irradiated V_2O_5 , $\text{P}_{2.5}\text{V}$, P_5V , P_{10}V , & P_{15}V composites.

Figure 2: FESEM images of (a) pristine and (b) Ni-irradiated V_2O_5

References:

- [1] N. K. Subramani, S. Kasargod Nagaraj, S. Shivanna, and H. Siddaramaiah, "Highly Flexible and Visibly Transparent Poly(vinyl alcohol)/Calcium Zincate Nanocomposite Films for UVA Shielding Applications As Assessed by Novel Ultraviolet Photon Induced Fluorescence Quenching," *Macromolecules*, vol. 49, no. 7, pp. 2791–2801, 2016, doi: 10.1021/acs.macromol.5b02282.
- [2] M. Farahmandjou, "Chemical Synthesis of Vanadium Oxide (V_2O_5) Nanoparticles Prepared by Sodium Metavanadate," *J Nanomed Res*, vol. 5, no. 1, pp. 2–5, 2017, doi: 10.15406/jnmr.2017.05.00103.
- [3] Z. Li, X. Wang, X. Li, and J. Zhang, "Exploration on the microwave-assisted synthesis and formation mechanism of polyaniline nanostructures synthesized in different hydrochloric acid concentrations Exploration on the Microwave-Assisted Synthesis and Formation Mechanism of Polyaniline Nanostru," no. July 2017, doi: 10.1002/pola.28707.

5.2.5

Gas-Sensing Measurement for Sensing NO/NO_2 gas using Prototype Setup at IUAC

Indra Sulania¹, GBVS Lakshmi², Avinash Kumar Singh², Vijay Jangra³ and V V Sivakumar¹

¹Inter University Accelerator Centre, Aruna Asaf Ali Marg, New Delhi 110067, India

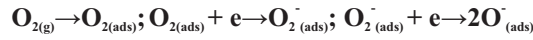
²Special Center for Nanoscience, Jawaharlal Nehru University, New Delhi.

³Department of Physics, Chaudhary Bansi Lal University, Bhiwani Haryana-127021

Introduction

Oxides of Nitrogen (NO_x) is one of the most dangerous air pollutants due to its toxicity for people, animals, and plants, as well as its role in generating acid rain and photochemical smog. Therefore, it is very important to sense it with high sensitivity and selectivity. The sensing process is closely related to chemisorption of O_2

and NO_x on the porous surface of sample electrode. Here we have used, Zn doped NiCo₂O₄ as porous surface to detect NO_x. When the sample is exposed to air, the chemisorbed oxygen molecules are adsorbed on the surface of the sample and grains which leads to the creations of active surface sites which captures electrons from conduction band, or donor level, which leads to the formation of chemisorbed oxygen ions (O²⁻) at <100 C, O⁻ at 100°C-300°C, and O²⁻ at > 300°C) and create holes on valence band as shown in Fig. 1 [1]. Our experiments were performed at 200°C, so the chemisorbed oxygen exists in the form of O⁻ ions which act as the active sites for NOx sensing. This is represented in the following equations:



The NOx gas sensing mechanisms of Zn doped NiCo₂O₄ follows:

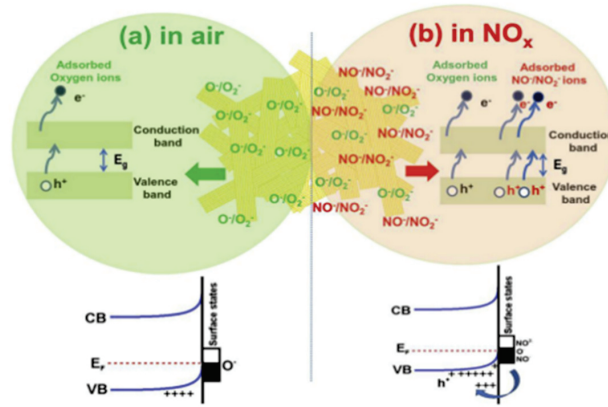
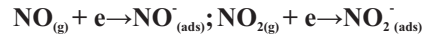


Figure 1: Interaction of sample in air and in NO_x environment

Experimental Details

The Gas sensing measurements were performed using an alloy of Zn doped NiCo₂O₄ thick film. The powdered sample was prepared by Solvothermal method [2]. The XRD spectrum of the sample is shown in figure 2, corresponds to the formation of NiCo₂O₄. The Zn doped composition is represented by the symbol MPR8.

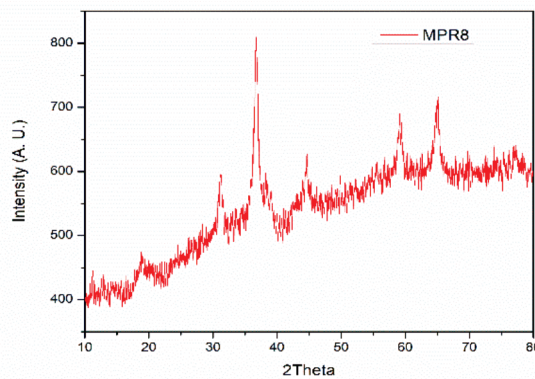


Figure 2: XRD spectra of powdered sample of Zn doped NiCo₂O₄

Thick layer was deposited on corning glass by drop casting. The resistance of the film was found to be in M range. The set-up was tested for NO_x gas. As the gas was inserted inside the glass chamber, the resistance was found to decrease immediately. The gas was pumped out of the chamber with the help of an air pump and the resistance was increasing again. This cycle was repeated for 6 to 7 times. This indicates that the alloy of Zn doped NiCo₂O₄ is sensitive and selective to NO_x gas [3].

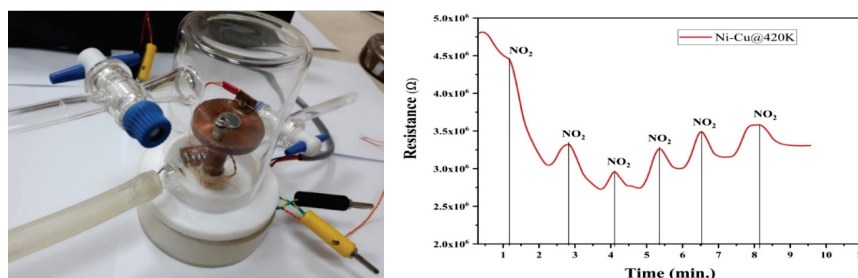


Figure 3. (a) Prototype setup at IUAC. (b) NO_x gas sensing plot using Zn doped NiCo₂O₄ composite carried out at 420 K temperature.

Results and Discussion

The operating temperature highly influences the gas sensing behaviors of metal oxides. Hence, we initially carried out measurements at RT and slowly increased the temperature to reach 200°C. Fig. 3(b) shows the typical response behavior of the sample at ~420 K towards 50 ppm of NO_x (oxidizing gas).

Conclusion: This setup has successfully demonstrated gas sensing but it requires the following modifications to get the setup competitive enough to detect the gases with sensitivity and selectivity.

Modifications: 1) The vacuum inside the chamber is not proper due to the leakages. Therefore, a stainless-steel chamber to be designed and implemented. 2) The proper mixing chamber to be used to study the selectivity. 3) Mass-flow controller is needed to know the precise concentrations of the gas entered inside the chamber so that the present qualitative analysis can be improved to quantitative analysis. 4) Setup require dedicated electronic modules such as temperature controller, Source meter etc. with proper data acquisition system.

Reference:

- [1] Vijay Kumar et al. Characterization of mesoporous Zn doped NiCo₂O₄ rods produced by hydrothermal method for NO_x gas sensing application; *Journal of Alloys and Compounds* 773 (2019) 158-167.
- [2] Vijay Kumar et al. Hybrid aqueous supercapacitors based on mesoporous spinel-analogous Zn-Ni-Co-O nanorods: Effect of Ni content on the structure and energy storage; *Journal of Alloys and Compounds* 882 (2021) 160712-160720.
- [3] N Afzalet al., NO_x sensors based on semiconducting metal oxide nanostructures: progress and perspectives, *Sens. Actuators B Chem.* 171 (2012) 25-42.

5.2.6

Luminescence tuning in Cr doped BiFeO₃ thin-films by Au¹⁹⁺ (100 MeV) irradiation

Harish Kumar Meena¹, Khushbu Meena¹, Fouran Singh², Vishnu Chauhan², Sushil Kumar Jain³, Balram Tripathi^{4*}

¹*Department of Physics, University of Rajasthan, Jaipur-302004, India*

²*Inter-University Accelerator Centre, New Delhi-110067, India*

³*Department of Physics, Manipal University Jaipur, Jaipur-303007, India*

⁴*Department of Physics, S S Jain PG(Auto.) College, Jaipur-302004, India*

*E-mail: balramtripathi1181@gmail.com

To find the effects of swift heavy ion (SHI) irradiation on the structural and optical properties of bismuth ferrite and Cr-doped bismuth ferrite thin films, the thin films deposited as pristine and with Cr doping in wt% of 10%, 20%, and 30% using spin coating system. The films were deposited at 5000 RPM for 35 seconds of thickness 200 Å to 300 Å. The spin coating was repeated for 5 times to obtain films of adequate thickness of 300 Å and annealed at 500°C for 1hr. These films were irradiated by 100 MeV Au¹⁹⁺ ions at the fluence 10¹³ ions cm⁻² with current 0.5 pA (particle nanoampere) using UD Pelletron accelerator at Inter-University Accelerator Centre (IUAC), New Delhi. The films were fixed at the ladder inside the vacuum chamber at the high vacuum (~10⁻⁶) during irradiation. The ion beam was focused to a spot of 10 mm diameter and scanned over an area of 1×1 cm² using a magnetic scanner to cover the complete sample surface for uniform irradiation. The SHIs move through the material, their bombardment can create disorder in the form of point defects, cluster defects, or a perturbed atomic distribution. [1].

Cr-doped bismuth ferrite (BCFO) thin films are deposited on glass substrates using spin coater in order to customise the multiferroic and optical properties. Bismuth ferrite materials are more suitable to prepare ferroelectric photovoltaic devices and to increase power conversion efficiency (PCE). The influence of Cr-doped bismuth ferrite thin films on optical, bonding, and surface properties have been investigated via various characterization techniques like, UV-VIS, Photo luminescence, FT-IR, and SEM. The X-ray diffraction spectra of Cr-doped bismuth ferrite thin films reveals the rhombohedral perovskite structure with crystalline size distribution of 6 nm to 10 nm. The bonding of Cr in BFO thin films was confirmed by Fourier Transform Infrared (FT-IR) Spectra. The homogenous surface morphology and distribution of Cr in the BFO thin films are confirmed by scanning electron microscopy (SEM) images. According to observations from optical absorption spectra, the optical luminescence was found to be enhanced with the band gap tuned in between 2.75 eV and 2.59 eV via (Au¹⁹⁺) SHI irradiation.

The type of irradiation ions, synthesis parameters, stoichiometry, and material type all play an important role in the material's modification. The incident ion's mass, irradiation energy, and fluence have a significant impact on the radiation-induced changes. [2]. After the irradiation, to study of the structural properties we characterized XRD measurement of the thin films at IUAC, New Delhi and to investigate the optical properties we carried out the UV-visible and PL measurements of thin films. We found that the band gap of the BCFO thin film decreases, allowing the photovoltaic effect to occur even at low energies.

References: -

- [1] N. Tripathi, S. Rath, Thin Films ECS. J. Solid State Sci. Technol. 2014, 3(3) P21.
 [2] P. Prabukanthan, K. Asokan, D. Kanjilal, R. Dhanasekaran, J. Semiconductor Science and Technology. 23 (2008) 125042.

5.2.7 Proton irradiation of 8051 microcontroller at IUAC

Charu Sharma¹, R.P.Behera², B.K. Panigrahi³, Ambuj Tripathi⁴

¹Indira Gandhi Centre for Atomic Research, A CI of Homi Bhabha National Institute, Kalpakkam, 603 102, Tamilnadu, India

²Real Time Systems Division, Indira Gandhi Centre for Atomic Research, Kalpakkam, 603 102, India

³RRF, Department of Atomic Energy, Mumbai

⁴Inter University Accelerator Centre

To study the performance of commercial off-the-shelf (COTS) device of the instrument and control system of a nuclear power plant under severe accident conditions is critical to the successful and reliable operation of the plant. In the accidental scenario, the adverse environment of ionizing radiation affects the performance of the I&C system and it leads to inaccurate and incomprehensible results. It is important to understand the single event effects (SEE) induced by protons and other high energetic particles for successful operations. In order to understand the SEE induced by proton, 8051 microcontrollers were irradiated with 25 MeV protons in the general purpose scattering chamber (GPSC) of 15 UD Pelletron accelerator in online condition at the Inter University Accelerator Centre (IUAC) in New Delhi, India.

The total energy deposited by the decelerating proton is given by its stopping power and the energy transferred per unit mass of material is referred as dose and it is given by the formula:

$$\text{Dose (rad)} = 1.6 \times 10^{-5} \times \text{Fluence (cm}^{-2}\text{)} \times S \text{ (MeV- cm}^2\text{/mg)}$$

where, S is the stopping power. The SRIM Monte Carlo simulation code is used to compute S and another common radiation damage exposure unit known as atomic displacements per atom (dpa).

In this work, three micro controller chips were irradiated with 25 MeV proton in 15 UD Pelletron accelerator (shown in fig.1) at the Inter University Accelerator Centre (IUAC) in New Delhi, India. The experiment was conducted in online conditions. The experiments were performed at room temperature with the ion fluence with the dose rate of 6×10^9 /sec. The chips with their associated circuit boards were mounted on the ladder of the accelerator as and all the connections of the cables come out through the feed through (fig.2) of the accelerator. The chips were written using a specific program to provide an output that flash the associated LEDs, as well as sending the output data to the PC *via* a serial communication port. The power supply and the PC were placed in the control room and connected to the board *via* connecting wires through the patch panel. Fig.3 shows the beam was focused using the quartz, placed on the ladder. After the beam was focused and the flux was tuned, the power was turned on. The output of the program loaded into the micro controller was recorded on the PC *via* RS232 communication until the output data display was stopped. The board was then removed from the accelerator for functional evaluation and the error in the memory array was recorded.



Fig. 1- Proton ion beam chamber



Fig. 2- Cable connections to feedthrough



Fig. 3- Focussing beam on quartz

Based on the analysis of the data, it was observed that proton irradiation affects the functionality of chips, as they were failed to perform the given task. The chips were irradiated with a maximum fluence of 8.06×10^{11} ions/cm² and single event upset was observed. It was also observed that the micro controllers regained their functionality after reprogramming.

5.2.8 Enhanced non-linear optical properties of Au nanoparticle in C₆₀ by Thermal and Athermal annealing.

Darpan Khandelwal¹, Amena Salim¹, Jyotsna Bhardwaj¹, Fouran Singh², Rahul Singhal¹

¹Department of Physics, Malaviya National Institute of Technology Jaipur, JLN Marg, Malviya Nagar, Jaipur 302017, India

²Inter University Accelerator Centre, Vasant Kunj, New Delhi, Delhi 110067, India

Nanocomposite thin films constituting noble metal-matrix have been synthesized for analyzing their enhanced non-linear optical properties by the impact of treatment with heavy energy ion source followed with subsequent thermal annealing. Au-C₆₀ nanocomposite thin coatings have been synthesized by means of thermal co-evaporation resistive heating approach under a very high vacuum on carbon coated Cu grid, quartz, and silicon in which nanoparticles of noble metal Gold are rooted in fullerene. RBS is executed for computing accurate concentration (~4.2%) of Au NPs and thickness (~45 nm) of film. The as-synthesized gold-fullerene (C₆₀) nanocomposite samples were bombarded with a 90 MeV Ti ion source at several fluences varying from 1×10^{12} ions/cm² to 5×10^{13} ions/cm². The sample irradiated at the highest fluence was annealed at various temperatures i.e., 200°C, 400°C, and 500°C for span of 30 minutes in a high-temperature furnace in the Ar atmosphere. On 500°C, a clear indication of SPR at 530 nanometres was observed, which confirms the increase in the size of nanogold particles of substantial size. The same result is later supported by TEM analysis. Surface features of Au-C₆₀ thin film are studied by AFM along with SEM. Entire make over of fullerene into non-crystallized carbon can be figured out by Raman measurements, where there is existence of characteristic D and G bands of non-graphitized at the highest fluence. XPS has been exercised to figure out the chemical states present in the samples.

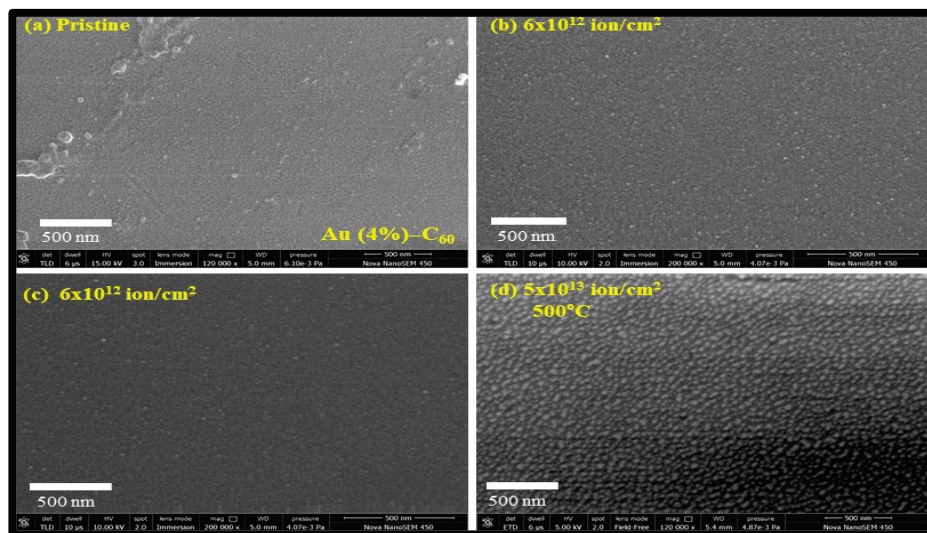


Fig.1 2-D SEM images of Au-C₆₀ nanocomposite at pristine and different fluences with a dose of 90 MeV Ti beam.

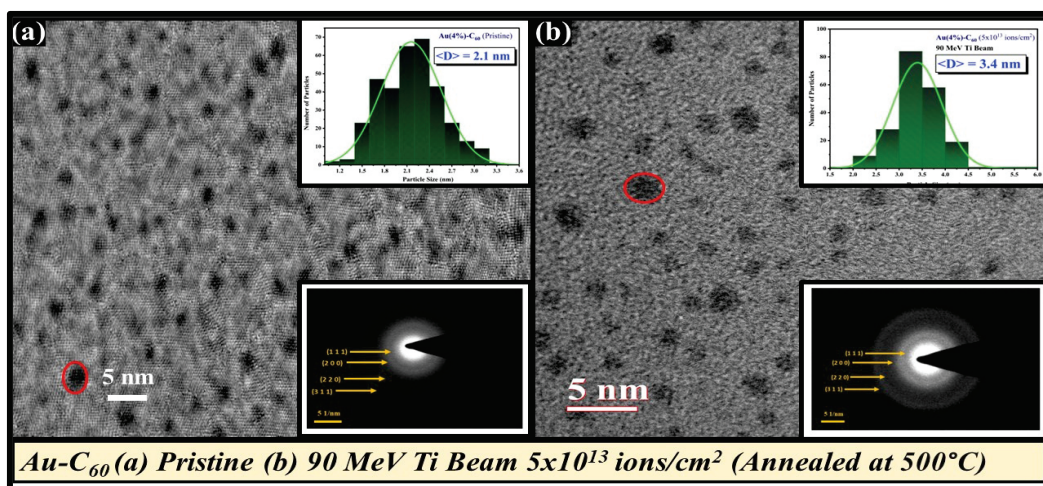


Fig.2 2-D TEM Images Au-C₆₀ NC Thin films. The upper and lower inset shows the size variation of NPs and the selected area electron diffraction pattern, respectively.

5.2.9 Study of structural and electronic properties of mono-layer and few-layer MoS₂

Mayur Khan¹, Sunil Kumar¹, Ambuj Mishra¹, Indra Sulania¹, Madhvendra Nath Tripathi², Ambuj Tripathi¹

¹Materials Science Group, Inter-University Accelerator Centre, New Delhi 110067, India.

²Department of Pure & Applied Physics, Guru Ghasidas Vishwavidyalaya (Central University), Koni, Bilashpur 495009, India

Due to their appealing electrical, optical, and catalytic properties of 2D-transition metal dichalcogenide (TMD) materials such as MoS₂, the creation of a MoS₂-based sensor, among its various uses, demands the large-scale production of a thin film of MoS₂ layer. In this work, the synthesis of the few-layers of MoS₂ was done on a SiO₂/Si substrate, and there are between 9 and 11 layers of MoS₂, according to AFM and Raman spectroscopy. We utilised XRD and Raman spectroscopy for macroscopically structural observation, AFM and TEM for microscopically structural observation. However, the practical electronic band gap and band structure properties were explored using UV-Vis and Photoluminescence spectroscopy, as well as their comparison with theoretically calculated band structures and density of state using Density Functional Theory. Refer Khan M. et al., Materials Today: Proceedings, 2022 Feb. for more details [1]. Moreover, XRD reveals the hexagonal structure of a few layers of MoS₂, with the observed (002) plane, 6.14 Å interplanar distance, and 12.28 Å lattice parameter. The hexagonal crystal structure of MoS₂ as well as the stacking of MoS₂ layers were revealed by TEM and HRTEM studies. The calculated band gap using DFT at various symmetry points was compared to the observed PL and UV-Vis spectra corresponding to the various energy levels. The development of the VBM and CBM at symmetry points was described using PDOS and DOS diagrams. The study of band structural properties will contribute in the advancement of MoS₂-based potential applications in solar cells, photodetection, and FET fabrication.

The DFT and DFT+U computational study has been done to understand the biaxial strain effect on electronic band structures, structural, and elastic properties of monolayer MoS₂. Significant changes in the bond distances, bond angles, electronic structures, and effective mass of electron m_e^* (hole m_h^*) are observed under biaxial strain. The Bulk modulus decreases (increases) by increasing the tensile (compressive) biaxial strain. The band-gap values of unstrained 1L-MoS₂ are estimated as 1.78 (1.81) eV within the GGA (GGA+U) approximations; however, direct band gap varies from 1.74 (1.76) to 1.92 (1.95) eV within a region of 0.3(0.4) % tensile to 1.13(1.11) % compressive strains. Beyond this strain region, direct nature of the band gap becomes indirect, and further increment causes semiconductor to metallic transition. Direct band-gap tuning and observed small effective mass values of electrons and holes carriers under applied strain indicate the enhanced optoelectronic properties in strained monolayer MoS₂. For more details refer Khan M. et. al Journal of Materials Research, 2022 Oct [2].

References:

- [1] Khan, Mayur, Sunil Kumar, Ambuj Mishra, Indra Sulania, Madhvendra Nath Tripathi, and Ambuj Tripathi. "Study of structural and electronic properties of few-layer MoS₂ film." *Materials Today: Proceedings* (2022).
- [2] Khan, Mayur, Madhvendra Nath Tripathi, and Ambuj Tripathi. "Strain-induced structural, elastic, and electronic properties of 1L-MoS₂." *Journal of Materials Research* 37, no. 20 (2022): 3340-3351.

5.2.10 Influence of defect dynamics on the nano-hardness of NiCoCrFePd high entropy alloy under high dose Xe³³ irradiation and 120 MeV Au⁷⁷ irradiation

Abid Hussain¹, S.A. Khan¹, Sandeep K. Sharma², Kathi Sudarshan², Saurabh K. Sharma⁵, Chetan Singh⁴, P. K. Kulriya³

¹Materials Science Group, Inter University Accelerator Centre, New Delhi 110067, India

²Radiochemistry Division, Bhabha Atomic Research Centre, Mumbai 400085, India

³School of Physical Sciences, Jawaharlal Nehru University, New Delhi 110067, India

⁴Department of Materials Science and Engineering, Indian Institute Technology, New Delhi, 110067, India

⁵Mechanical, Aerospace and Nuclear Engineering, Rensselaer Polytechnic Institute, Troy, NY, 12180, USA

NiCoCrFePd high entropy alloys (HEAs) are one of the best radiation resistant alloys among the several HEAs studied till date. [1,2] The Pd incorporation dramatically changes the local structure by inducing an appreciable short-range ordering and strong lattice distortion. [3,4] Thus, the investigation of defect migration and its effect on the mechanical properties in NiCoCrFePd HEA is studied with the help ion beam irradiation. By the application of positron annihilation Dopplers broadening spectroscopy, and transmission electron microscopy, we provided for the first time an experimental evidence of vacancy generation and its evolution with ion fluence in one of the derivatives of Cantor-Wu alloy namely NiCoCrFePd under the room temperature irradiation using 1.05 MeV Xe³³ low energy ion beam facility (LEIBF) available at Inter-University Accelerator Centre (IUAC). The positron dopplers broadening spectroscopy (PADBS) along with the application high resolution transmission electron microscope (HR-TEM) used to evaluate the defect

generation at various ion fluences ranging from 1×10^{16} ions/cm² to 9×10^{16} ions/cm². We have established a relationship in defect generation and its effect on the hardness of the NiCoCrFePd HEA.^[5]

Further, to investigate the effect of high energy ion beam in the defect generation in NiCoCrFePd HEA, 120 MeV Au⁺⁷ ion irradiation was carried out using the 15 UD Pelletron tandem accelerator available at IUAC, New Delhi. The irradiation was carried out at several ion fluence ranging from 3.310^{12} ions/cm² to 110^{14} ions/cm² in order to evaluate the stability as well to investigate the type of defect produced by the irradiation with increase in ion fluence. By the application of positron life time spectroscopic measurement (PALS) and high-resolution transmission electron microscopy (HR-TEM) we are able to mark the type of defects produced by the Au beam and its evolution with increase in the ion fluence. The increase in τ_1 from 151.9 ± 2.0 ps to 158.0 ± 4.0 ps which indicates the generation of monovacancies at the initial ion fluence and generates the micro-strain as observed from the x-ray diffraction analysis. With increase in the ion fluence to 1×10^{14} ion/cm² further decreases the life time to 137.4 ± 3.0 ps which indicates the formation of vacancy clusters and dislocation formation also observed from the HR-TEM investigations. We have also established a relationship between the defect produced and its influence on the nano hardness of NiCoCrFePd by the application nano indentation hardness measurement. These studies are important in terms of understating the dynamics of defects produced by the ion beams and their evolution with ion fluences, which further will help in designing a radiation resistant alloy.

References:

- [1] Yang, Tai-ni, et al. "Influence of irradiation temperature on void swelling in NiCoFeCrMn and NiCoFeCrPd." *Scripta Materialia* 158 (2019): 57-61.
- [2] Shi, Shi, et al. "Evolution of ion damage at 773K in Ni-containing concentrated solid-solution alloys." *Journal of Nuclear Materials* 501 (2018): 132-142.
- [3] Ding, Qingqing, et al. "Tuning element distribution, structure and properties by composition in high-entropy alloys." *Nature* 574.7777 (2019): 223-227.
- [4] Zhang, Fuxiang, et al. "Lattice distortion and phase stability of Pd-Doped NiCoFeCr solid-solution alloys." *Entropy* 20.12 (2018): 900.
- [5] Hussain, Abid, et al. "Influence of defect dynamics on the nanoindentation hardness in NiCoCrFePd high entropy alloy under high dose Xe+3 irradiation." *Materials Science and Engineering: A* 863 (2023): 144523.

5.2.11 Effect of nitrogen implantation on the structural, optical, and electrical properties of V₂O₅ thin films on different substrates

Tanuj Kumar^{1*}, Bhanu Priya¹, Priya Jasrotia¹, Indra Sulania², D. Kanjilal²

¹Department of Nanoscience & Materials, Central University of Jammu, Jammu, 181143, India

²Inter University Accelerator Centre, Aruna Asif Ali Marg, New Delhi 110067, India

*Corresponding Author: tanuj.nsm@cjammu.ac.in, +91 9992910750

1.1 Introduction:

In recent years, there has been growing scientific interest in synthesizing and modifying vanadium oxides (VO_x), particularly V₂O₅, due to their potential applications in electrochemical activity, thermochromism, optics, and electronics. V₂O₅ is the most stable phase of VO_x with a band gap energy of 2.2-2.3 eV in bulk form. Different polymorphs of V₂O₅, including α -V₂O₅, β -V₂O₅, and γ -V₂O₅, can exist depending on growth mechanisms and conditions[.]. Thin films of V₂O₅ at the nano and micro scale exhibit unique morphology and properties compared to bulk materials. Various methods such as physical vapor deposition, sol-gel, spray-pyrolysis, and spin coating have been used for synthesizing V₂O₅ thin films, with the structural and morphological properties being highly dependent on the synthesis process and substrate used[.]. Physical vapor deposition, specifically thermal evaporation, is an effective approach for obtaining quality films with good uniformity and porosity. Doping V₂O₅ thin films with cations such as Ag, Mo, Sn, Zr, Na, F, Cu, and Cr using different methods has been reported in the literature, resulting in tunable structural, optical, and electrical properties. For instance, Cu doping improves electrochemical properties, while Ag enhances electrical properties. Ion implantation using accelerators offers an alternative doping method for V₂O₅ films, but the role of substrates in influencing the phase structure and properties of V₂O₅ films has been rarely investigated by other authors.

1.2 Experimental work:

The surfaces of glass, n-Si (100), and sapphire substrates were cleaned using alcohol and acetone through a standard procedure. A uniform V₂O₅ thin film with a thickness of about 500 nm was then grown on the substrates using physical vapour deposition with a rotating target holder. The thin films were named as V₂O₅:Gl, V₂O₅:Si, and V₂O₅:Sp, corresponding to the substrates used. The base pressure during deposition

was maintained at 5×10^{-5} bar. To re-crystallize the V_2O_5 thin films, they were heated at 500°C for 6.5 hours. Subsequently, N^+ ions with an energy of 16 keV were implanted into the crystallized V_2O_5 thin films at IUAC, New Delhi, using a tabletop accelerator. Two different fluences of N^+ ions, namely 5×10^{12} and 1×10^{14} ions/ cm^2 , were implanted using an implanter current of $\sim 15 \mu\text{A}/\text{cm}^2\text{s}$.

1.3 Results and discussion:

1.3.1 XRD study

Figure 1 shows the X-ray diffraction (XRD) patterns of V_2O_5 thin films with a thickness of 500 nm deposited on glass, sapphire, and silicon substrates (referred to as $V_2O_5:\text{Gl}$, $V_2O_5:\text{Sp}$, and $V_2O_5:\text{Si}$, respectively). The films were annealed at 500°C for 6.5 hours and subsequently implanted with 16 keV N^+ ions at fluences of 5×10^{12} and 1×10^{14} ions/ cm^2 . All the samples exhibit crystalline behavior, with diffraction peaks mainly attributed to the α - V_2O_5 orthorhombic phase (Pmmn space group, JCPDS card No. 01-089-2482). In the annealed thin film, additional peaks corresponding to the β - V_2O_5 tetragonal phase (Pmmn space group, JCPDS card No. 00-045-1074) appear at (200) and (002) crystallographic planes, along with the peaks of α - V_2O_5 [3].

In the glass substrate, the peak at 12.5 shows a dominant presence of β - V_2O_5 as compared to sapphire and silicon samples, with the peak orientation along the surface and an increasing relative intensity with fluence. In contrast, in sapphire, the α - V_2O_5 (200) peak at 15.3 dominates, and the relative intensity decreases with fluence. In silicon, the peak at 20.3 is dominated by the α - V_2O_5 phase, and the peak intensity increases [4]. Thus, a mixture of α - V_2O_5 and β - V_2O_5 phases is observed in the annealed V_2O_5 thin film. After N^+ implantation at a fluence of 5×10^{12} ions/ cm^2 on the V_2O_5 thin film, new peaks appear at (110) and (020) at 21.70 and 41.330 values of 2θ , respectively. With further N^+ treatment at a fluence of 1×10^{14} ions/ cm^2 , the peak at (020) disappears. The XRD patterns of the N^+ irradiated V_2O_5 samples differ from those of the pristine ones in terms of the relative intensities and positions of the peaks.

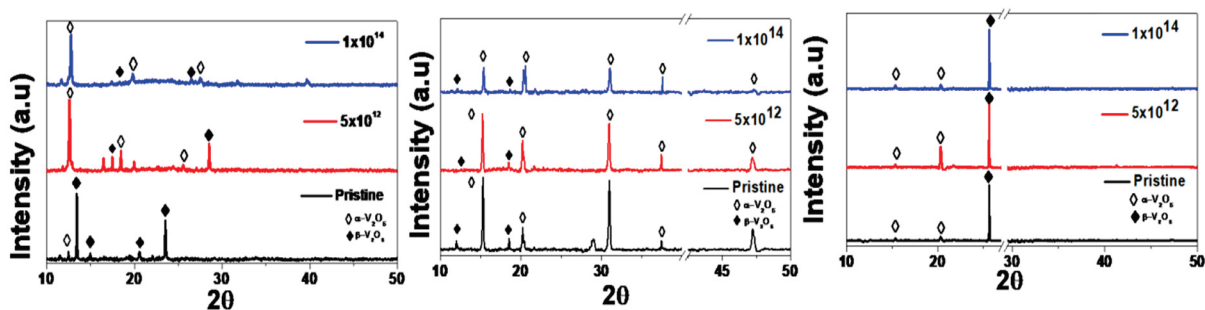


Fig. 1 XRD spectra of V_2O_5 thin film deposited on glass, sapphire, and silicon substrates.

1.3.2 FTIR analysis

The Fourier-transform infrared spectra of $V_2O_5:\text{Gl}$ after thermal treatment at 500°C for 6.5 hours and N^+ implantation at fluences of 1×10^{14} ions/ cm^2 are illustrated in Figure 2(a). The structural determination of orthorhombic V_2O_5 crystals is evident from the peak position of the vanadyl mode ($\text{V}=\text{O}$) at 1068 cm^{-1} , which is consistent across all samples. In crystalline V_2O_5 , the IR band of $\text{V}=\text{O}$ is typically observed at $1017\text{--}1021 \text{ cm}^{-1}$. The annealed sample at 500°C shows an additional peak around 506 cm^{-1} , attributed to the bending vibration of the V-O-V bond. Furthermore, two broad peaks at approximately 750 cm^{-1} and 894 cm^{-1} correspond to the symmetric and asymmetric stretching of the V-O-V bond, respectively.

The presence of N^+ implantation is also evident in the IR spectra. The symmetric N-O stretch appears at 1261 cm^{-1} , which is consistent with the N-O stretch range of $1360\text{--}1290 \text{ cm}^{-1}$. Additionally, the N_3 stretch is observed at 2157 cm^{-1} . The peaks in the $400\text{--}700 \text{ cm}^{-1}$ region correspond to symmetric stretching of V-O-V , which gradually shifts to lower wave numbers and merges with the bending V-O-V peak.

Comparing the FT-IR peak positions and bond attributions with literature data, it can be observed that the annealed $V_2O_5:\text{Gl}$ sample at 500°C has higher strength of V-O-V and $\text{V}=\text{O}$ bonds, which gradually decreases with increasing ion fluence for N^+ implanted samples. This suggests that the annealed sample has a more crystalline nature compared to the N^+ implanted samples.

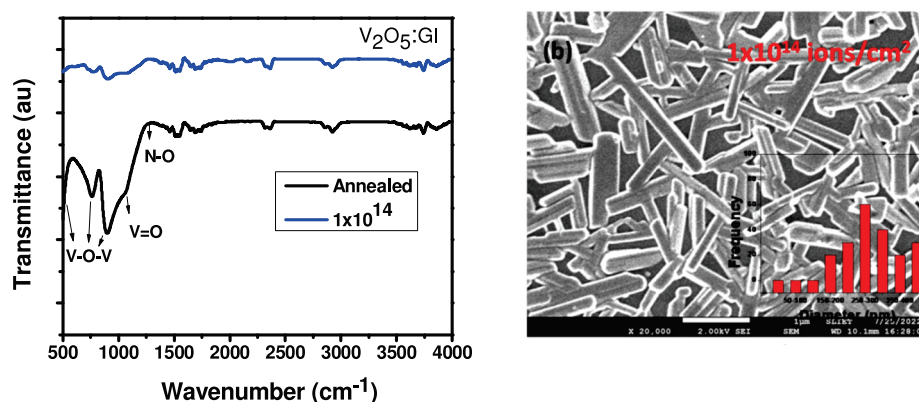


Fig. 2 (a) FTIR spectra of V_2O_5 films. (b) FESEM images of film after irradiation

1.3.3 FESEM study

The FESEM images of V_2O_5 thin film on a silicon substrate are shown in Figure 2 (b). Nanorod formation is observed in these samples, with an average diameter of 142 nm for the pristine film and 304 nm for the film irradiated at a fluence of 1×10^{14} ions/ cm^2 . Well-defined nanorod structures are visible after irradiation. Previous studies by R. Suresh et al. have shown that V_2O_5 particles tend to have uneven diameters due to aggregation. However, in Co- V_2O_5 SEM pictures, the emergence of nanorods with diameters ranging between 20 and 50 nm within the V_2O_5 clusters is observed. The development of these nanorods is believed to be due to surface diffusion caused by thermodynamics, as reported in literature [].

1.4 Conclusion

The structural characterization revealed that N^+ implantation did not affect the crystal structure of the pristine V_2O_5 sample, and all the nanoparticles were predominantly of the orthorhombic α - V_2O_5 phase, with traces of monoclinic β - V_2O_5 . The FESEM images of the V_2O_5 thin film on a glass substrate showed that the nanoparticles or grains were spherical and randomly scattered across the entire substrate surface. However, on the silicon substrate, nanorod formation was observed in the samples. After irradiation, well-defined nanorods were observed, resulting in an increase in the average diameter of the nanorods from 142 nm to 304 nm. This suggests that the irradiation process induced the formation of distinct nanorod structures on the silicon substrate, while maintaining the crystal structure of the V_2O_5 nanoparticles on the glass substrate.

References:

- [1] B. Priya, P. Jasrotia, I. Sulania, D.K. Chaudhary, R. Gupta, A. S. Verma, R. Kumar, T. Kumar, ECS Advances, (2023).
- [2] S. Kumar, A. Qadir, F. Maury, N. Bahlawane, ACS applied materials & interfaces, 9 (2017) 21447-21456
- [3] B. Priya, P. Jasrotia, I. Sulania, R. Kumar, R.K. Pandey, T. Kumar, Applied Surface Science, 619 (2023) 156592.
- [4] D. Kumar, B. Priya, P. Jasrotia, A. Kumar, V. Singh, J. Jire, R. Kumar, P.K. Kulriya, Frontiers in Materials, (2022) 728.
- [5] A. Venkatesan, N.K. Chandar, S. Arjunan, K. Marimuthu, R.M. Kumar, R. Jayavel, Materials Letters, 91 (2013) 228-231.
- [6] R. Suresh, K. Giribabu, R. Manigandan, S. Munusamy, S.P. Kumar, S. Muthamizh, A. Stephen, V. Narayanan, Journal of Alloys and Compounds, 598 (2014) 151-160.

5.2.12 A Combinative Study Investigating the LSPR Tuning of Embedded Gold Nanoparticles in Si_3N_4 matrix upon 120 MeV Au^{9+} Swift Heavy Ion Irradiation

Pariksha Malik¹, Pankaj Srivastava¹, Debalaya Sarker², Dileep Kumar Gupta², Santanu Ghosh^{1*}

¹Department of Physics, Indian Institute of Technology Delhi, New Delhi-110016, India

²UGC-DAE Consortium for Scientific Research, Indore, Madhya Pradesh 452017, India

The synthesis and modification of materials and nanostructures by means of ion irradiation has been the topic of substantial research and is a procedure that is routinely utilised in the primary industries that are involved in the production of microelectronics [1]. The production of optical wave guides in insulating materials is just one of the many uses of swift heavy ions (SHIs), which have a wide variety of applications [2]. Applications in sensing and photonics are extremely important uses for metallic nanostructures such as nanorods and nanoparticles. The occurrence of bands that exhibit localised surface plasmon resonance (LSPR) within the visible spectrum is one of the additional optical properties that shape anisotropy bestows onto Au

nanoparticles. Given that the plasmonic responses of these systems are determined by the dielectric properties of the host matrix [3] it would be great if the method that was outlined for a-SiO₂ could be applied to other dielectric materials such as silicon nitride (Si₃N₄). The focus of the current research is on the ion-shaping of gold nanoparticles that have been encased in Si₃N₄ via plasma accelerated chemical vapour deposition (PECVD). In this study, the ion shape of Au NPs in Si₃N₄ that had been bombarded with 1x 10¹¹, 1x 10¹², and 1x 10¹³ ions cm⁻² of 120MeV Au⁹⁺ was investigated. Irradiated samples were examined with X-TEM, Grazing Incident XRD, WAXS, SAXS, and UV-spectroscopy Vis's in order to investigate the microstructural and optical properties of the samples at varying fluences. In order to investigate the local distribution of Au NPs as well as their structural and morphological alterations, a Thermo Scientific Themis 300 G3 Transmission Electron Microscope equipped with a thermal field emission electron gun was used at an energy of 300 kV in the HRTEM mode (Point resolution 0.2 nm) with a High-Resolution Transmission Electron Microscope (Point resolution 0.2 nm). This was done so that more information regarding the structural and morphological changes that took place in the Au NPs could be gleaned from it. The TEM plane samples were created by using Gatan PIPS while the samples were maintained at a temperature of liquid nitrogen. This was done in order to prevent any modifications from taking place during the process of Ar ion sputtering in the PIPS apparatus. This was done to ensure that there would be no need for any revisions. Null ellipsometry at 632.8 nm was utilized in order to ascertain the films' thickness, as well as their composition and refractive index. Irradiating the produced Si₃N₄/Au NPs/ Si₃N₄/Si nanostructured films with 120 MeV Au⁹⁺ ions at one of three separate fluences of ions at room temperature yielded the following results: 1E11 (1x10¹¹), 1E12 (1x10¹²), and 1E13 (1x10¹³) cm⁻². The surface of each film was maintained in such a way that it faced in a direction that was perpendicular to the path that the ion beam was travelling. Throughout the duration of the experiment, the beam current was kept at 0.76 pA, while the pressure inside the irradiation chamber was kept at 2.8 x10⁻⁶ torr. An electromagnetic scanner was used to scan the beam a region that was 1.0 cm² in size. The calculation that was carried out using the SRIM code from 2006 yielded the following results: the range of 120 MeV Au ions in Si₃N₄ is 22.66 μm, which is a substantial amount greater than the thickness of the films. Because of this, the likelihood of Au ions being found in the films that have been exposed is quite remote. It is plausible to suppose that the electrical and nuclear stopping powers (Se = 10.3 keV nm⁻¹ and Sn = 0.2 keV nm⁻¹)[3] remain the same over the entirety of the film's thickness.

References:

- [1] A. V. Krasheninnikov, K. Nordlund, *JAppl Phys.* 107 (2010).
- [2] P. Mota-Santiago, H. Vazquez, T. Bierschen, F. Kremer, A. Nadzri, D. Schauries, F. Djurabekova, K. Nordlund, C. Trautmann, S. Mudie, M. C. Ridgway, P. Kluth, (2018).
- [3] P. Mota-Santiago, F. Kremer, A. Nadzri, M. C. Ridgway, P. Kluth, *Nucl Instrum Methods Phys Res B.* **409**, 328–332 (2017).

5.2.13 Enhancing room temperature ferromagnetism in pure MoS₂ by Ar ion irradiation

Sharmistha Dey^a, Pankaj Srivastava^a, Fouran Singh^b and Santanu Ghosh^a

^aNanostech Laboratory, Department of Physics, Indian Institute of Technology Delhi, New Delhi 110016, India

^bMaterials Science Division, IUAC, New Delhi-110067, India

Defects are omnipresent in Solids. A sufficient number of defects in solids can alter their optical, electrical, and magnetic characteristics [1]. Nowadays, defect-driven ferromagnetism is a vast area of research work. Due to defects, nonmagnetic materials exhibit ferromagnetism without the doping of magnetic material (as there is a solubility problem of magnetic materials in semiconductors due to different crystal structures). Hence, defect-induced room temperature ferromagnetism (RTFM) is a really interesting topic. There are several types of defects like structural defects, vacancies, interstitial, surface defects, and strain. Generally, magnetism can be induced from partially filled or half-filled “d” orbitals but here, ferromagnetism is induced due to defects, so this is called d⁰ ferromagnetism. There are some research articles that show d⁰ ferromagnetism in oxides and nitrides like ZnO [2], GaN [3], HfO₂ [4], etc. Generally, semiconductors are diamagnetic at room temperature. But if it is possible to create ferromagnetism in a semiconductor at room temperature as a result of defects, then this will be highly interesting work for spintronics applications. One can induce defects by various methods, like variation in annealing temperature [5], varying deposition parameters [6], plasma treatments, and by irradiation [3]. Among these, ion irradiation is a very strong tool to create defects in solids in a very controlled manner. In a low energy regime, there is a creation of defects and damages due to nuclear energy loss. Nowadays, transition metal dichalcogenides (TMDCs) are very convenient materials for mechanical, electrical, optoelectronics as well as magnetic studies, due to their very interesting properties, like thickness-dependent band gap, Vander Waal interaction between two layers, etc. Among these properties, magnetic properties measurements in low dimensional TMDCs have not been elaborately studied till now. So, the study of defect-induced room temperature ferromagnetism in transition metal chalcogenides (MoS₂) will be a very interesting topic of research.

The preparation of MoS₂ thin films is done by the chemical vapor deposition process (CVD). All the parameters for CVD growth (Deposition temperature, Gas flow rate, Substrate type and position, etc.) are optimized. Basic characterization of MoS₂ pristine sample is done by XRD and Raman. From XRD and Raman data, it is clearly visible the pure phase formation of 2H-MoS₂ phase. Surface morphology study was performed by FESEM from which the formation of nano-wall like structure is clearly visible. Surface composition analysis is done by XPS, shows pure phase formation of MoS₂ thin films. Magnetic measurements have also been done for pristine samples by SQUID. Pristine MoS₂ sample shows ferromagnetism at room temperature. Then the films were irradiated at Inter University Accelerator Centre (IUAC), New Delhi with 40 keV Ar⁺ ions at ion fluences from 1×10^{13} ions/cm² to 1×10^{16} ions/cm² with current of 500 nA. XRD and Raman are performed for all the irradiated samples and it is evident that there is structural change as the intensity is decreasing with increasing ion fluences. To study the effects on magnetic properties of the irradiation, SQUID measurements and also other characterizations are under process. As MoS₂ is a semiconductor and if one can tune room temperature ferromagnetism in it due to ion irradiation then it will be very helpful for spintronics applications.

References:

- [1] Sarkar A, Sanyal D, Nath P, Chakrabarti M, Pal S, Chattopadhyay S, Jana D and Asokan K 2015 Defect driven ferromagnetism in SnO₂: a combined study using density functional theory and positron annihilation spectroscopy *RSC Advances* 5 1148–52
- [2] Singh P, Mishra V, Barman S, Balal M, Barman S R, Singh A, Kumar S, Ramachandran R, Srivastava P and Ghosh S 2021 Role of H-bond along with oxygen and zinc vacancies in the enhancement of ferromagnetic behavior of ZnO films: An experimental and first principle-based study *Journal of Alloys and Compounds* 889 161663
- [3] Singh P, Ghosh S, Mishra V, Barman S, Roy Barman S, Singh A, Kumar S, Li Z, Kentsch U and Srivastava P 2021 Tuning of ferromagnetic behavior of GaN films by N ion implantation: An experimental and first principle-based study *Journal of Magnetism and Magnetic Materials* 523 167630
- [4] Bharathi K K, Venkatesh S, Prathiba G, Kumar N H and Ramana C V 2011 Room temperature ferromagnetism in HfO₂ films *Journal of Applied Physics* 109 07C318
- [5] Gao X, Man B, Zhang C, Leng J, Xu Y, Wang Q, Zhang M and Meng Y 2017 The important role of Ga vacancies in the ferromagnetic GaN thin films *Journal of Alloys and Compounds* 699 596–600
- [6] Roul B, Rajpalke M K, Bhat T N, Kumar M, Kalghatgi A T, Krupanidhi S B, Kumar N and Sundaresan A 2011 Experimental evidence of Ga-vacancy induced room temperature ferromagnetic behavior in GaN films *Appl. Phys. Lett.* 99 162512

5.2.14 Study on damage of Gd₂O₃-CeO₂ under electronic energy loss and nuclear energy loss regime: comparison between bulk-like and nanostructure

Waseem Ul Haq,¹ Vinita Grover², Fouran Singh³, Sanjay Kumar³, Parswajit Kalita⁴, Santanu Ghosh^{1*}

¹Department of Physics, Indian Institute of Technology (IIT) Delhi, New Delhi 110016 India.

²Chemistry Division, Bhabha Atomic Research Centre (BARC), Mumbai 400085. India.

³Material Science Group, Inter-University Accelerator Centre (IUAC), New Delhi 110067, India.

⁴Department of Physics, University of Petroleum & Energy Studies (UPES), Dehradun, 248007 India.

To understand the physical phenomena responsible for radiation damage of the materials used in nuclear reactors, and thus study their operation life and/or efficiency, it is required to simulate the condition by exposing them to energetic ions. Ceria (CeO₂) has been proposed as one of the inert matrices for the transmutation of minor actinides in the futuristic inert matrix fuel (IMF) concept. The inert matrix should also consist of burnable poison to compensate the initial reactivity of fuel. In this context, Gadolinium (Gd) is an excellent burnable poison with a high neutron absorption cross-section. In view of this, Gd₂O₃-CeO₂ nano-powders were synthesized and sintered at 800°C and 1300°C to obtain different grain sizes and morphology. FESEM and TEM were carried out to study the grain size of pristine pellets. The sintered pellets were irradiated with 80 MeV Ag ions (electronic energy loss (Se) regime) at room temperature to emulate the effect of fission fragments. For analysis of the effect of grain size on the irradiation-induced structural degradation at different fluences, GIXRD and Raman spectroscopy were performed. Significantly large damage has been observed for the smaller grain-sized samples (sintered at 800 C) as compared to the large grain-sized sample (sintered at 1300 C). Neither of the samples amorphized under present experimental conditions as indicated by the presence of the Raman active T_{2g} mode (centred at 462 cm⁻¹) and all XRD peaks of fluorite cubic structure up to highest fluence employed (1×10^{14} ions/cm²). The radiation tolerance behaviour of the samples is understood with the help of thermal spike simulation, which indicates higher transient lattice temperatures with longer durations upon irradiation. Gd-doped ceria thus possesses good radiation stability in the S_e regime indicating its potential for application in IMFs.

In order to investigate the effects of Low energy ion beam irradiation on the structural and behavioural change in Gd-doped Ceria, we prepared the three different-grained size samples and employed various

characterization techniques. After initial characterization via XRD, Raman Spectroscopy and FESEM, these samples were exposed to 400 keV Kr⁺ ions at different fluences at IUAC, New Delhi. GIXRD patterns & Raman Spectroscopy show that there are significant changes in the Gd-doped Ceria post-irradiation. XPS measurement and detailed analysis of the irradiated samples are under process.

Simultaneously we have prepared the two manuscripts of above-mentioned works and shall be submitted immediately after XPS measurements.

5.2.15 Radiation Damage Effects on Nano-Crystalline Zirconolite Ceramic Compositions

Swetha R¹, Merry Gupta², Sanjay Kumar K.², S. K. Sharma³, P. K. Kulriya⁴ and P. V. L. Narayana¹

¹Department of Nuclear Physics, Andhra University, Visakhapatnam 530003, Andhra Pradesh, India

²Inter-University Accelerator Centre, Aruna Asaf Ali Road, New Delhi 11067, India

³Rensselaer Polytechnic Institute, New York; SPS, Jawaharlal Nehru University; Inter-university Accelerator Centre, India

⁴SPS, Jawaharlal Nehru University New Delhi, India

To safeguard the Human life and the environment from the hazardous wastes expelled out during Nuclear Fuel processing, the immobilization of minor actinides and alkaline-earth metal has been a key concern for nuclear industry. Initially Zirconolite was synthesized following the basic methodology i.e. solid state reaction techniques. Later a polycrystalline nano-powder of CaZrTi₂O₇ pellets were synthesized using ball-milling for Nd, Ce and Yt- doped Zirconolite were irradiated using 15 UD Pelletron tandem accelerator at Inter University Accelerator Centre (IUAC), New Delhi with current of 1pA. All the Pellets and TEM grids were mounted on a target ladder placed inside the high vacuum (~10⁻⁶ torr) chamber during irradiation with 2 MeV Kr⁺ ions for the ion fluence varying from 1 × 10¹⁴ to 2 × 10¹⁶ ions/cm². X-ray diffraction (XRD) studies showed that zirconolite was not amorphized even on irradiation up to a fluence order of 2 × 10¹⁶ ion/cm². Fig-1 given below shows the XRD peaks of Zirconolite at various fluences. Transmission electron microscopy (TEM) images of the pristine sample exhibited well separated grains with average size of about 0.46 μm. Thus, XRD along with TEM investigation was performed for the radiation damage study of nano-crystalline Zirconolite ceramic composite. TEM images of nano-crystalline pristine Zirconolite, SAED pattern and grain boundary between two grains divided by misorientation were given in the below Fig-2. Other measurements and analysis are under process.

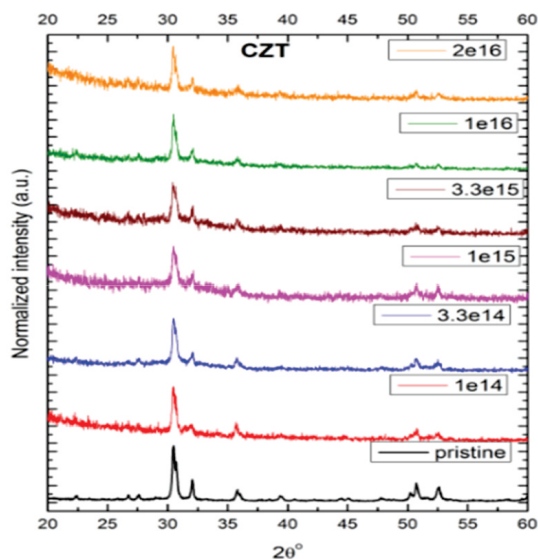


Fig -1

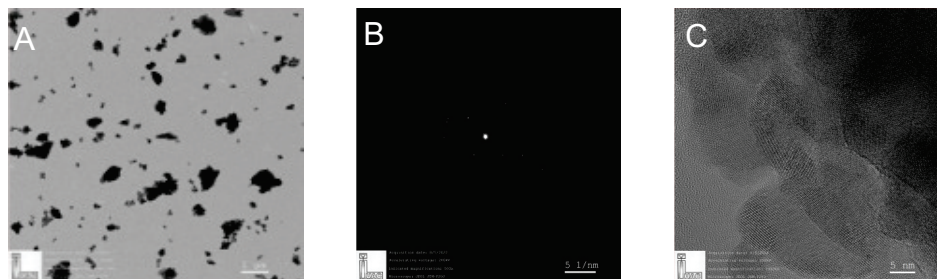


Fig-2(a) TEM images of Nano-crystalline pristine Zirconolite (b) SAED pattern and (c) Grain boundary between two grains.

References:

- [1] W.J. Weber, R.C. Ewing, C.R.A. Catlow, T. Diaz de la Rubia, L.W. Hobbs, C. Kinnoshita, H.J. Matzke, A.T. Motta, M. Nastasi, E.K.H. Salje, E.R. Vance, S.J. Zinkle, Radiation effects in crystalline ceramics for the immobilization of highlevel nuclear waste and plutonium, *J. Mater. Res.* 13 (1998) 6.
- [2] S.X. Wang, G.R. Lumpkin, L.M. Wang, R.C. Ewing, Ion irradiation-induced amorphization of six zirconolite compositions, *Nucl. Instr. Meth. B* 166–167 (2000) 293.
- [3] M. Gilbert, C. Davoisne, M. Stennett, N. Hyatt, N. Peng, C. Jaynes, W.E. Lee, Krypton and helium irradiation damage in neodymium–zirconolite, *J. Nucl. Mater.* 416 (2011) 221.
- [4] W. Sinclair, A.E. Ringwood, Alpha-recoil damage in natural zirconolite and perovskite, *Geochem. J.* 15 (1981) 229.
- [5] R.C. Ewing, L.M. Wang, Amorphization of zirconolite: alpha-decay event damage versus krypton ion irradiation, *Nucl. Instr. Meth. B* 65 (1992) 319. [6] K.L. Smith, N.J. Zaluzec, G.R. Lumpkin, In situ studies of ion irradiated zirconolite, pyrochlore and perovskite, *J. Nucl. Mater.* 250 (1997) 36.
- [6] Kaur, R., Gupta, M., Kulriya, P. K., & Ghumman, S. S.: 'Phase analysis and reduction behaviour of Ce dopant in zirconolite', *J Radioanal Nucl Chem*, 1-10, 2019.

5.2.16**Synthesis and characterization of Transition metal oxides and their application as humidity and Gas Sensors**

Peramjeet Singh¹, N.K. Pandey¹, V.V. Siva Kumar², I. Sulania², R.R. Awasthi³, V. Verma¹, B. Kumar¹, N. Yadav¹, S. Srivastava¹, A.K. Verma¹, A. Dawar¹

¹*Sensors and Materials Research Laboratory, University of Lucknow, Lucknow, U. P. (226007), India.*

²*Inter-University Accelerator Centre, New Delhi (110067), India.*

³*KMC Language University Lucknow, Lucknow, U.P. (226013), India.*

The importance of nanoscale materials, especially, Bismuth trioxide (Bi₂O₃), in the production of energy, photonics, humidity sensors, gas sensing [1], supercapacitors, catalysts, and solar cells has gained attention. Due to the broad use of Bi₂O₃ in both research labs and industries as humidity and gas sensors is quite significant [1]. Further, MoO₃ is one of the potential candidates for lithium batteries [2]. The material MoO₃ doped Bi₂O₃ exhibits extraordinarily high conductivity due to its different phases and orientations in the periodic table [3, 4]. Sayyed et al. reported that when borate glass has high concentrations of metal oxides like Bi₂O₃ and MoO₃, it attenuates gamma photons between 0.356 MeV and 1.33 MeV the most [5].

In this report, attempts have been made to improve the processes used to synthesize multi-component metal oxide and develop a method for synthesizing multiple phases of Bi₂O₃/MoO₃ nanocomposite. The chemical structure, optical properties, surface roughness, and microstructure have been studied using XRD, AFM, UV-Vis, and FT-IR at IUAC, New Delhi [6, 7]. The fabricated material was used to investigate its potential as a humidity sensor and gas sensor. We synthesized a pure sample of molybdenum trioxide at three different temperatures: 400 °C, 500 °C, and 600 °C. We also synthesized bismuth oxide-doped molybdenum trioxide, SnO₂-doped MoO₃, and TiO₂-doped MoO₃ at 500 °C and irradiated the samples with gamma rays at energies of 0.1 kGy, 10 kGy, and 50 kGy to observe the significant changes in the said properties for application in sensors.

References:

- [1] A. Venkatanarayanan, and E. Spain, *Comprehensive Materials Processing* (2014), 47–101. doi:10.1016/b978-0-08-096532-1.01303-0.
- [2] W. Lu, X. Chen, M. Xue, Y. Cui, and Q. Zhuang, *Int. J. Electrochem. Sci.*, 13 (2018) 275 – 286. doi: 10.20964/2018.01.04.
- [3] T. Takahashi, T. Esaka, and H. Iwahara, *Journal of applied electrochemistry* 7(1977) 31-35. <https://doi.org/10.1007/BF00615527>.
- [4] T. Takahashi, and H. Iwahara, *Journal of Applied Electrochemistry* 3, 65–72 (1973). <https://doi.org/10.1007/BF01119469>.
- [5] M.I. Sayyed, K.M. Kaky, O.K. Gaikwad, O. Agar, U.P. Gawai, and S.O. Baki, *Journal of Non-Crystalline Solids* 507 (2019) 30–37. <https://doi.org/10.1016/j.jnoncrysol.2018.12.010>.
- [6] Highly sensitive pure molybdenum trioxide thin films at a higher annealing temperature for liquefied petroleum gas and humidity sensing at room temperature, Peramjeet Singh, N.K. Pandey, V.V. Siva Kumar, Vernica Verma, Ajeet Singh, Priya Gupta, and B.C. Yadav, *Applied Physics A* (2023) 129:250. <https://doi.org/10.1007/s00339-023-06491-7>.
- [7] Analysis of the optical, chemical, surface, and humidity sensing characteristics of nanostructured Bi₂O₃-doped MoO₃ materials, R.R. Awasthi, V.V. Siva Kumar, V. Verma, B. Kumar, I. Sulania, N. Yadav, S. Srivastava, A.K. Verma, A. Dawar, *Materials Today: Proceedings xxx (xxxx) xxx*. <https://doi.org/10.1016/j.matpr.2023.01.398>.

5.2.17 Tuning of electrical properties through field effects for manganite-based n-n Junctions: Role of Swift Heavy Ion Irradiation

Mayur Parmar¹, P.S. Solanki¹, Ambuj Tripathi², N.A. Shah¹

¹Department of Physics, Saurashtra University, Rajkot – 360 005, Gujarat, India

²Inter University Accelerator Centre, Aruna Asaf Ali Marg, New Delhi, 110 067, India.

In order to investigate the modifications in the properties of manganite-based thin films through the n-n junctions based field effect behavior, proposed polycrystalline films of n-type $\text{La}_{0.3}\text{Sr}_{0.7}\text{MnO}_3$ and $\text{Gd}_{0.3}\text{Sr}_{0.7}\text{MnO}_3$ were synthesized using low-cost CSD method wherein, for prepared solutions of $\text{La}_{0.3}\text{Sr}_{0.7}\text{MnO}_3$ lanthanum (III) acetate hydrate, strontium acetate (II) and manganese (II) acetate tetrahydrate 99.99 % trace metal basis have been used whereas, for the preparation of GSMO gadolinium (III) acetate hydrate, strontium acetate (II) and manganese (II) acetate tetrahydrate 99.99 % trace metal basis used as starting precursors thereafter, desired LSMO (100 nm) and GSMO (100 nm) layer has been grown over STO substrate. To prepare the n-n junction on prepared films, firstly cadmium acetate is used as starting precursor to prepare the solution followed by the preparation of CdO (50 nm) layer on manganite-based thin films. The final obtained product of manganite-based n-n junction films are CdO (50 nm) / LSMO (100 nm) / STO and CdO (50 nm) / GSMO (100 nm) / STO film which will further be characterized.

During the next sanctioned year of the research project, the main focused area will be to tune the electrical properties through field effects of manganite-based n-n junction films with the application of swift heavy ion irradiation. For this purpose, SHI irradiation on prepared films with 200 MeV energy Ag^{+15} ions with different ion fluence of i.e., 1×10^{11} ions/cm², 1×10^{12} ions/cm², 1×10^{13} ions/cm² will be carried out. Several characterizations i.e., structural (XRD), microstructural (AFM), and electrical properties (I-V, R-T, Dielectric, a.c. Conductivity, Impedance) will be performed after SHI irradiation of the prepared films.

References:

- [1] D. Venkateshwarlu, Himanshu Dadhich, Bhargav Rajyaguru, Sukriti Hans, M. Ranjan, R. Venkatesh, V. Ganesan, P.S. Solanki, N.A. Shah, *Materials Science in Semiconductor Processing* 136 (2021) 106154
- [2] Hiroshi Nakatsugawa, Miwa Saito, Yoichi Okamoto, *Materials Transactions*, 60(6) (2019), 1051-1060

5.2.18 Tuning of charge carriers in Bi₂Te₃ thin films via swift heavy ion irradiation

Jyoti Yadav^{1,3}, Anoop M D¹, Nisha Yadav¹, N. Srinivasa Rao¹, Fouran Singh³, Ankur Jain^{2,5}, Takayuki Ichikawa⁴, Kamalendra Awasthi¹, Rini Singh² and Manoj Kumar¹

¹Department of Physics, Malaviya National Institute of Technology Jaipur, Rajasthan, 302017, India

²Graduate School of Engineering, Hiroshima University, Higashi-Hiroshima, 739-8527, Japan

³Inter-University Accelerator Centre (IUAC), New Delhi - 110067, India

⁴Natural Science Centre for Basic Research and Development, Hiroshima University, Higashi-Hiroshima, 739-8530, Japan

⁵Centre for Renewable Energy and Storage, Suresh Gyan Vihar University, Jagatpura, Jaipur-302017, India

Irradiation with swift heavy ion (SHI) is an excellent approach towards creating extrinsic defects and strain in the films. SHIs, the beam of ions having energy up to hundreds of MeV is used to bombard the samples and these highly energetic ions can induce cylindrical tracks of a few nanometer diameter along the ion path. It is known that the physical properties of Bi-Te based alloys strongly depend upon the lattice defects and grain boundaries justifying wide studies of nanostructures of these alloys for various applications. However, thin films of Bi-Te alloys are preferred for their device application. Therefore the study of the effects of ion irradiation on semiconductors has always been interest of researchers due to properties affected by strain and defects. To report irradiation tool as an effective approach to tune the Fermi level in Bi₂Te₃ films, Ni ion of energy 100 MeV is used at five different fluences (5×10^{11} , 1×10^{12} , 3×10^{12} , 5×10^{12} , 1×10^{13} ions/cm²). The high energy ions penetrated through thickness of the films to the substrate. The structural, morphological, optical, and electrical properties of the pristine and irradiated films were studied in detail. The observed transition in conductivity suggested the controlling of charge carriers through irradiation. Through ion beam irradiation-induced defects, the Fermi level is stabilized in the centre of the bulk band gap in Bi₂Te₃ thin films. [for details, see *Journal of Mat. Sci. Mat. in Electronics*. 34 (2023) 175]

The XRD pattern exhibited the polycrystalline nature with a single phase of Bi₂Te₃ in pristine and irradiated

thin films, perfectly matching with the standard data (JCPDS-00-015-0863). The pristine and irradiated Bi₂Te₃ thin films correspond to the rhombohedral crystal structure with the R-3m space group. The observed increase in intensity of the peak could be due to the mass diffusion across the grain boundaries resulting in an increase in the average grain size. [for details, see *Macromol. Symp.* 399 (2021) 2100079]. To investigate the modifications in band structure, low-temperature transport studies were carried out. The temperature-dependent resistivity measurements in the temperature range (4 K-300 K) suggests the semiconducting nature of thin films. [for details, see *Appl. Phys. A.* 127 (2021) 5130]. The temperature dependent resistivity measurements in temperature range 4-300 K show that the vacancies created and distribution of irradiation induced defects plays significant role in transport properties. [for details, see *Mater. Lett.* 306 (2022) 130923]. The transport properties of the thin films are greatly influenced by ion irradiation, which can be better understood by the transport of charge carriers under the magnetic field. Hence, the Hall coefficient values at a fixed magnetic field of 0.2 T in the temperature range from 300 K down to 4 K is studied. For the pristine and the lowest ion dose irradiated thin films, *n*-type conductivity is observed. The variation of the Hall coefficient with temperature shows tuning of Fermi level towards the center of the bulk conduction band and bulk valence band. The diffusion of Te atoms due to the displacement of atoms resulted in change of charge carriers from *n*-type to *p*-type. The position of Fermi level in between the band gap confirms the suppression of bulk conductivity. Further increase in the fluence acceptor like defects was predominantly generated resulted in the crossover from films of *n*-type majority carriers to the films of *p*-type majority carriers. Interestingly, at fluence 5×10^{12} ions/cm² the film again tried to get into the region of *n*-type but at the highest fluence 1×10^{13} ions/cm² with *p*-type conductivity compensation of bulk charge carriers could successfully be achieved. The highest three fluences show the Hall coefficient very close to zero and the Fermi level seems to be stabilized near the zero Hall coefficient. The zero Hall coefficient value confirms the Fermi level position at the middle of the band gap. The observed zero Hall coefficient might be due to the generation of free charge carriers which is because of the native defects and strain created during irradiation. Ion irradiation might suppress the bulk conductivity. Hence, by probing the surface states possibly we might get the clear evidence of surface dominated carrier transport through ion beam irradiation.

References:

- [1]. Jyoti Yadav, Anoop M D, Nisha Yadav, N. Srinivasa Rao, Fouran Singh, Ankur Jain, Takayuki Ichikawa, Kamalendra Awasthi, Rini Singh and Manoj Kumar, *Journal of Mat. Sci.: Mat. In Electronics* 34 (2023) 175.
- [2]. Jyoti Yadav, Anoop MD, Rini Singh, Nisha Yadav, N. Srinivasa Rao, Fouran Singh, Takayuki Ichikawa, Ankur Jain, Kamalendra Awasthi, and Manoj Kumar, *Macromol. Symp.* 399 (2021) 2100079.
- [3]. Jyoti Yadav, Anoop MD, Rini Singh, Nisha Yadav, N. Srinivasa Rao, Fouran Singh, Kamalendra Awasthi, and Manoj Kumar, *Appl. Phys. A.* 127 (2021) 5130.
- [4]. Jyoti Yadav, Anoop M D, Rini Singh, Nisha Yadav, N. Srinivasa Rao, Fouran Singh, Ankur Jain, Takayuki Ichikawa, Kamalendra Awasthi, and Manoj Kumar, *Mater. Lett.* 306 (2022) 130923.

5.2.19 Low Energy Ion-Induced Structural and Morphological Modifications in NiO Thin films

Lolly Maria Jose,¹ V V Sivakumar², Arun Aravind¹

¹Centre for Advanced Functional Materials, Department of Physics, Bishop Moore College, Mavelikara., India.

²Inter University Accelerator Centre, New Delhi, India.

In order to investigate the effects of low energy ion beam irradiation on the structural, optical, and electrical and properties of NiO thin films, we deposited NiO thin films on glass substrate using RF Magnetron Co-sputtering technique using NiO ceramic target. The distance between the target and substrate was adjusted at 7 cm. Prior to deposition, the chamber was evacuated to a base pressure of 10^{-6} mbar. The working pressure was maintained at 2×10^{-2} mbar while the radio frequency power was 80W. The deposition was done for 30 minutes keeping the substrate temperature at 100°C. After the required pre-irradiation characterizations, the films were irradiated using Negative Ion Implanter beam facility (NIIBF) at Inter University Accelerator Centre (IUAC), New Delhi with 50 keV N⁺ ions at three different ion fluences, 5×10^{15} ions/cm², 1×10^{16} ions/cm² and 5×10^{16} ions/cm² with current of 1 pA (particle nanoampere). All the films were pasted to the target ladder placed inside the high vacuum ($\sim 10^{-6}$ torr) chamber during ionbeam irradiation. Beam was irradiated in a direction perpendicular to the sample surface over an area of 1×1 cm².

To investigate the structural and morphological changes because of the irradiation, XRD and AFM measurements of the irradiated thin are conducted. XRD patterns of NiO pristine and irradiated thinfilms with different ion fluences are shown in Fig. 1. Moreover, the intense multiple peaks from different planes of thin films indicate that the NiO thin films are polycrystalline in nature and exhibit good crystalline quality. Intense peak from different planes depicts the polycrystalline and good crystalline nature of the samples. Irradiation with different fluences caused a significant variation in peak intensity. The intensity of the diffraction peak corresponding to the (111) plane was found to increase with the increase in fluence except for 1×10^{16} ions/cm². Increase in peak intensity is related to the reduction in density of defects following the

interaction of ions with the material [1]. From AFM images (Fig.2), it was understood that the average roughness of the film varies in a non-uniform manner. Further analysis and characterizations including optical, morphological and electrical analysis are under process.

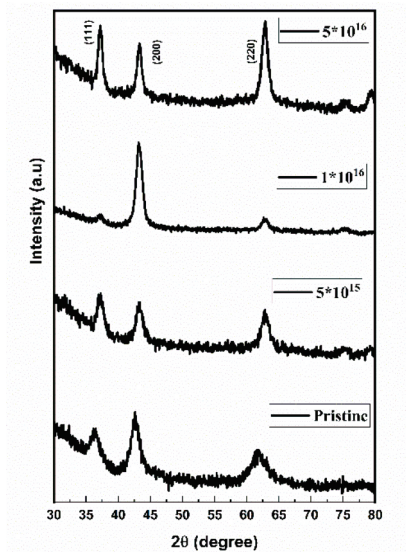


Figure 2 XRD spectrum of pristine and 50keV Nitrogen irradiated NiO thinfilms at fluences $5*10^{15}$, $1*10^{16}$ and $5*10^{16}$ ions/cm².

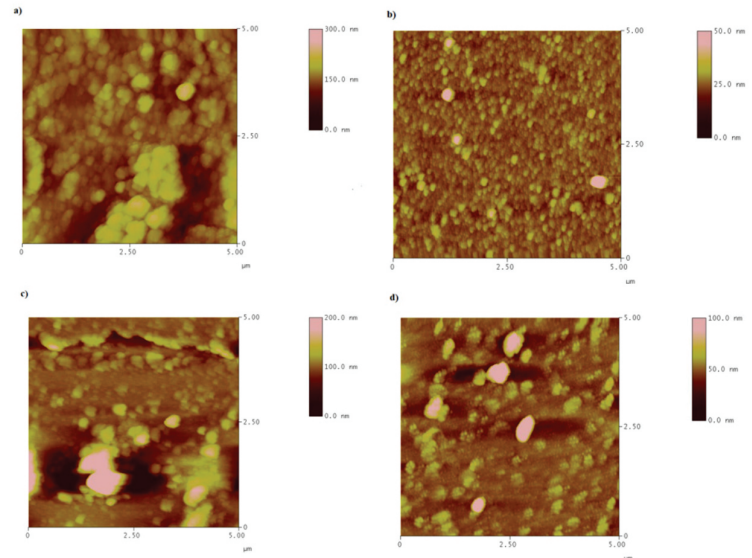


Figure 1 AFM images of a) pristine and 50keV Nitrogen irradiated NiO thinfilms at fluences a) $5*10^{15}$, c) $1*10^{16}$ d) $5*10^{16}$ ions/cm².

References:

[1] V Chauhan, D Gupta, N Koratkar and R Kumar, Scientific Reports.11(2021) 17672.

5.2.20

Sulfur ion irradiation studies on PNP transistors at different biasing conditions

Darshan M.¹, Arshiya Anjum¹, Pushpa N.², Meena R. C.³, Ambuj Tripathi³ and Gnana Prakash A. P.^{1*}

¹Department of Studies in Physics, University of Mysore, Manasagangotri, Mysore-570 006, India.

²Department of PG Studies in Physics, JSS College, Ooty Road, Mysore-570 025, India.

³Inter University Accelerator Centre, Aruna Asaf Ali Marg, New Delhi-110 067, India.

Integrated circuits (IC's) are miniature electronic circuits that are made up of millions of semiconductor devices such as transistors, diodes, resistors etc. IC's are the building block of modern electronics and has numerous application. Transistors are biased in certain required ways in these IC's according to the application. Space is an extreme environmental condition filled with energetic photons and charged particles that can cause severe degradation in the performance and operating life of the semiconductor devices and intern leads to the failure of space missions [1-2]. Thus, it's important to study the reliability of these devices before employing them.

The PNP transistors were exposed to 100 MeV sulfur ions (S^{8+}) in 15 UD Pelletron Accelerator at Inter University Accelerator Centre (IUAC), New Delhi, India. The irradiation was performed at different biasing conditions (0V, +1V and -1V) with fluence ranging from $1.34*10^9$ ions/cm² to $2.68*10^{11}$ ions/cm² with current of 0.15 pA (particle nanoampere) which is equivalent to a dose range of 300 krad(Si) to 60 Mrad(Si). The ion irradiation and measurements were done *in-situ* to avoid the time dependent annealing of radiation defects created in the device. The experimental chamber was maintained at a vacuum of 10^{-6} mbar. The key electrical parameters like Gummel characteristics, excess base current ($\Delta I_B = I_{Bpost} - I_{Bpre}$), dc current gain (h_{FE}), output characteristics and collector saturation current (I_{CSat}) were studied as a function of total dose, and some of the results are shown below. Variation of current gain for 100 MeV S^{8+} ion irradiated PNP transistor biased at +1V is shown in Fig. 1. It can be observed in Fig. 2 that the degradation in electrical parameters is more for the devices irradiated at +1V and -1V than at 0V due to the combined effects of irradiation and biasing. The reason attributing to this is increased thermal gradient due to the application of electric field which causes damage to the device by creating cracks and dislocations in the material. When the transistors were biased during irradiation the generated charge carriers due to irradiation are accelerated due to applied electric field this leads to the increase in the current density in collector base region leading to the creation of local hotspots which increases the thermal resistivity. In transistors, the degradation in current gain due to biasing during irradiation highly depends on transistor geometry. The emitter base and collector base depletion regions play a crucial role by providing larger area for recombination of generated charge carriers due to irradiation.

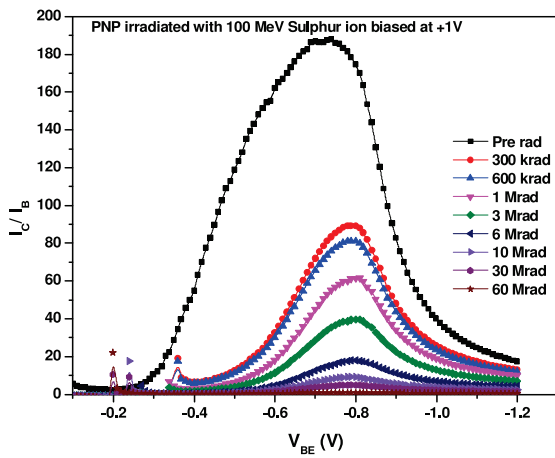


Fig. 1 Variation of current gain for 100 MeV S^{8+} ion irradiated transistors biased at +1V.

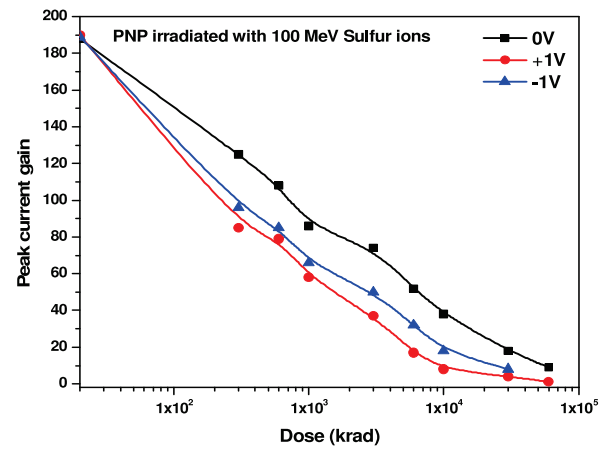


Fig. 2 Variation of peak current gain for 100 MeV S^{8+} ion irradiated transistors biased at 0V, +1V and -1V

References:

- [1] Schafer, Benjamin Carrion, and Zi Wang. IEEE Trans. on Computer-Aided Design of Integ. Circ. and Syst. 39 (2019) 2628-2639.
- [2] Hegde, Vinayakprasanna N., K. C. Praveen, T. M. Pradeep, John D. Cressler, and AP Gnana Prakash. Microelectronics Reliability 137 (2022) 114754.
- [3] Johnston, A. H., G. M. Swift, and B. G. Rax. IEEE transactions on nuclear science 41 (1994) 2427-2436.

5.2.21

A comparison of low temperature and room temperature swift heavy ion irradiation effects on N-channel MOSFETs

Arshiya Anjum¹, Darshan M.¹, Pushpa N.², Meena R. C.³, Ambuj Tripathi³, Gnana Prakash A. P.^{1*}

¹Department of Studies in Physics, University of Mysore, Manasagangothri, Mysore-570006, India.

²Department of PG Studies in Physics, JSS College, Ooty Road, Mysore-570025, India.

³Inter-University Accelerator Centre (IUAC), Aruna Asaf Ali Marg, New Delhi-110067, India.

The electronic systems which operate under adverse ambient conditions that lie outside the domain of commercial or even military specifications are called as extreme environment electronics (EEE). The N - channel depletion metal oxide semiconductor field effect transistors (MOSFETs) are the fundamental components for many EEE applications which requires the devices to operate reliably for a long time at extreme temperatures and radiation harsh environments. The incident ionizing radiation can cause an accumulation of charges to build up at the sensitive interface i.e., at Si/SiO₂ and thereby degrade the performance of the devices [1]. Thus, it is very important to study the radiation response of MOSFETs at different temperatures.

The MOSFETs were exposed to 80 MeV Nitrogen ions (N^{6+}) at room temperature (300 K) as well as low at temperature (100 K) at Inter University Accelerator Centre (IUAC), New Delhi in the fluence range of 2.4×10^9 to $7.14 \times 10^{11} N^{6+}$ ions/cm². The corresponding equivalent dose is 100 krad to 30 Mrad and the devices were grounded during irradiation. The electrical characterizations were done before and after irradiation at 300 K using Keithley dual source meter 2636A. The electrical characteristics of MOSFET such as threshold voltage (V_{th}), density of oxide trapped charges (ΔN_{ot}), density of interface trapped charges (ΔN_{it}), transconductance (g_m), mobility (μ) and leakage current (I_L) were studied as a function of total dose. The low temperature irradiation results were compared with the room temperature irradiation results. Fig. 1 and Fig. 2 respectively depict the variation in V_{th} and μ of MOSFETs irradiated with N^{6+} ions at 300 K and 100 K. A significant decrease in V_{th} and μ was observed after irradiation due to the creation of interface and oxide trapped charges at the Si/SiO₂ interface of the device [2]. From the results, it is observed that the MOSFETs irradiated at 300 K show more degradation than devices irradiated at 100 K. This is because at low temperatures the thermal energy of electrons decreases and thus they freeze out in the valence band only, resulting in the very less number of charge carriers for the conduction. Hence, the MOSFETs show significant radiation hardness at low temperatures.

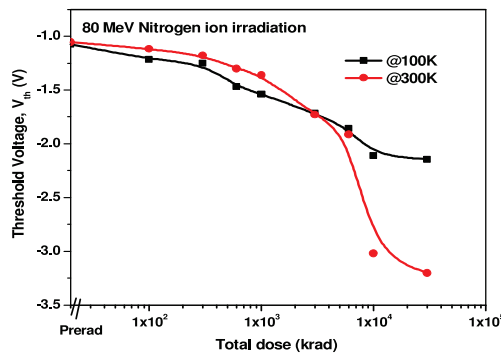


Fig. 1: Variation in V_{th} with total dose at 300K and 100K

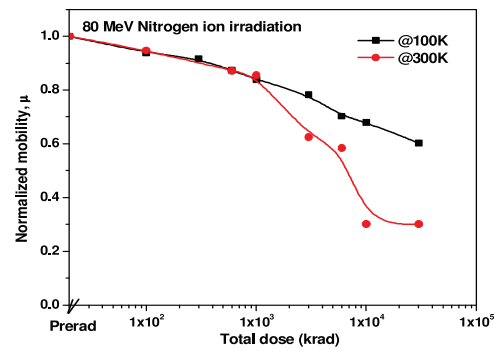


Fig. 2: Variation in μ with total dose at 300K and 100K

References:

- [1] V. N. Hegde, K. C. Praveen, T. M. Pradeep, J. D. Cressler and A. P. Gnana Prakash, Microelectronics Reliability 137 (2022) 114754.
- [2] Arshiya Anjum, T. M. Pradeep, V. N. Hegde, N. Pushpa, Ambuj Tripathi and A. P. Gnana Prakash, IEEE Transactions on Device and Materials Reliability 9 (2019) 696-703.

5.2.22 Cryogenic temperature effects on NPN transistors irradiated with 80 MeV Nitrogen ion

Darshan M.¹, Arshiya Anjum¹, Pushpa N.², Meena R. C.³, Ambuj Tripathi³ and Gnana Prakash A. P.^{1*}

¹Department of Studies in Physics, University of Mysore, Manasagangotri, Mysore-570 006, India.

²Department of PG Studies in Physics, JSS College, Ooty Road, Mysore-570 025, India.

³Inter University Accelerator Centre, Aruna Asaf Ali Marg, New Delhi-110 067, India.

Semiconductor devices are used in various applications such as communication systems, navigation systems, power systems and in scientific instruments such as gamma ray telescope used to detect high energy radiation from distant objects etc. Transistors are one of the widely used semiconductor devices in space applications due to their high linearity, small size, low power consumption and switching speed. The devices operating in space environment are prone to radiation effects and other extreme environment effects such as extreme high and low temperatures, corrosive and pressure gradient condition etc. which can cause degradation to the electrical parameters of the device. Thus, it is very important to evaluate the radiation hardness of these devices for different radiations under different extreme environmental conditions [1-2].

In the present study the transistors were exposed to 80 MeV nitrogen ions (N^{6+}) using 15 UD Pelletron Accelerator at Inter University Accelerator Centre (IUAC), New Delhi, India. The irradiation was performed at room temperature and at cryogenic temperature (100 K) with the dose range of 300 krad(Si) to 60 Mrad(Si) which is equivalent to fluence ranging from 7.15×10^9 ions/cm² to 1.43×10^{12} ions/cm² with current of 0.5 pA (particle nanoampere). The experimental chamber was maintained at a vacuum of 10^{-6} mbar and all the terminals of the transistors were grounded during the irradiation. The key electrical parameters like Gummel characteristics, excess base current ($\Delta I_B = I_{Bpost} - I_{Bpre}$), dc current gain (h_{FE}), output characteristics and collector saturation current (I_{CSat}) were studied as a function of total dose. Fig. 1 shows the current gain degradation of NPN transistor irradiated with 80 MeV N^{6+} ions at 100 K temperature and Fig. 2 shows the variation in peak current gain for different doses for room temperature and 100 K irradiated transistors. It can be observed that the degradation in electrical parameters is more for the devices irradiated at low temperature than at room temperature. This is due to the reduced mobility of charge carriers, increased trapped charge effect, surface damage, and increased phonon scattering at low temperature [3]. At low temperature, the mobility of charge carriers reduces due to low thermal energy. This decrease in mobility can lead to a reduction in the transistor current and an increase in the resistance which in turn increases the number of trapped charges in the device structure.

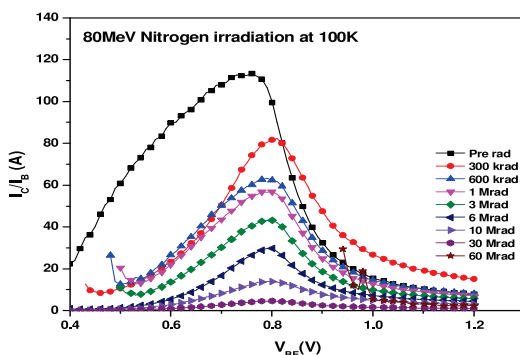


Fig. 1 Variation of current gain for 80 MeV N^{6+} ion irradiated transistors at 100 K.

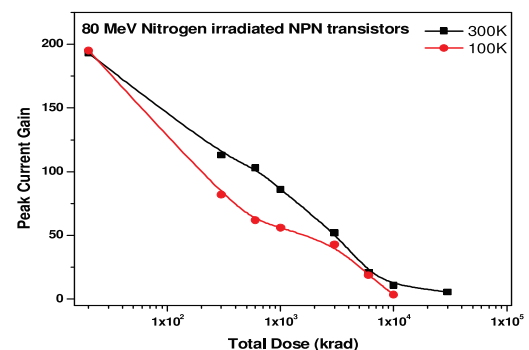


Fig. 2 Variation of peak current gain for 80 MeV N^{6+} ion irradiated transistors at 300K and 100 K.

References:

- [1] Sotskov, Denis I., Vadim V. Elesin, Alexander G. Kuznetsov, Nikita M. Zhidkov, Igor O. Metelkin, Konstantin M. Amburkin, Dmitry M. Amburkin, Nikolay A. Usachev, Dmitry V. Boychenko, and Varvara V. Elesina. *IEEE Trans. on Nucl. Sci.* 67 (2020) 2396-2404.
- [2] Pradeep, T. M., Vinayakaprasanna N. Hegde, N. Pushpa, Ambuj Tripathi, K. Asokan, and A. P. Gnana Prakash. *Rad. Eff. and Def. in Solids* 174 (2019) 859-872.
- [3] Asheghi, M., Y. K. Leung, S. S. Wong, and K. E. Goodson. *Applied Physics Letters* 71 (1997) 1798-1800.

5.2.23

The effect of gate biasing during swift heavy ion irradiation on N-channel depletion MOSFETs

Arshiya Anjum¹, Darshan M.¹, Pushpa N.², Meena R. C.³, Ambuj Tripathi³, Gnana Prakash A. P.^{1*}

¹Department of of Studies in Physics, University of Mysore, Manasagangothri, Mysore-570006, India.

²Department of PG Studies in Physics, JSS College, Ooty Road, Mysore-570025, India.

³Inter-University Accelerator Centre (IUAC), Aruna Asaf Ali Marg, New Delhi-110067, India.

Metal–oxide semiconductor field-effect transistors (MOSFETs) are extensively used in space applications because of their faster switching speeds and simple drive requirements when compared to bipolar transistors. The charged particles being abundant in space (like protons, electrons and heavy ions) can incident on MOS devices, and deposit their energy in the device structure via two modes i.e., electronic ionization and atomic displacements, producing ionization and displacement damage, respectively. The ionizing radiation primarily affects the insulating layer i.e. SiO₂ and Si/SiO₂ interface of MOSFETs. Ionization damage produce oxide traps and interface traps in SiO₂ and Si/SiO₂ interface respectively, resulting in the device degradation. The density of these trapped charges is greatly dependent on the bias voltage applied during the irradiation, and they too can modify the overall charge-dependent properties of MOS devices [1]. Therefore, it is very interesting and essential to study the gate polarization effects on MOSFETs during irradiation.

The 100 MeV Sulphur ion (S⁸⁺) irradiation was carried out at Inter University Accelerator Centre (IUAC), New Delhi, India. The devices were irradiated with different gate biases ($V_{GS} = -4, 0$ and $+4$ V) at room temperature. The irradiation experiments were conducted at different radiation fluences ranging from 4.47×10^8 to 4.47×10^{11} S⁸⁺ ions/cm² with different gate biases as mentioned above. The corresponding equivalent dose is 100 krad to 100 Mrad and the beam current was of the order of 0.15 pA. The electrical characterizations were done before and after irradiation at 300 K using Keithley dual source meter 2636A. The electrical characteristics of MOSFET such as threshold voltage (V_{th}), density of oxide trapped charges (ΔN_{ot}), density of interface trapped charges (ΔN_{it}), transconductance (g_m), mobility (μ) and leakage current (I_L) were studied as a function of total dose at different gate voltages. The obtained results were compared with the different biasing voltages applied during irradiation. Fig. 1 represents the subthreshold characteristics of MOSFETs irradiated with 100 MeV S⁸⁺ ions at $V_{GS} = 0$ V. It can be observed from the figure that as the radiation dose increases the drain current (I_D) swings towards the negative gate voltage. A similar trend was observed for the devices irradiated at $V_{GS} = +4$ and -4 V. But the drain current became leaky after 30 Mrad of total dose for the devices irradiated at $+4$ V. Therefore, the V_{th} of 100 MeV Sulphur ion irradiated MOSFETs was measured up to 30 Mrad of total dose only. The Fig. 2 depicts the variation of V_{th} with respect to total dose for 100 MeV Sulphur ions irradiated MOSFETs at different bias voltages. It can be seen that the gate bias during irradiation enhances the device degradation. Also, the degradation in V_{th} is more for the positive gate biased ($V_{GS} = +4$ V) MOSFET. This is because when the devices are positively biased, the radiation-induced electron-hole pairs can not recombine and results in the large amount of charge yield. Hence, the maximum degradation was observed for the devices irradiated at positive bias to the gate.

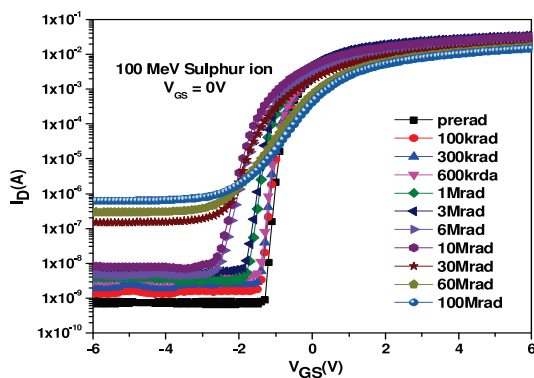


Fig. 1: Variation in V_{th} with total dose at 300K and 100K

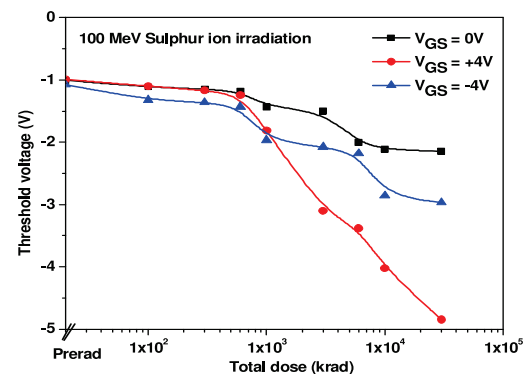


Fig. 2: Variation in μ with total dose at 300K and 100K

References:

- [1] Jianqun Yang, Xingji Li, Chaoming Liu and D. M. Fleetwood, *Microelectronics Reliability* 82 (2018) 124-129.
- [2] A. P. Gnana Prakash, S. C. Ke and K. Siddappa, *Semicond. Sci. Technol.* 18 (2003) 1037–1042.

5.2.24 Swift Heavy Ion Irradiation Studies on SrTiO₃ Thin Film-Based Resistive Switching Devices

Amit Kumar Shringi¹, Mubashir Mushtaq Ganaie² and Mahesh Kumar¹

¹Department of Electrical Engineering, Indian Institute of Technology Jodhpur, Jodhpur-342030, India.

²Department of Physics, Indian Institute of Technology Jodhpur, Jodhpur-342030, India.

Resistive random-access memory (RRAM) is an emerging non-volatile memory (NVM) technology have huge potential to replace conventional flash memories for storage applications. Moreover, these devices offer a high tolerance towards the harsh radiation environment and hence can be game changers as a dense and compact memory option for memory applications in such conditions as nuclear plants and space. The current flash technology offers radiation resistance only upto a dose of a few krad thus these devices show abrupt behaviour in radiation-prone areas and need radiation-hard packaging of the device which further increases the cost and size. Besides that, the other charge base memories are also radiation sensitive with further downscaling. The limitations of these memory technologies to working in radiation harsh conditions result in the unavailability of high-density and fast memories. Hence there is a great demand for radiation-hard NVM technologies to be deployed in such environments to perform stable memory operations. For radiation stability analysis the RRAM devices have been explored and tested for different ionic radiation environments. Metal oxides including TiO₂, ZnO, HfO₂, BiFeO₃ and BaTiO₃ have been widely studied for radiation stability in various electronic device applications and the results show the potential of these materials to be used in such conditions. The radiation exposure alters the structural properties and stoichiometry due to irradiation upto a certain level and the higher exposure may lead to data loss in RRAM devices. Hence heavy ion irradiation with lower fluence can affect the device's performance and their retention capabilities. Furthermore, the CBRAM where the metal ion migration through the switching layer governs the filament formation and dissolution also offer the radiation hard RRAM performance. The perovskite oxide layers including LaFeO₃, BaTiO₃ and AlFeO₃ have been used as switching layers for resistive switching applications. [1-2] There are very few studies on the irradiation effect on perovskite oxide-based RRAM and it needs to be explored more for their use in a radiation harsh atmosphere. As resistive switching is a trap-assisted and vacancy-governed phenomenon, radiation exposure can significantly improve the device performance. We explore the radiation stability of SrTiO₃ thin film-based RRAMs against the varying fluence of swift heavy ions. Therefore, SrTiO₃ thin films were exposed to the Au⁹⁺ ions of 120 MeV energy for a different fluence of ions by varying the exposure time. Further, the surface morphological and RRAM properties were investigated concerning the ion exposure. The performances of the fabricated devices before and after irradiation were compared and analysed for the various performance parameters of RRAM.

We observe that the average surface roughness is drastically reduced as the irradiation fluence was increased. The highest roughness has an irregular pattern concerning influence and it was 126 nm, 117 nm, 99 nm, and 107 nm for pristine, 3.3×10^{11} ions/cm², 6.6×10^{12} ions/cm² and 1×10^{13} ions/cm² respectively. The average surface roughness was 12.32 nm, 10.69 nm, 9.49 nm, and 7.65 nm for devices pristine, 3.3×10^{11} ions/cm², 6.6×10^{12} ions/cm² and 1×10^{13} ions/cm² respectively. The devices show stable RRAM performance even after the irradiation for the voltage sweep from -4 V to 1.5 V for more than 200 cycles. However, there is a significant reduction in the switching ratio from 655 (pristine) to 10 (1×10^{13} ions/cm²) but the retention curves reveal the stable data retention capability irrespective of irradiation for a period of about 8000 seconds. The abrupt switching behaviour changes to soft filament formation as the ion fluence increases showing the potential for neuromorphic application. A significant reduction after irradiation also confirms the reduced power consumption. The stable performance after irradiation and the same operating voltage proves the potential of these devices to be used in radiation harsh environment.

References:

- [1] Amit Kumar Shringi, Atanu Betal, Satyajit Sahu, and Mahesh Kumar, "Write-once-read-many-times resistive switching behavior of amorphous barium titanate based device with very high on-off ratio and stability", Appl. Phys. Lett. 118, 263505 (2021)
- [2] Amit Kumar Shringi, Atanu Betal, Satyajit Sahu, Michael Saliba and Mahesh Kumar, "Resistive Switching and Synaptic Behavior of Perovskite Lanthanum Orthoferrite Thin Film for Neuromorphic Computing", IEEE Transactions on Electron Devices, 69(11)(2022), pp. 6465-6470.

5.2.25 A Study of the Co-doping Effect on the Thermoluminescence Properties of Nanocrystalline SrSO₄:Dy,Er

Anant Pandey¹, Devanshi Sharma¹, Birendra Singh², Ambuj Tripathi²

¹Department of Physics, Sri Venkateswara College, University of Delhi, Benito Juarez Marg, New Delhi-110021.

²Inter-University Accelerator Centre, Aruna Asaf Ali Marg, New Delhi-110067.

In order to study the thermoluminescence (TL) property of nanophosphors for ion beam dosimetry, strontium sulphate doped/co-doped with different lanthanides was synthesized using the chemical co-precipitation technique [1]. In order to prepare the nanophosphor, the following salts: strontium nitrate (AR, 99.9%), ammonium sulphate (AR, 99%), and dysprosium (III) chloride hexahydrate were used as starting materials in the correct stoichiometric ratio because of their high solubility in water. Initially, SrSO₄ doped solely with Dy was prepared. In co-precipitation procedure, the resultant precipitate obtained after mixing the reactants was washed using centrifuge machine and then dried on a heating mantle for 4 hours. The obtained sample was subjected to annealing at 900°C for 2 hours. Different concentrations of Dy ranging from 0.1 mol% to 0.5 mol% were synthesized and irradiated with gamma rays from a Co-60 source with a test dose of 10 Gy to investigate dopant concentration optimization. After analyzing the TL response of all the concentrations, it was found that the optimized concentration was 0.3 mol% for Dy.

After optimizing the concentration, the nanophosphor's response to different gamma-radiation doses ranging from 10 Gy to 7 KGy was studied. The nanophosphor was further irradiated with carbon ion beams of two different energies i.e. 65 MeV and 85 MeV at 5 different fluences for each energy and with 1 pA current using 15 UD Pelletron tandem accelerator at the Inter-University Accelerator Centre (IUAC), New Delhi [2]. Further to enhance the nanophosphor's thermoluminescence efficiency vis-à-vis its suitability for ion beam dosimetry, the nanophosphor was co-doped with erbium. The co-doped nanophosphor was prepared with the following dopant concentrations: [Dy (0.2 mol%), Er (0.1 mol%)], [Dy (0.15 mol%), Er (0.15 mol%)], [Dy (0.1 mol%), Er (0.2 mol%)]. Their TL response was studied and investigated for enhancing our understanding of the physical process involved in the TL emission.

References:

- [1] Bahareh Samariha and Khadijeh Rezaee Ebrahim Saraee, Journal of Luminescence Volume 198, June 2018, Pages 389-399
- [2] Kanika Sharma, Shaila Bahl, Birendra Singh, Pratik Kumar, S.P. Lochab and Anant Pandey, Radiation Physics and Chemistry, Volume 145, April 2018, Pages 64-73

5.2.26

Study of low energy negative ion implantation on ZnO-based inorganic/organic hybrid thin films for optoelectronic device applications

M S Abdul Azeez¹, Gnyaneshwar Dasi¹, Thyda Lavanya¹, Koppula Naresh¹, Kuppuswamy Thangaraju¹

¹Organic optoelectronic device laboratory, Department of Physics, National Institute of Technology Warangal-506004, India

Alq₃ incorporated ZnO (Alq₃/ZnO) hybrid thin films were prepared by cost effective sol-gel derived spin-coating process to study its impact on optoelectronic properties and subsequent optoelectronic devices such as Solar cells, OLED, and UV Photodetector. The sol-gel derived spin-coated pristine ZnO and Alq₃/ZnO hybrid thin films were deposited at room temperature using the precursor solutions preparation as mentioned in the previous report [1]. These films were characterized for their optical, structural, and morphological studies using the UV-visible, XRD, SEM, and Photoluminescence (PL), Hall effect measurement. The Hall effect measurements at room temperature show that the conductivity increases while increasing Alq₃ content. It is also evident from UV-vis spectroscopy that transparency takes a hit with an increase in Alq₃ concentration. The XRD analysis showed that the [002] peak intensity is decreasing with increase in Alq₃ concentration. The incorporated Alq₃ molecules may preferably be adsorbed at the grain boundaries of ZnO crystallites along the plane (002) orientation having the higher surface energy and SEM characterization reveals the particle morphology in the hybrid thin film ascertains the adsorption of Alq₃ molecules at the grain boundaries of ZnO and formation of Alq₃ complex molecules capped ZnO nanoparticles. The change in the morphological features of hybrid thin films with increasing Alq₃/ZnO molar ratio is in support of decreasing crystallite size in the XRD studies [2]. The result demonstrates a significant influence on the optoelectronic properties with the Alq₃ incorporation ZnO, prompting the performance of optoelectronic devices fabricated with these samples [2].

In order to investigate the effects of the low energy implantation on the structural, optical, and electrical properties of ZnO and Alq₃ incorporated ZnO hybrid thin films, we fabricated these films by spin coating method at NIT Warangal. The speed and acceleration time was fixed to be 2000 rpm for 30 secs respectively. After phase analysis, the films were implanted at Inter University Accelerator Centre (IUAC), New Delhi with 25 keV O⁺ ions at three different ion fluences i. e. 5×10¹⁴ ions/cm², 1×10¹⁵ ions/cm² and 5×10¹⁵ ions/cm² with current of 700 nA. Silver (Ag) and aluminum (Al) ions were also implanted onto a different set of these films at 50 keV with ion fluences 5×10¹⁵ ions/cm², 1×10¹⁶ ions/cm² and 5×10¹⁶ ions/cm² with current of 850 nA. All the films were fixed to the target ladder placed inside the high vacuum (10⁻⁶ torr) chamber during irradiation. Implantation was performed in the direction perpendicular to the sample surface. The ion beam

was focused to a spot of 10 mm diameter and then scanned over an area of $1 \times 1 \text{ cm}^2$ using magnetic scanner to cover the complete sample surface for uniform irradiation. To investigate the structural changes because of the irradiation, we have carried out the optical, and XRD measurements of the irradiated thin films at room temperature at our home institute NITW. To study the effects on electrical, and magnetic properties of the implantation the other measurements and analysis are under process.

References:

- [1] Gnyaneshwar Dasi, R Ramarajan and Kuppaswamy Thangaraju, AIP Conference Proceedings 060015(2018), doi:10.1063/1.502875
- [2] Gnyaneshwar Desi, R Ramarajan, D. Paul Joesph, S. Vijayakumar, Jae-Jin Shim, M. Arivananthan, R. Jayavel, Kuppaswamy Thangaraju, Thin solid films 710 (2020) 138265.

5.2.27 Effects of 120 MeV Ag^{9+} swift heavy ion irradiation on the structural, optical and electrical properties of pristine and Ni doped BiFeO_3 thin films grown by pulsed laser deposition

M. Nadeem^a, Wasi Khan^b, Shakeel Khan^a, Fouran Singh^c, R.J. Choudhary^d, S.R. Sahu^d, Sumesh Rana^d, R. Venkatesh^d, D.K. Shukla^d and Shahid Husain^b

^aDepartment of Applied Physics, Z.H. College of Engineering & Technology, Aligarh Muslim University, Aligarh 202002, India.

^bDepartment of Physics, Aligarh Muslim University, Aligarh 202002, India.

^cInter-University Accelerator Centre, Aruna Asaf Ali Marg, New Delhi 110067, India.

^dUGC-DAE Consortium for Scientific Research, Khandwa Road, Indore 452017, India.

In order to investigate the effects of the swift heavy ion (SHI) irradiation on the structural, optical, and electrical properties of BiFeO_3 and Ni-doped BiFeO_3 thin films, the targets of composition $\text{BiFe}_{1-x}\text{Ni}_x\text{O}_3$ ($0 \leq x \leq 0.07$) were synthesized via sol-gel method. [1] In this work, the effects of swift heavy ion (SHI) irradiation on the structure, morphology, and optical and electrical properties of pristine and Ni-doped BiFeO_3 thin films have been explored. The thin films with composition of $\text{BiFe}_{1-x}\text{Ni}_x\text{O}_3$ ($x = 0, 0.01, 0.03$, and 0.05) were deposited on the n-type single crystal Si(100) substrates through pulsed laser deposition technique. Further, irradiation on the thin films was performed with 120 MeV Ag^{9+} ions at different ion fluences, i.e. 1×10^{13} , 5×10^{13} and 1×10^{14} ions/cm². To investigate the effects of SHI irradiation on the aforementioned properties, all the films have been characterized by various analytical techniques, such as X-ray diffraction (XRD), Raman spectroscopy, atomic force microscopy, scanning electron microscopy, energy dispersive X-ray spectroscopy, UV-visible diffuse reflectance spectroscopy, and using a two-probe resistivity setup. The effects of the irradiation on the crystal structure and phase of the thin films were analyzed by the XRD and Raman measurements, and it has been observed that irradiation tends to amorphize the thin films. A decrease in the band gap has been observed for the irradiated thin films with the increase of ion fluence. The current-voltage plots of all the unirradiated and irradiated thin films demonstrate the rectifying diode type characteristics. [2].

References:

- [1] M. Nadeem, Wasi Khan, Shakeel Khan, Mohd Shoeb, Shahid Husain and Mohammad Mobin, Mater. Res. Express 5 (2018) 065506.
- [2] M. Nadeem, Wasi Khan, Shakeel Khan, Fouran Singh, R.J. Choudhary, S.R. Sahu, Sumesh Rana, R. Venkatesh, D.K. Shukla and Shahid Husain, Thin Solid Films 760 (2022) 139487.

5.2.28 Electrical and optical properties of Cu ion implanted TiO_2

Subhashree Sahoo¹ Indra Sulania², and Pratap K. Sahoo¹

¹School of Physical Sciences, National Institute of Science Education and Research (NISER) Bhubaneswar, An OCC of Homi Bhabha National Institute, Jatni-752050, Khurda, Odisha, India.

²Inter University Accelerator Centre, New Delhi 110067, India.

TiO_2 is a wide band gap n-type semiconductor with a wide range of applications starting from photocatalysis to resistive switching devices. The electrical and optical properties of this material can be improved by inserting suitable dopants into it. Ion implantation is a suitable technique to dope the material upto desired thickness. In resistive switching devices, defects (oxygen vacancy) plays a significant role as it make a conducting path in the sample. So by ion implantation we can create defect that lead to improve the conductivity of the samples. Again, the Fano effect, which arises due to interference between continuous electronic states and discrete phonon states can be tuned by playing with the concentration of charge carriers in the conduction band.

To study the optical and electrical properties of TiO_2 , we synthesized TiO_2 thin film using RF sputtering deposition technique. The prepared sample was amorphous in nature, so we annealed the sample in muffle furnace for one hour at 400°C . It is well known that the conductivity can be improved by inserting proper elements into the host material. The main purpose of this work is to study the Resistive switching behavior of the anatase TiO_2 thin films. We implanted Cu in the fluence range 1×10^{15} – 2×10^{16} ions/ cm^2 . The XRD and Raman spectroscopy data revealed the pure anatase phase of the samples. The surface morphology of samples was studied using AFM. The AFM image of TiO_2 thin film before and after Cu ion irradiation (2×10^{16} ions/ cm^2) is presented in figure 1(a) and (b) respectively. It is observed that the roughness of samples increases from 0.21 nm to 2.8 nm with ion irradiation. For the study of optical properties, we collected the UV-visible spectra of the pure and Cu ion irradiated samples. Figure 2(a) shows the absorbance spectra of pristine and 2×10^{16} ions/ cm^2 Cu ion implanted TiO_2 . The optical band gap of samples were calculated using Tauc plot as shown in figure 2(b). The band gap is observed to be decreased from 3.8 eV to 3.7 eV upon incorporation of Cu into the TiO_2 matrix. The reduced bandgap is attributed to formation of midgap states. It is reported that the incorporation of Cu into the TiO_2 may substitute the Ti atom, hence creating defects. It is also probable that some oxygen vacancy will be created in the samples.[1] These defects may enhance the conductivity of the TiO_2 matrix. We are on the way to fabricate the resistive switching devices and study the effect of these implanted ions on the electrical properties of the samples. In addition, we are planning to study effect of dopants on optical properties, mainly the Fano effect, and anharmonicity using Raman spectroscopy.[2]

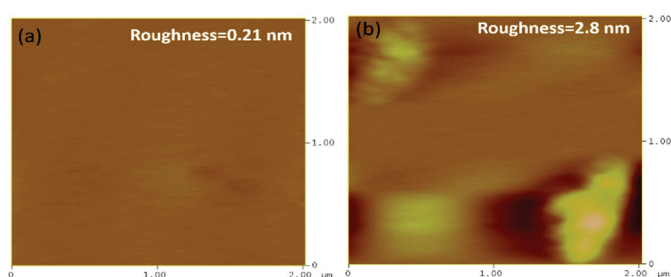


Fig 1: AFM image of (a) Pristine TiO_2 (b) 2×10^{16} ions/ cm^2 Cu implanted TiO_2

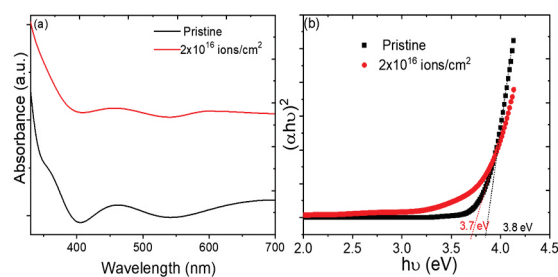


Fig 2: (a) Absorbance and (b) Tauc plot of pristine and 2×10^{16} ions/ cm^2 Cu implanted TiO_2

References:

- [1] Subhashree Sahoo, Gurupada Ghorai, Kalyan Ghosh, Bidyadhar Das, Mrinal K Sikdar, and Pratap K Sahoo, AIP Advances, 11(10) (2021)105013.
- [2] Subhashree Sahoo and Pratap K Sahoo, Journal of Applied Physics 133 (2023)144301.

5.2.29

Reaction-Diffusion-Driven Stoichiometric Gradient in Coevaporated Superconducting NiBi_3 Thin Films

Bidyadhar Das¹, Tapas Ranjan Senapati¹, Ashok Kumar Yadav², G. R. Umamathy³, Sambhu Nath Jha⁴, Kartik Senapati¹, and Pratap Kumar Sahoo¹

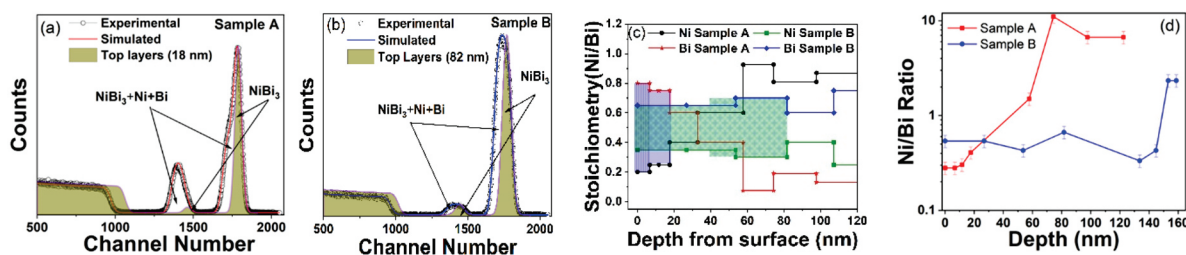
¹School of Physical Sciences, National Institute of Science Education and Research, An OCC of Homi Bhabha National Institute, Jatni 752050 Odisha, India.

²Atomic and Molecular Physics Division, BARC, Mumbai 400085, India.

³Inter University Accelerator Centre, New Delhi 110067, India.

⁴Beamline Development and Application Section, BARC, Mumbai 400085, India.

NiBi and NiBi_3 are the two thermodynamically stable intermetallic alloys of Ni-Bi system with melting temperatures 742 K and 927 K respectively. Interestingly, both the alloys are superconducting with superconducting transition temperatures of 4.25 K and 4.1 K respectively. Further, NiBi_3 phase has gained attention in the scientific community because of the special properties of co-existence of superconductivity and ferromagnetism where the same electrons are responsible for both superconductivity and ferromagnetism. The synthesis process of NiBi_3 phase plays an important role in the describing its superconducting and magnetic property. Polycrystalline and single crystal NiBi_3 in bulk form are fabricated using solid state method wherein the mixture of Ni and Bi in the ratio 1:10 is annealed at a temperature of 1373 K for many hours in a furnace. In case of thin film, polycrystalline NiBi_3 is synthesized when Ni film is deposited on Bi film or vice-versa. It is spontaneously formed at the interface of Ni-Bi by diffusion of Bi into Ni matrix irrespective of the higher radius of Bi. Since the melting temperature of Bi is very less (544 K) than that of Ni (1728 K), Bi is more mobile in the Ni matrix and diffuses to form NiBi_3 alloy. However, there is no control over the diffusion process and NiBi_3 is formed non-uniformly at the interface. Therefore, the synthesis of a single NiBi_3 thin film with filtering of excess Ni and Bi remained a challenge.



Experimental and simulated RBS spectra of (a) sample A (b) sample B (c) Depth profile from simulated RBS spectra (d) Ni/Bi ratio from (c)

In this work, for the first time, we have co-deposited Ni and Bi simultaneously by varying the deposition rate of Bi (0.2 and 0.4 Å/s) and keeping the deposition rate of Ni fixed (0.1 Å/s). Sample with deposition of Ni (0.1)Bi (0.2) is addressed as Sample A whereas that with deposition Ni(0.1)Bi(0.4) is addressed as Sample B. Field emission scanning electron microscopy (FESEM), X-ray diffraction (XRD) technique, Rutherford backscattering spectrometry (RBS), X-ray absorption spectroscopy (XAS), SQUID based magnetometer, Physical property measurement system (PPMS) were used to characterize the samples. The XRD pattern shows the presence NiBi₃ phase in addition to Ni and Bi phases in both the samples. However, the relative intensity of NiBi₃ increases with respect to Ni and Bi in case of higher Bi deposition rate signifying the decrease in impurity Ni and Bi. RBS data of both samples show that a thicker NiBi₃ layer (82 nm) is formed for higher Bi deposition rate whereas a very few nm (10 nm) of stoichiometric NiBi₃ is formed with non-linear variation towards the substrate for lower Bi deposition rate. The analysis of XAS data also signifies the reduction in Ni phase with increase in the content of NiBi₃ phase for higher Bi deposition rate. A sharp superconducting transition is observed for higher Bi deposition rate whereas the transition has a width for lower Bi deposition rate. Most importantly, the superconducting transition temperature is enhanced for higher Bi deposition rate. The presence of non-stoichiometric NiBi₃ and higher percentage of Ni impurity lowers the transition temperature of lower Bi deposition rate. The magnetic measurements of both the samples show ferromagnetic behavior in the temperature range 5 K-300 K. However, the coercive field significantly decreases for higher Bi deposition rate signifying the transition towards soft ferromagnetic phase. The fitting of coercive field versus temperature shows that the sample with lower Bi deposition rate is fitted by exponentially decaying curve whereas the curve for sample with higher Bi deposition rate fits well with strong pinning behavior below 50 K whereas weak pinning behavior dominates at higher temperatures. Thus, the variation of Bi deposition rate in co-deposition technique results in the synthesis of thicker NiBi₃ film with reduction in impurity Ni and Bi and enhancement in the superconducting transition temperature (for details see J. Crys. Growth, 23, (2023), 2, 980-988.

References:

- [1] Bidyadhar Das¹, Tapas Ranjan Senapati¹, Ashok Kumar Yadav², G. R. Umaphathy³, Sambhu Nath Jha⁴, Kartik Senapati¹, and Pratap Kumar Sahoo¹ J. Crys. Growth, 23, (2023), 2, 980-988

5.2.30

Irradiation induced interface and magnetic study of Zinc ferrite/insulator/cobalt ferrite multilayers

Sanjeev Gautam^a, Shaffy Garg^c, Ramcharan Meena^b, Navdeep Goyal^c

^aAdvanced Functional Materials Lab., Dr. S. S. Bhatnagar University Institute of Chemical Engineering & Technology, Panjab University, Chandigarh, 160 014, India

^bMaterials Science Division, Inter-University Accelerator Centre, New Delhi - 110 067, India

^cDepartment of Physics, Panjab University, Chandigarh 160 014, India

The objective of the research project proposal (UFR-63323) spanning from June 26, 2018, to June 25, 2022, is to synthesize and characterize oxide multilayers for their potential application in magnetic tunnel junctions (MTJ). The thin film targets are prepared using optimized synthesized powder samples, and thin films are fabricated and optimized using an RF/DC sputtering machine at the host lab facilities at Panjab University. However, due to COVID-19, there was a delay in the fabrication process, and the preliminary investigation for the modification in interface properties of the multilayers was carried out on January 27-28, 2022, during the allocated beamtime at IUAC, New Delhi. Systematic characterization of the multilayers, including high-resolution X-ray diffraction (HRXRD) and X-ray reflectometry (XRR), as well as X-ray absorption spectroscopy-total fluorescence yield (XAS-TFY), was conducted during beamtime allocation at Indus-II, RRCAT, Indore. HRXRD measurements were performed on selected samples at the 8D POSCO beamline of Pal, South Korea. The results were analyzed and compiled for potential publication.

A book chapter “Design of ferrite based magnetic tunnel junction, Shaffy Garg, Jatinder Pal Singh, Keun Hwa Chae, K. Asokan, Navdeep Goyal, Sanjeev Gautam” to the Elsevier book entitled “Ferrite

nanostructured magnetic materials: Technology and Applications” (ISBN:9780128237182) Edited by J.P. Singh et. al has been published.

5.2.31 **Dissolution of Mg(OH)₂ by swift heavy ion irradiation in CoFe₂O₄/MgO/ZnFe₂O₄ multilayer thin films**

Sanjeev Gautam¹, Shaffy Garg^{1, 2}, Mandeep Kaur^{1, 2}, Anshu Gupta³, Ramcharan Meena⁴, Suvankar Chakraverty³, Young Hwa Jung⁵, Jitendra Pal Singh⁶, Navdeep Goyal²

¹*Advanced Functional Materials Lab., Dr. SSB UICET, Panjab University, Chandigarh, 160 014, India*

²*Department of Physics, Panjab University, Chandigarh 160 014, India*

³*Institute of Nano Science & Technology, Sector-81, Mohali, Punjab, India*

⁴*Inter-University Accelerator Centre, New Delhi, India*

⁵*Pohang Accelerator Lab, Pohang University of Science and Technology, Pohang, South Korea*

⁶*Manav Rachna University Faridabad, Haryana, India*

This study aims to resolve the issue of impurity formation in metallic multilayer thin films used for magnetic tunnel junctions (MTJs) and hence enhancing the interface sharpness. A single target system was utilized to form the multilayer, and swift heavy ion irradiation was used to dissolve the impurity phases that were formed due to lower vacuum in the RF sputtering system. Pristine MgO/Si(100) thin films and CoFe₂O₄/MgO/ZnFe₂O₄/Si(100) multilayer thin films were prepared using the RF sputtering technique. These thin film structures were irradiated with 75 MeV oxygen-ion fluence and 200 MeV silver-ion fluence to investigate structural modifications. High-resolution X-ray diffraction (HRXRD) revealed that the MgO thin film had impurity peaks that were dissolved by O-ion and Ag-ion irradiation, but the Ag-ion irradiation was more intense and made the samples almost amorphous. The multilayer stack of cobalt-ferrite/MgO/zinc-ferrite is irradiated with Ag-ion at 1x10¹² ions/cm² showing that Mg(OH)₂ phase was completely dissolved, and only a less intense (311) peak corresponding to the ferrite structure appeared. However, the O-beam dissolves the impurity phases in a controlled manner. This behaviour of both beams is also explained by the SRIM simulation. The study demonstrates that SHI-irradiation can effectively dissolve impurities in a controlled manner, potentially reducing the cost of MTJ production by eliminating the need for a multi-targeted system and improving MTJ efficiency by improving interface properties.

This work completes the main objective of the research project, i.e. improving the interface properties to enhance the MTJ efficiency of the multilayer stacks.

The IUAC-UGC project for beamtime utilization (UFR-63323) is duly acknowledged along with IUAC collaborator Dr. K. Asokan/Mr. Ramcharan Meena in these publications.

5.2.32 **Influence of Low Energy Ion Irradiation on Hafnium Oxide Thin Films**

Sikta Mandal¹, Udai P. Singh¹ and Pravin Kumar

¹*School of Electronics Engineering, KIIT Deemed to be University, Bhubaneswar-751024, India*

²*Materials Science Division, Inter-University Accelerator Centre, New Delhi- 110067, India*

The aim of the proposed work is to understand in a better way whether hafnium oxide (HfO₂) can be used as a material for non-volatile memory and to establish a physical mechanism (carrier mediated and defect mediated) for it. For this, firstly, the HfO₂ films have been deposited on silicon substrates by atomic layer deposition. Next, the presence or absence of oxygen vacancies needs to be investigated by XPS measurement. ZnO has already been explored widely [1]. Not much literature exists on HfO₂. However, resistive switching property attributed to oxygen vacancies has been reported recently. It seems that oxygen vacancy profile plays an important role in exhibiting the property in oxides. [2]. Thus, HfO₂ has been chosen for further systematic studies.

In order to investigate the same thin films of HfO₂ have been deposited on both p- silicon and n- silicon substrates by both Thermal ALD and Plasmonic ALD processes. Two sets of films were deposited n-Si and two other sets were deposited on p-Si. The sets of films differed in thickness. The n-Si Set 1 consisted of films having 100 nm thickness and Set 2 consisted of films having 200 nm thickness. It was similar for the sets of films deposited on p-Si. The films were then irradiated using Low Energy Ion Beam Facility (LEIBF) at Inter-University Accelerator Centre (IUAC) using Xe⁸⁺ with a current of 1μA. The n-Si sets were irradiated at different ion fluences of 7 e14, 9 e14, and 1 e15 ions/cm² and the p-Si sets were irradiated using different fluences of 1.5 e15, 2 e15, and 2.5 e15 ions/cm². All the films were fixed to the target ladder placed inside the high vacuum chamber during irradiation. Irradiation was performed in the direction perpendicular to the sample surface. The ion beam was focused to a spot of 10 mm diameter and then scanned over an area of 1×1 cm² using magnetic scanner to cover the complete sample surface for uniform irradiation. To investigate the structural changes and the effects on optical and electrical properties because of the irradiation, we have

carried out the XRD, UV and Hall Effect measurements of the irradiated thin films at room temperature at Thin Film Photovoltaic Lab, KIIT University. For surface roughness and defect analysis, we have used the AFM and FTIR measurements at IUAC, New Delhi.

References:

- [1] D. K. Mishra, P. Kumar, Manoj Kumar Sharma, J. Das, S. K. Singh, B. K. Roul, S. Varma, Ratnamala Chatterjee, V. V. Srinivasu, D. Kanjilal; *Physica B* 405; 2010; 2659–2663.
- [2] Manoj Kumar Sharma, Dilip Kumar Mishra, Sabyasachi Ghosh, Dinakar Kanjilal, Pankaj Srivastava, Ratnamala Chatterjee; *Journal of Applied Physics* 110; 063902; 2011; 1-7.

5.2.33 Effects of gamma radiation on structural, optical, and electrical properties of SnO₂ thin films.

Rashmi Kajal^{1*}, B.R. Kataria², K. Asokan^{3,4}, Devendra Mohan¹

¹ Department of Physics, Laser Laboratory, GJUS&THisar 125001, Haryana, India

² Department of Nano Science and Advanced Materials, Saurashtra University, Rajkot 360 005, India

³ Materials Science Division, Inter-University Accelerator Center, Aruna Asaf Ali Marg, New Delhi 110067, India

⁴ Department of Physics & Centre for Interdisciplinary Research, University of Petroleum and Energy Studies (UPES), Dehradun, Uttarakhand, 248007, India

The objective of the present research is to look into the structural changes and alteration of morphological, optical, and electrical properties of n-type tin oxide thin films with gamma radiation. The powder precursor of tin oxide SnO₂ (purity 99.99%) from Sigma Aldrich was used to prepare the target. A 20 mm pellet was prepared and sintered the target at 1200°C for 24 hours in the air. Finally, films were deposited on the FTO substrate by maintaining 400 temperature via the pulsed laser deposition (PLD) method, and the target-to-substrate distance was kept at 4cm inside the chamber.

The SnO₂ films having a thickness of 200 nm were irradiated for the doses, (0, 75, 100, 125, and 200 kGy) using a ⁶⁰Co gamma source, the 1200 Gamma Chamber, installed at the Inter-University Accelerator Centre, New Delhi having a dose rate of 2.029 kGy/hr. X-ray diffraction was carried out in SmartLab 3kW Make-Rigaku for all samples in the range of 2θ between 20° and 80° using the CuKα radiation (λ=1.54059Å). The Raman spectroscopy was carried out in the system Alpha300/WITec. Optical characterization was performed by using an ultraviolet-visible spectrometer (Hitachi UV-3300) in the range of 200–800 nm. The I-V measurements were carried out at ±5V after gamma irradiation at various temperatures. The I-V characteristics were measured in two probe setups using the Keithley source electrometer (model-6517B) at a different temperature range from 270K to 400K using a silver paste to make contacts. The Hall measurement van der Pauw method was carried out at room temperature in a magnetic field of 0.5 T using a Hall effect measurement system at IUAC, New Delhi.

5.2.34 Structural, Optical, and dielectric characteristics of PLD deposited SnO₂-TiO₂ composite thin films

Rashmi Kajal^{1*}, K. Asokan^{2,3}, B.R. Kataria³, Pankaj Solanki^{4,5}, Devendra Mohan¹

¹ Department of Physics, Laser Laboratory, GJUS&THisar 125001, Haryana, India

² Material Science division, Inter-University Accelerator Center, Aruna Asaf Ali Marg, New Delhi 110067, India

³ Department of Physics & Centre for Interdisciplinary Research, University of Petroleum and Energy Studies (UPES), Dehradun, Uttarakhand, 248007, India

⁴ Department of Nano Science and Advanced Materials, Saurashtra University, Rajkot 360 005, India

⁵ Department of Physics, Saurashtra University, Rajkot 360 005, India

The main objective of this report is to study the impact of TiO₂ content in SnO₂ thin film where the PLD method was used to obtain SnO₂ and TiO₂:SnO₂ (75%, 25%) composite thin films. A 20mm pellet was prepared with SnO₂ and sintered the target at 1200°C for 24 hours in air rich environment. Finally, films were deposited on the FTO substrate by maintaining 400 temperature via the pulsed laser deposition (PLD) method, and the target-to-substrate distance was kept at 4 cm inside the chamber. X-ray diffraction was carried out in SmartLab 3 kW Make-Rigaku for all samples in the range of 2θ between 20° and 80° using the CuKα radiation (λ=1.54059 Å). The Raman spectroscopy was carried out in the system Alpha300/WITec. The Hall measurement van der Pauw method was carried out at room temperature in a magnetic field of 0.5 T using a Hall effect measurement system at IUAC, New Delhi.

5.3 ACCELERATOR MASS SPECTROMETRY AND GEOCHRONOLOGY

5.3.1 Palaeo-Geomorphic Features and The Environment: A Study of Sai-Ganga Interfluve, Uttar Pradesh, India

Shashi Shekhar Shukla¹, Padmini Pani¹, and Rajveer Sharma²

¹Centre for the Study of Regional Development, Jawaharlal Nehru University, New Delhi, India

²Inter University Accelerator Centre, New Delhi, India

Paleo-geomorphic features are geological structures or landforms that were formed in the past and are still preserved in the present-day landscape. These features provide valuable information about the history of an area in terms of past environmental conditions, climate changes, and geological events that have shaped the earth's surface in geological times. In this study, the palaeo-geomorphic features of Sai-Ganga interfluve have been explored. The study area has an abundance of palaeo-geomorphic landforms like- palaeochannels, crevasses splay, palaeo-oxbow lakes etc.

Apart from mapping these palaeo-landforms, it is also necessary to establish the geochronology of such landforms. In this study, two geochronological methods are being used. In the case of landscape dating, radiocarbon dating can be used to determine the age of various features in the landscape, such as peat bogs, alluvial deposits, and glacial moraines. In this study, the sediment samples have been collected from alluvial deposits of palaeo-channels, oxbow lakes, and palaeo-crevasses splay for OSL and radiocarbon dating.

In the first batch of the analysis, a total of 12 samples were pre-processed for radiocarbon dating. Two samples were rejected due to very low carbon content. A total of 10 samples were graphitized for the AMS analysis. One radiocarbon date has been established for each of the ten sampling trenches made in the field at selected sites. The calibrated age ranges between ~5000 to ~27000 years cal BP for various landforms at varying depths. The radiocarbon dates suggest that most of the palaeochannels in the area were active before 12000 cal BP. The oldest date was achieved for Umran Tal, as ~27000 cal BP at a depth of 3 meters. Based on the obtained dates, it is evident that the palaeo-geomorphic features in the study area have preserved the geological records at least as far back as the late Pleistocene.

5.3.2 Understanding the ¹⁴C Dynamics in the Terrestrial and Aquatic Ecosystem

Sabyasachi Rout¹, Sonali Yadav¹, Madhav K. Murari², Rajveer Sharma², Vandana Pulhani¹

¹Bhabha Atomic Research Centre, Mumbai, India

²Geochronology, Inter-University Accelerator Centre, New Delhi, India

¹⁴C in the environment is derived from both natural sources (Cosmic) and anthropogenic activities (atmospheric nuclear weapon testing & from Nuclear fuel cycle). Increased input of carbon dioxide in the atmosphere due to anthropogenic activities like fossil fuel burning, deforestation, industrial growth etc., has disturbed the distribution and dynamics of carbon isotopes in the environmental matrices [1-3]. Seawater is the main sink for atmospheric carbon dioxide and ¹⁴C/¹²C ratios in marine biota are prime indicators of impact of climate change. Soil is the main interface between atmosphere, hydrosphere, lithosphere and biosphere. ¹⁴C dynamics in soils are governed by several physical processes (eg. soil structure, soil aggregation, soil erosion), chemical processes (eg. sequestration by soil components either mineral or organic) and soil biological processes (eg. Microbes, fauna, soil biochemistry). The relative importance of such processes varied remarkably among the various biomes and with change in region [2-3]. Though many studies are reported in literature on ¹⁴C in environment, there is still a lack of understanding of the dynamics of newly assimilated ¹⁴C to plants, soil, aquatic system, lost to the atmosphere and aquatic systems. To understand the environmental transport/dynamics of ¹⁴C, ¹⁴C/¹²C ratio in all the matrices forming part of the dynamic chain is required. Comparison of the isotopic ratios in different matrices give information about the source, transport pathways and age of assimilated C. Furthermore, understanding ¹⁴C dynamics would allow a realistic modelling of the accidental release of ¹⁴C by nuclear industry, which in turn would be useful in Radiological Environmental Impact Assessment (REIA). To fulfil this requirement the study was planned to understand the ¹⁴C dynamics in biosphere and develop a mathematical model for ¹⁴C dynamics in environment. For better understanding and development of ¹⁴C dynamic model large set of data (¹⁴C/¹²C ratio) from each of the compartments and matrices involved is required. In the preliminary stage for the study, 17 samples from different matrixes such as: soil (2no's), sediment (1), vegetation (5 no's) air (2 no's) water (3 no's) and fish (4 no's) were analysed using accelerator mass spectroscopy (AMS) facility at Inter University Accelerator Centre (IUAC), New Delhi. Before, AMS analysis, samples were processed and graphitised using graphitisation facility at IUAC. Though the no. of samples analysed is very less to achieve the objective of this study, preliminary results were helpful to estimate the ¹⁴C isoflux to the atmosphere and its effect on ¹⁴C isoflux to the atmosphere. Isoflux is derived using equation 1.

$$\text{Isoflux} = \text{Flux (Carbon)} \times \Delta^{14}\text{C}_{\text{DIS}} \quad (1)$$

Where, $\Delta^{14}\text{C}_{\text{DIS}}$ is the difference between reservoir and atmosphere (%). This isoflux is used to calculate the changes in ^{14}C atmospheric budget as presented in equation 2.

$$\frac{dC_a \Delta a}{dt} = F_r (\Delta_r - \Delta_a) + F_{oa} (\Delta_{oa} - \Delta_a) + F_{ff} (\Delta_{ff} - \Delta_a) + F_c (\Delta_c - \Delta_a) + F_n (\Delta_n - \Delta_a) \quad (2)$$

Where, C_a is atmospheric CO_2 burden, F_r is CO_2 flux out of the terrestrial biosphere, F_{oa} is flux from ocean to atmosphere, F_{ff} is flux to the atmosphere from fossil fuel emissions, F_c is flux from natural cosmogenic production of ^{14}C and F_n flux due to atmospheric nuclear weapon testing and nuclear power plant industries and Δ is ^{14}C value of the denoted flux. The calculated values of isoflux (presented in Table 1) were found lower than the earlier reported value of post bomb period (in 1995), which indicates a decreasing trend of difference between reservoir and atmosphere (%). [4].

Table 1: Estimated ^{14}C isoflux and its impact on $\Delta^{14}\text{CO}_2$

Reservoir	Reported Flux F to atmosphere (Pg C y ⁻¹) [4]	$\Delta^{14}\text{C}$ difference (%)	Isoflux (Pg C %o y ⁻¹)	Impact on $\Delta^{14}\text{CO}_2$ (%o y ⁻¹)
Ocean (Ocean to atmosphere)	85±21	-55.405	-4709±1163.5	-5.25±1.296
Terrestrial Mangroves	52±11	24.089	1252±265	1.4±0.295
Terrestrial Mango leaves	52±11	6.077	316±66.8	0.35±0.074
Nuclear weapon Testing	8E-13	8.5E14	680	0.757
Cosmogenic Production	6.5±8E-13	8.5E14	5525±680	6.15±0.757
Fossil Fuels	6.4±0.6	-995	-6368±597	-7.1±0.665

The impact of isoflux on atmospheric $^{14}\text{CO}_2$ is calculated assuming CO_2 mixing ratio of 421 ppm, preliminary inferred that, ^{14}C atmospheric budget trending towards pre bomb era. However more data is required to confirm this hypothesis. Though, it is possible to derive the transfer factor of ^{14}C from source compartment to sink compartment, more samples need to be analysed. Moreover, more data with a good statistics from each matrices is needed for the development of the model.

List of publication

1. Estimation of ^{14}C isoflux to the atmosphere: Impact on atmospheric $\Delta^{14}\text{CO}_2$. Sonali Yadav,

Sabyasachi Rout, Madav K. Murari, Rajveer Sharma, Amol. Chandrakar, Vandana Pulhani, A. Vinod Kumar. (Accepted for DAE-BRNS symposium on Nuclear and Radiochemistry-2023)

References:

- [1]. https://www.irs.n.fr/EN/Research/publications-documentation/radionuclides_sheets/environment/Documents/Carbone_UK.pdf
- [2]. Dynamics of Carbon 14 in soils: A review, C. Tamponnet. *Radioprotection*, Suppl. 1, vol. **40** (2005) S465-S470
- [3]. Radiocarbon and Soil Carbon Dynamics, Susan Trumbore. *Annu. Rev. Earth Planet. Sci.* 2009. 37:47–66
- [4]. Turnbull, J.C., Graven, H., Krakauer, N.Y. (2016). Radiocarbon in the Atmosphere. In: Schuur, E., Druffel, E., Trumbore, S. (eds) *Radiocarbon and Climate Change*. Springer, Cham. https://doi.org/10.1007/978-3-319-25643-6_4

5.3.3

Validation of Liquid Scintillation Spectrometry-Based Carbon-14 (^{14}C) Measurements Techniques by AMS and Development of Reference Materials for Environmental Monitoring Applications around Nuclear Power Plants

Arya Krishnan K.¹, Bharath¹, Pankaj Kumar,² Sundeep Chopra², Karunakara N^{1*}

¹Centre for Advanced Research in Environmental Radioactivity (CAREER), Mangalore University, Mangalagangothri, 574199, India

²Inter-University Accelerator Centre, Aruna Asaf Ali Marg, Near Vasant Kunj, New Delhi, 110067, India

Carbon-14 (^{14}C) is a pure beta emitter ($T_{1/2} = 5730 \pm 40$ y, $E_{\text{max}} = 156.5$ keV) and occurs naturally in the environment due to cosmic ray induced production in the atmosphere. The long-term mean value of specific activity of natural atmospheric carbon has been determined to be 226 ± 1.1 Bq of ^{14}C per kg of carbon (Bq kg⁻¹ ^{14}C) in the air-borne CO_2 which is equal to 100% pMC (percent of modern carbon) with the year 1950 as the

reference date (Karlén et al., 1964; Libby, 1965; Stenström et al., 2000; Roussel-Debet et al., 2006). This leads to an annual effective dose of $\sim 12 \mu\text{Sv}$ to man (UNSCEAR, 1977). Knowledge on the release rates of ^{14}C from nuclear facilities is essential because of its long half-life, environmental mobility, and ease of assimilation into living matter. ^{14}C is the most significant radionuclide released from a nuclear power plant (NPP) that will contribute significantly to the collective radiation dose to exposed population. The Centre for Advanced Research in Environmental Radioactivity (CARER), a national facility with the state-of-the-art facilities for radioecological studies, has undertaken a detailed study on ^{14}C around the NPP in India.

The main objectives of the present study includes (i) standardisation of method based on sample oxidation and Liquid Scintillation Spectrometry (LSC) based ^{14}C measurements and validation of it by AMS technique (ii) development of a secondary reference material which is specific and representative of the environment of nuclear power plants of India for use in radioecology laboratories of India. A method was optimized for the determination of ^{14}C in the ambient air with the development of a simple setup for the regeneration of CO_2 from carbonate sample and saturating the absorber in <45 min for direct determination of activity by liquid scintillation counting (LSC). A minimum detectable activity value of $14 \text{ Bq kg}^{-1}\text{C}$ for a counting time of 300 min ($8 \text{ Bq kg}^{-1}\text{C}$ for 1000 min) was achieved by this method. The validation of the method was performed by analysing (i) BaCO_3 precipitate obtained from the air samples by AMS at Inter-University Accelerator Centre, New Delhi (Pankaj Kumar et al., 2015; Rajveer Sharma et al., 2019), and (ii) IAEA quality assurance materials (IAEA C3, cellulose). The second objective of the project was to develop a reference material for ^{14}C for use in the environmental survey laboratories of India. In this regard, a “pre-bomb” wood material which has the potential to be developed as a reference material was identified. Subsamples of this wood material were analysed by AMS method at IUAC for the quantification of carbon-14. Carbon-14 analyses of the samples using Liquid Scintillation Spectrometry were performed at CARER and the results were observed to be in good agreement with the AMS data. Hence, the pre-bomb wood material which is available in bulk could be used as a secondary reference material.

method based on thermal oxidation and the LSC was standardised for the determination of ^{14}C activity in soil and sediment samples and quantification of excess activity in the vicinity of the nuclear facilities and validated through the AMS measurements. The method involves the following important steps: (i) combustion of the sample in a tube furnace system, (ii) trapping the CO_2 generated from the sample in NaOH solution, (iii) precipitation of absorbed CO_2 as BaCO_3 , (iv) regeneration of CO_2 by acid hydrolysis of BaCO_3 in a specially designed regeneration setup to saturate in an amine-based absorber, (v) mixing with a liquid scintillator, and (vi) liquid scintillation analysis. Upon optimisation of the method, its successful application to quantify small excess ^{14}C activity in the vicinity of the NPP was demonstrated by analysing soil samples collected from the Kaiga NPP region. Soil samples were collected from six locations in the vicinity of the Kaiga NPP and analysed by the method standardised in this study. The validation of the method was performed by analysing the aliquots of the samples by the AMS at IUAC, New Delhi. Soil samples from the clean-air region were analysed and this data was used for quantifying the excess ^{14}C activity in the vicinity of the NPP.

The ^{14}C specific activity results obtained from the LSC method, developed in this study, were in good agreement with the AMS data. The deviation of the results obtained from the LSC method was $<3\%$ in comparison with the AMS method which confirmed that the method standardised in this study is capable of yielding accurate results. The excess ^{14}C activity in the vicinity of the NPP was quantified in comparison with ^{14}C specific activity data for the samples collected undisturbed clean-air region. The maximum excess activity in soil was $10 \text{ Bq kg}^{-1}\text{C}$. The data conclusively demonstrate that the method standardized in the present study is suitable for assessing the impact of the NPP on the surrounding environment. The method standardized in the present study is also applicable to the analysis of sediment samples.

References:

- [1] Karlén, I., Olsson, I.U., Kiillberg, P., Kilicci, S., 1964. Absolute determination of the activity of two ^{14}C dating standards. *Arkiv for Geofysik* 4:465–471.
- [2] Kumar, P., Chopra, S., Pattanaik, J.K., Ojha, S., Gargari, S., Joshi, R., Kanjilal, D., 2015. A new AMS facility at Inter-University Accelerator Centre, New Delhi. *Nucl. Instrum. Methods Phys. Res. B.* 361, 115 - 119. <https://doi.org/10.1016/j.nimb.2015.03.078>.
- [3] Libby, W.F., 1965. *Radiocarbon Dating*. 2nd edition (1st Phoenix edition). Chicago: University of Chicago Press.
- [4] Roussel-Debet, S., Gontier, G., Siclet, F., Fournier, M., 2006. Distribution of carbon 14 in the terrestrial environment close to French nuclear power plant. *J. Environ. Radioact.* 87, 246–259.
- [5] Sharma, R., Umopathy, G.R., Kumar, P., Ojha, S., Gargari, S., Joshi, R., Chopra, S., Kanjilal, D., 2019. AMS and upcoming geochronology facility at Inter University Accelerator Centre (IUAC), New Delhi, India. *Nucl. Instrum. Methods Phys. Res. B.* 438, 124 - 130, <https://doi.org/10.1016/j.nimb.2018.07.002>.
- [6] Stenström, K., Erlandsson, B., Mattsson, S., Thornberg, C., Hellborg, R., Kiisk, M., Per Persson, P., Skog, G., 2000. ^{14}C emission from Swedish nuclear power plants and its effect on the ^{14}C levels in the environment. Internal report LUNDFD6/(NFFR-3079), Lund University.

[7] United Nations Scientific Committee on the effect of atomic radiation (UNSCEAR), 1977. Sources and effects of Ionizing radiation, United Nations, New York

5.3.4

Ventilation of Northern Indian Ocean during the last glacial-interglacial cycle

Kumari Nisha^{ab}, Sushant Suresh Naik^a, and Pankaj Kumar^c

^aCSIR- National Institute of Oceanography, Dona-Paula, Goa 403004, India

^bSchool of Earth, Ocean and Atmospheric Sciences, Goa University, Goa 403004, India

^cInter-University Accelerator Centre (IUAC), New Delhi 110067, India

In order to reconstruct the ventilation age changes in the northern Indian Ocean for the last glacial-interglacial cycle, AMS radiocarbon dating of foraminifera from a gravity core SSD-044/GC-01 (3160 m water depth), collected from northern Indian Ocean was carried out at the Inter-University Accelerator Centre (IUAC), India. Here the ventilation ages of deep water are reported as the radiocarbon age difference between paired bottom water-dwelling benthic foraminifera and surface-dwelling planktic foraminifera (B-P) based on Broecker et al., 1984, which represents deep-surface radiocarbon age offset. In order to cover the objectives of this research, samples from specific intervals such as Last Glacial Maximum (LGM), Henrich Stadial 1 (HS1), Bølling-Allerød (B-A), Younger Dryas (YD) and Holocene were used. The reconstructed benthic-planktic (B-P) ventilation ages for the deep water suggest that there have been many significant changes during the last 25 kyr. The apparent age difference between coexisting benthic and planktic foraminifera during the LGM was ~3000 ¹⁴C years indicating incursion of ¹⁴C-depleted deep water into the northern Indian Ocean. The observed poor ventilation during the last glaciation shows that the northern Indian Ocean was a part of the glacial ocean aged carbon pool. Similar to the LGM, deep-water ventilation in the northern Indian Ocean during the HS1 (~17.5-14.5 kyr BP) remained poor. At the start of the B-A (~14.5 kyr BP) there was an abrupt reversal in the ventilation age, decreasing to as low as ~1500 years indicating better ventilated water in the northern Indian Ocean at that time. During the YD (~12.8-11.5 kyr BP) there was again an increase of ~300 ¹⁴C years in ventilation age of the deep water. Ventilation age during the Holocene was less (~1500 year) indicating better ventilation water at the core site. This study thus supports the role of Southern Ocean in modulating atmospheric CO₂ variations during the last deglaciation. The output from this research has been published in Earth and Planetary Science Letters (IF: 5.785) titled '**Radiocarbon evidence for reduced deep water ventilation of the northern Indian Ocean during the last glacial maxima and early deglaciation**' (Nisha et al., 2023).

References:

- [1] Broecker, W., Mix, A., Andree, M., Oeschger, H., 1984. Radiocarbon measurements on coexisting benthic and planktic foraminifera shells: potential for reconstructing ocean ventilation times over the past 20 000 years. Nuclear Instruments and Methods in Physics Research Section B: Beam Interactions with Materials and Atoms, 5(2), 331-339.
- [2] Nisha, K., Naik, S.S., Kumar, P., Banerjee, B. and Murty, P.R., 2023. Radiocarbon evidence for reduced deep water ventilation of the northern Indian Ocean during the last glacial maxima and early deglaciation. Earth and Planetary Science Letters, 607, p.118067.

5.3.5

¹⁴C age dating of foraminifera and bivalve shells from the cold seep and oxygen minimum zone sediments

A. Mazumdar, A. Peketi, K. Siva, M. Sadique, A. Ghosh, S. Pavan, A. Zatale

Geological Oceanography, CSIR-National Institute of Oceanography, Donapaula, Goa-403004

Cleaned planktonic foraminifera samples were processed and analyzed at IUAC, Delhi, to determine ¹⁴C dates. The samples form different sediment cores from the oxygen minimum zone off the east coast of India and methane cold seep sites off the Krishna-Godavari and Mannar basins.

Radiocarbon dating is carried out in the core SSD065/GC1 collected from the oxygen minimum zone of the Bay of Bengal at water depths of 287 mbsl, and the core shows a distinct sedimentation pattern. Based on sediment type, the core may be subdivided into four zones (Olive green sediment zone: surface - 46 cmbsf, white calcareous sediment: 46 - 240 cmbsf, black sediment: 240 - 410 cmbsf, olive green sediment: 410 - 600 cmbsf). The core ages of the sediment range from 19.468 - 42.125 Ka. The top 46 cm of olive green sediment deposited within 19.5 ka during suboxic bottom water condition is characterized by moderately high CRS (pyrite, 0.15 - 1.25 wt %) and reactive iron content (0.18 to 1.77 wt %) but low TIC content (0.5 - 3 wt %). The low concentration of calcium carbonate in this zone may suggest high influx of terrigenous material after the sea level rise during the post-glacial period. The white calcareous sediment zone deposited during 19.5 - 35.7 Ka (~46 to 245 cmbsf) is characterized by high TIC content (6.5 - 10.27 wt %) but low CRS (0.002 - 0.8 wt %) and reactive iron content. The deposition of this sediment zone rich in biogenic material probably took

place during the Last Glacial Maximum (LGM) in the late Pleistocene. The high biogenic calcium carbonate concentration during LGM may be related to high productivity as well as reduced terrigenous supply. Furthermore, the low pyrite content in the zone may be due to low organic matter content in the calcareous rich sediment, resulting in low sulfate reduction. The black color sediment zone (237 – 398 cmbsf) deposited during 35.7 – 42.1 Ka is characterized by relatively high CRS and reactive iron content but low TIC content. The black color of the sediment may be due to highly anoxic conditions that prevailed during 35 – 42 ka which is also evident from intense pyritization in the zone. Overall, the sedimentation pattern observed in the core suggests variable influence of terrigenous influx/ biogenic material during different periods. The sediment composition has a profound impact on the overall sediment biogeochemistry.

The radiocarbon dates off Mannar basin cold seep sites (SSD70-GC-5) ranges up to 34 kilo years and the sedimentation rate 26.45 cm/kyr (between 3.4 to 5.3 kyr B.P.) to 1.9 cm/kyr (between 5.7 to 18.5 kyr B.P.) with an average sedimentation rate of 13.06 cm/kyr. The TOC and TN values range from 1.2 to 10 wt % and 0.2 to 0.9 wt%, respectively. Between the time interval of 19-24 Kyr, i.e., the Last glacial maxima, both sedimentation rate and TOC content increases. The TOC and T.N. show parallel trends, and the strong positive correlation between these two parameters suggests that a large fraction of total nitrogen is dominantly organic bound. The average molar C/N ratio of the studied core is around 11.8 ± 2.12 (n=328), and the stable carbon isotope values of the organic matter range from -19.2 to -21.8 ‰. The C/N and the $\delta^{13}\text{C}$ values suggest a dominance of marine organic matter input to the sediment. This observation is further supported by the n-alkane distribution pattern where the short-chain n-alkanes dominate. The high TIC content (up to 8.36 wt %) throughout the core and much-depleted $\delta^{13}\text{C}$ values of the authigenic carbonate indicates AOM (Anaerobic Oxidation of Methane) related microbial processes taking place in this cold seep site.

The core SSD45/4/G4 from the cold seep region of the K-G basin contains methane hydrate and free methane gas. Mo isotopic and organic geochemical characterization are presently being carried out. Analysis of the radiocarbon dating (^{14}C) of planktic foraminifera suggests the core preserves a record of 35 kyr and the calculated sedimentation rate fluctuates between 6.89 to 39.18 cm/kyr. In the present study, we have measured n-alkane and Mo concentrations in the sediments along with isotope ratios of archaeal lipid biomarkers and Molybdenum (Mo). Multiple Mo concentration spikes were observed, possibly suggesting paleo-seepage activity which is further supported by Mo- isotope ratios. In sediments younger than approximately 13.5 kyr, enriched Mo isotope ratios correlate with Mo concentrations at some depth intervals, likely indicating paleo seepage activity. Conversely, below the age of 13.5 kyr sedimentation rate has increased from 7.65 cm/kyr to 38.9 cm/kyr at a depth of 460cm, which likely falls within the range of LGM corresponding to the depleted Mo isotope ratio and Mo concentration spike.

The core SSD45/4/G4 was subjected to organic geochemical analysis. The presence of methanotrophic archaeal lipid biomarkers, including irregular isoprenoids such as 2,6,10,15,19- pentamethylcosane (PMI) and Crocetane (2,6,11,15-tetramethyl hexadecane) along with isotopically depleted carbon isotope ratios (-118 to -80 ‰ VPDB) of lipid biomarkers signifies that anaerobic oxidation of methane (AOM) and enhanced abundances of methanotrophic archaeal biomass are governed by methane emission.

5.3.6 Development of Paleo-earthquake History in the western part of Central Seismic Gap along the Himalayan Frontal Thrust (HFT), Kumaun Himalaya: Multi-Dating approach

R. Jayangondaperumal^{1,2}, A. Brice¹, A. Pandey¹, P. S. Rao³, P. Kumar⁴, M. K. Murari⁴, S. Chopra⁴

¹Wadia Institute of Himalayan Geology, Dehradun

²Dept.of Geology, Central University of Punjab, Bathinda, Punjab

³Dept. of Geology, University of Delhi, New Delhi

⁴Geochronology project, Inter-University Accelerator Centre (IUAC), Delhi, India

Over the past 200 years, the northwestern Himalayan region has experienced numerous large earthquakes, which have been recorded both historically and through instruments. As a result, many studies have been conducted on active faults and paleoseismology in the area over the last few decades. The region between North-Central India and Western Nepal, known as the "Central Seismic Gap," (Khattari, 1987) has not experienced significant earthquakes recently but has been studied by several researchers in the last decade. However, the paleoearthquake history of the area remains unclear (e.g., Kumar et al. 2006; Jayangondaperumal et al. 2013; Rajendran et al. 2019). We excavated a trench across the fault scarp at Chourgalia town in Uttarakhand that will provide information on the timing of previous earthquake events. The age of these events will be determined using radiocarbon dating of charcoal fragments collected from the trench while comparing the concentration of cosmogenic radionuclides ^{10}Be and ^{26}Al from pebbles in the hanging and footwall of the trench will help match both walls. The presence of multiple layers in the trench suggests that there have been multiple earthquake events in the past. The radiocarbon dating has already been

completed at IUAC, which hints at a great medieval earthquake event. To infer the correlation between the units of the hanging wall and the footwall, nine bulk sediment samples were collected from the trench exposure. Along with these, three sediment samples were collected from the top of the hanging wall to correlate them with the trench units and to know whether they have a coeval depositional age.

The ^{10}Be concentrations were measured using two types of analysis, i.e. meteoric and in-situ. For the meteoric ^{10}Be concentration, the samples were sieved to collect the grains of size 75-125 μm in diameter. Approximately 2-3 g of sediment was collected for the chemical treatment. Of the collected sample, weighed sample between 0.8-1 g was taken. The samples were kept in vials with 10 ml 6N HCl overnight to react with CaCO_3 . They were then kept in a thermoshaker for ~5 hours at $\sim 80^\circ\text{C}$ at 500 RPM, with the lid of the vial kept a bit loose to let the gases pass. Once completed, the vials were centrifuged at 5000 RPM for 5 mins to settle the sediments at the bottom. The liquid was drained in a clean beaker (washed with soap water and MQ water). The residual solid was then filled with 10 ml MQ water and again centrifuged. The liquid was poured into the beaker, and the process was repeated three times. The collected liquid was then added with 2ml H_2O_2 to dissolve organic matter. The liquid was then dried on a heating plate, and the residual solid was added with 10 ml 1N HCl. Of this solution, 1ml was collected separately for ICPMS analysis and a ^9Be spike of known concentration was added to the rest of the solution, then dried on a heating plate. The dried sample was loaded for column separation. In column separation, anion and cation separation were carried out. The collected sample was then sent for further analyses to measure ^{10}Be concentration.

For in-situ ^{10}Be concentration analysis, the felsic pebbles were washed thoroughly and dried. The pebbles were then crushed to a size of 250-500 μm in diameter using rock crusher. The sample was then treated with 1N HCl and 1N HNO_3 acid solution for 24 hours to remove impurities, and then dried. The dried sample was then differentiated using magnetic separator to remove magnetic minerals.

Further analysis are ongoing at IUAC to infer the ^{10}Be concentration in the collected sediment samples that would be helpful in correlating the units of hanging wall and footwall. These inferences will be helpful in interpreting the precise age of the recent surface rupturing great earthquake event in the NW Himalayas.

References:

- [1] Khattri, K. N. "Great earthquakes, seismicity gaps and potential for earthquake disaster along the Himalaya plate boundary." *Tectonophysics* 138.1 (1987): 79-92.
- [2] Jayangondaperumal R., Thakur V.C., Joevivek V., Rao P.S., Gupta A.K. (2018) Active Faults of the Kumaun and Garhwal Himalaya. Springer Natural Hazards. Springer, Singapore-150pp. https://doi.org/10.1007/978-981-10-8243-6_3.
- [3] Kumar, Senthil, et al. "Paleoseismic evidence of great surface rupture earthquakes along the Indian Himalaya." *Journal of Geophysical Research: Solid Earth* 111.B3 (2006).
- [4] Rajendran, C. P., Sanwal, J., John, B., Anandasabari, K., Rajendran, K., Kumar, P., ... & Chopra, S. (2019). Footprints of an elusive mid 14th century earthquake in the central Himalaya: Consilience of evidence from Nepal and India. *Geological Journal*, 54(5), 2829-2846.

Papers under review in collaboration with IUAC:

1. Arjun Pandey, R. Jayangondaperumal, Ishwar Singh, Atul Brice, Rao Singh Priyanka, Atul Kumar, Pradeep Srivastava, Pankaj Kumar. "Possible surface rupture of the 1714 CE earthquake at the backthrust outboard of the Indo-Bhutan range front" under review in **Tectonophysics**.
2. Ishwar Singh, Arjun Pandey, Rajeeb Lochan Mishra, Rao Singh Priyanka, R. Jayangondaperumal, P. Morthekai, Pradeep Srivastava, V. Srivastava, Pankaj Kumar and Sundeep Chopra. "Holocene vertical uplift rate along the Mishmi Thrust, Eastern Himalayan Syntaxis strain partitioning in the outer deformation front of Mishmi hills, under review in **Tectonophysics**.
3. Atul Brice, R. Jayangondaperumal, Rao Singh Priyanka, Arjun Pandey, Rajeeb Lochan Mishra, Ishwar Singh, Yashpal Sundriyal, Pankaj Kumar, Sandipta Prasad Dash. "Basement topography controls the propagation of great earthquakes in the Himalaya: Insight from paleoseismology" under review in **Geology**.

5.3.7

Paleomonsoon and Paleoenvironment study using multi-proxy data from marine and lake archives

Gupta, Anil Kumar¹, Palar, Biswajit², Santra Abhijeet¹, Paul, Madhurima², Parhi Arpita¹, Ghosh Puja¹, Ghosh Mainak¹, Roul, Soumya Ranjan¹ and Kumar, Pankaj³

¹Department of Geology and Geophysics, Indian Institute of Technology Kharagpur, Kharagpur- 721302, India

²Centre for Ocean, River, Atmosphere and Land Sciences, Indian Institute of Technology Kharagpur, Kharagpur 721302, India

³Inter University Accelerator Center (IUAC), New Delhi.

The Indian Summer Monsoon (ISM) is a complex atmospheric phenomenon that depends on insolation,

ocean circulation and wind movements. In order to understand the past variability and intensity of the ISM over the Indian sub-continent, sediment cores were collected from ten lakes from eastern India. Total fourteen cores of length 5.10m, 3.5m, 1.06m, 1.36m, 1.12m, 4.88m, 6.30m, 5.11m, 5.94m, 5.02m, 0.85m, 0.35m, 1.44m and 0.38m were obtained from Hansadanga, Nowpara, Sartola, Karajgram, Mathura Beel, Duma Baor and Panchita-Chanda lakes, respectively, located in the Nadia, Burdwan and North 24 Pragma districts of West Bengal. Six cores of length 7.17 m, 14.93 m, 9 m, 11.70 m, 7.8 m and 7.5 m were obtained from Chilika, Anshupa and Tampara lakes in Ganjam and Cuttack districts of Odisha, respectively using gravity and auger drilling method. The samples are sub-sampled at 5 mm and some at 10 mm intervals. The age of 41 approved samples (including bulk sediments, gastropods and bivalvia) from different lakes was done at the AMS radiocarbon facility of IUAC, New Delhi. The Samples were finely crushed using mortar and pestle and sieved to remove the detrital materials and plant roots. Afterwards, sediment samples were pre-treated in the Graphitization laboratory of IUAC using Acid- Base- Acid treatment and the ages were determined using the techniques after Sharma et al., 2019. Some coarse samples with low organic carbon concentrations are sent to IISER, Kolkata, to determine age from the OSL dating method.

The West Bengal lakes are mostly oxbow lakes of the lower Ganga plain, mainly formed in the Holocene period. Hence, these lakes are a good indicator of extreme events like floods and droughts and are also used for paleo-geographical study. Hansadanga lake covers the age range up to 12000 cal yr BP, whereas the Karajgram has a bottom age of nearly 20000 cal yr BP. The Sartola and Mathura Beel lakes have the age of 1339 cal yr BP and 1490 cal yr BP at depths of 287 cm and 129 cm, respectively. The analysis of the bottom samples below the mentioned depth of the above two lakes may cover mid to lower Holocene age. Radiocarbon dates of Chilika lake sedimentary cores have provided an age range upto nearly 25000 cal yr BP to Recent. Similarly, the coastal lake Tampara shows the age interval from 10000 cal yr BP to Recent. The Fluvial freshwater lake Anshupa provides an age range of 6200 cal yr BP to Recent. The radiocarbon age of these lakes record several climate events like Dark Ages Cold Period (DACP), Medieval Climate Anomaly (MCA) and Little Ice Age (LIA), 4.2 ka and 8.2 ka events, Younger Dryas as well as the LGM.

The grain-size analysis of these lakes has been completed. Samples are prepared for other proxy records, including XRF, XRD, TOC, Pollen and Stable isotope study (e.g. ^{13}C), and analysis will be done soon to reconstruct the past climate and environments. We have approval for 50 samples for AMS ^{14}C dating, and the preparation of the samples is currently going on at IUAC, New Delhi. Also, we have the approval for additional 30 samples, which will be done later.

References:

- [1] Majumder, J., Gupta, A. K., Kumar, P., Kuppusamy, M., & Nirmal, B. (2022). Late Quaternary variations in the Oxygen Minimum Zone linked to monsoon shifts as seen in the sediment of the outer continental shelf of the eastern Arabian Sea. *Palaeogeography, Palaeoclimatology, Palaeoecology*, 110891.
- [2] Sharma, R., Umopathy, G.R., Kumar, P., Ojha, S., Gargari, S., Joshi, R., Chopra, S. and Kanjilal, D. (2019). AMS and upcoming geochronology facility at inter university accelerator centre (IUAC), New Delhi, India. *Nuclear Instruments and Methods in Physics Research Section B: Beam Interactions with Materials and Atoms*, 438, 124-130.
- [3] Arun Kaushik, Anil K. Gupta, Steven C. Clemens, Pankaj Kumar, Prasanta Sanyal, Priyantam Gupta, Manoj Kumar Jaiswal, Abhayanand S Maurya, Sreya Sengupta, Rajveer Sharma, Rahul Pawar (2023). Palaeoclimatic reconstruction of northwest Himalaya since CE 475 using lake sediments from Taday Taal, Kumaun region. *Palaeogeography, Palaeoclimatology, Palaeoecology*. **(Being revised)**.
- [4] Sreya Sengupta, Anil. K. Gupta, Manoj Kumar Jaiswal, Pankaj Kumar, Prasanta Sanyal, Shilpa Pandey, Dhruv Sen Singh, Arun Kaushik, Anoop Kumar Singh, Biswajit Palar, Rajveer Sharma, Vartika Singh (2023). Paleoclimatic shifts in the Central Ganga Basin, northern India since the middle Holocene: evidence from lake multiproxy data. *Quaternary Science Reviews*. **(Communicated)**.

5.3.8

Reconstruction of surface and subsurface hydrography variation records from the Bay of Bengal Sediments

Komal Shinde¹ and Mohan K.²

¹*School of Advance Sciences Vellore Institute of Technology, Chennai, India*

²*School of Civil Engineering Vellore Institute of Technology, Chennai, India*

The Indian monsoon is one of the most powerful and dynamic circulation systems. The society, economy and agriculture systems are depending upon the monsoon. It is also a major source of rivers fresh water in India and neighboring countries. Where the majority of rivers deposited enormous sediment input from the Himalayas and the peninsular river in the Bay of Bengal (BoB) which is depending upon the intensity of the Indian monsoon. The seasonal reversal monsoon currents govern the Southwest (SW) and Northeast (NE) monsoon over the BoB. This study presents high-resolution micro paleo on to logical and geochemical measurements from a continuous succession of sediment core SK 336/GC-2 (water depth 814 m and core

depth 5.56 m length) to understand variation in past productivity, surface and subsurface hydrographic structure in response to the monsoon precipitation from the BoB. The exploited marine sediment core is situated in the western BoB which receives more freshwater input and is thus ideally situated to capture Indian monsoon precipitation and fluvial runoff. Hence this may also be reflecting the monsoonal variability in terms of changes in terrigenous input. We studied temporal fluctuations in planktic foraminifera, relative abundances of ecologically sensitive groups and species, and microhabitat categories which are used to infer previous changes in the sea bottom environment and to comprehend how monsoon-induced primary productivity-driven organic matter export flux and externally derived deep-water masses affected the deep-sea environment at the core site. In order to understand this temporal variation, it is required to date the species to establish the chronological age of sediment layers and therefore we analyzed five accelerated mass spectrometry (AMS) radiocarbon dates including top and bottom were obtained from clean white mixed planktic foraminifera (*Globigerina bulloides*, *Globigerinoides ruber*, *Neogloboquadrina dutertrei*, *Globorotalia menardii*, *Trilobatus sacculifer*, *Trilobatus quadrilobatus*) shells at Inter-University Accelerator Centre (IUAC), New Delhi. Measured results for all the samples are normalized to the standard sample OX II, and AMS delta ^{13}C values are used for the isotopic fractionation correction. Background value during the measurement was (0.385 ± 0.018) pMC (Percentage modern carbon) and that corresponds to $^{14}\text{C}/^{12}\text{C}$ ratio $(4.2474 \pm 0.1983) \times 10^{-15}$. The result was obtained with the percentage of modern carbon (pMC) and radiocarbon age in BP. This is further converted into the calendar year by applying approximate reservoir correction through the Bacon calibration program in R software. The calendar age is covering 33,000 years BP to the present (modern age). To study the frequency shift in SW and NE monsoons over this period the geochemical analysis of the sample is under process.

5.3.9 Exposure Dating of Glacigenic Sediments in the Higher Himalaya, INDIA

Sharma M.C.¹, Manna Ishita², Vishwas Poonam³, Das Suresh⁴, Mandal Sandip Tanu⁵, Kumar Pawan⁶, Elora Chakraborty¹

¹Centre for the Study of Regional Development, Jawaharlal Nehru University, New Delhi- 110067,

²Ernst & Young Global Limited, Gurgaon- 122002,.

³Department of Civil Engineering, Delhi Technological University, New Delhi- 110042,

⁴Amity Institute of Social Sciences, Amity University India, Kolkata- 700135,

⁵Mobius Foundation, New Delhi- 110067,

⁶Choudhary Bansi Lal University, Bhiwani, Haryana.

Our research-work pertains to determining near-precise timing of climate phases using strong chronological techniques, to ascertain the synchrony, magnitude and style of climatic events for western Himalaya (Himachal and Uttarakhand). In our investigation and analysis of palaeo-landform records the Upper Beas, Upper Chandrabhaga and Upper Bhagirathi river basins, using TCN (10Be, 26Al), Radiocarbon (14C) and OSL Dose estimation and for constraining the ages, it emerges that the climatic gradient with reference to two weather systems over these basins, and with the terrain factors heavily limited the existence of sampling material needed for these three methods through removal, as well as limiting the deposits to very few places.

From the Upper Beas and Upper Chenab (Jankar Chhu and Milang) catchments, Himachal Pradesh, our team has collected and processed 19+16 samples for Quartz extraction for 10Be isotopic measurements using 500kV Pelletron™ tandem accelerator at IUAC. AMS measured isotopic ratio and Q ICP-MS measured 9Be and spike 9Be from facilities at IUAC has helped measure 10Be atom/gm in each sample and used subsequently in CREP (Cosmo Ray Exposure Programme). Through the process our team has been able to develop a novel technique² of isodynamically separating quartz and feldspar from processed samples with the addition of Fe powder and subsequent isodynamic separation. Field emission scanning electron microscopy (FE-SEM) and Isodynamic separation (Frantz make) facilities at IUAC have helped develop this robust methodology of efficiently separating both the mineral for CRN as well as OSL Dating. 15 samples were processed for 10Be using the abovementioned facilities and protocols to study the chronology of past glaciations in the Gangotri basin and also to understand the palaeoclimatic conditions prevalent in the monsoon dominated catchment of Uttarakhand. Furthermore, X-ray fluorescence (XRF) spectroscopy as well as Q-ICPMS facilities have been used for 28 osl samples for dose rate determination. 14C measurements through the 500kV Pelletron Accelerator was undertaken at IUAC for sediments as well as cellulose samples to understand the Holocene climate dynamics of the monsoon dominated Upper Beas Basin using standard ABA and the BABAB protocols.

Dates (using both OSL and CRN) from the Upper Beas have helped ascertain three stages of Quaternary glaciation while those from Upper Chenab reflect five. Rare earth analysis of 30 terrace samples from Upper Beas through Q ICP-MS has aided in ascertaining their antiquity. Furthermore, dose rate estimation for U, Th and K through XRF and Q ICP-MS at IUAC has helped establish the chronology of glaciation in Sikkim Himalaya². Continuing research in collaboration with IUAC aims to put together the event chronology of the Northwestern Himalaya with dates from the Chandra and Bhaga upper catchments in Lahaul with 20

approved samples for ^{10}Be and ^{26}Al calculation and 1 ^{14}C core collected from the field, undergoing processing.

List of PhD Thesis:

- Ishita Manna: "Reconstructing Glacial Phases and Palaeo-environment in a part of Upper Beas Basin, Himachal Pradesh"
- Poonam Vishwas: "Evolution and Modification of River Terraces in the Upper Beas Basin, Himachal Pradesh"
- Suresh Das: "Mapping Glacial Dynamics in the Jankar Chhu Watershed, Lahaul Himalaya"
- Sandip Tanu Mandal: "Glacier Dynamics and Palaeo-Reconstruction in Milang Watershed, Lahaul Himalaya, Himachal Pradesh"
- Pawan Kumar: "Assessing Glacial Dynamics over Time and Space: Rudugaira and Kalapani Bamak, Northwest Garhwal Himalaya"
- Elora Chakraborty: "Glacial Facies, Surface Velocity and Event Chronology in Chandrabhaga Basin with special reference to Menthosa glacier, Northwest Himalaya."

References:

- [1] A. Singh, I. Manna, P. Kumar, A. Dawar, P. Kumar and M.K. Murari "A new and effective method for quartz-feldspar separation for OSL and CRN dating." *Quaternary Geochronology* 72 (2022): 101315.
- [2] P. Kumar, M.C. Sharma, S. Deswal, I. Manna, E. Ckkraborty and S. Prakash "Last Glacial Maximum and subsequent glacial chronology in the monsoon-dominated Sikkim Himalaya, India." *Palaeogeography, Palaeoclimatology, Palaeoecology* (2023): 111480.

5.3.10 Reconciling the Climate and tectonic evolution of Island Belt Uplift of Kachchh, Western India: A Multi Proxy Approach

Resmi M.R. M.¹, Gaurav Chauhan² and ³Pankaj Kumar

¹Department Asst. Professor, School of Earth Science, Banasthali Vidyapith 302021, India.

²Department Earth and Environmental Science, K.S.K.V. Kutchchh University, Bhuj 370001, India.

³Inter- University Accelerator Centre, New Delhi 110067-India.

The present study focused on the eastern part of the Great Rann, particularly in the island belt Quaternary deposits. Here, the Quaternary deposits preserved as island fringe deposits, river valley terraces, alluvial and colluvial deposits. Numerous Quaternary terrace sections have been identified in the island belt with remote sensing and GIS. To understand the interaction of paleoclimate, sea level change and tectonic activity in the IBU, the sediment samples collected from trenches/core of the terrace section near to island fringe deposits. Biomarker, Geochemical, Sedimentological analysis, OSL dating and AMS dating (Figure 1) done for the samples which are collected from the region (Tyagi et al., 2012; Resmi and Achyuthan, 2018). For AMS dating we have used both shell and sediment samples. The AMS dating of the samples is given in table 1. Additionally, archaeological sites in the Island like Juni Kuran at the western fringe of the Pachham Uplift will be explored to understand the connection between paleoclimatic variation and cessation of ancient settlement.

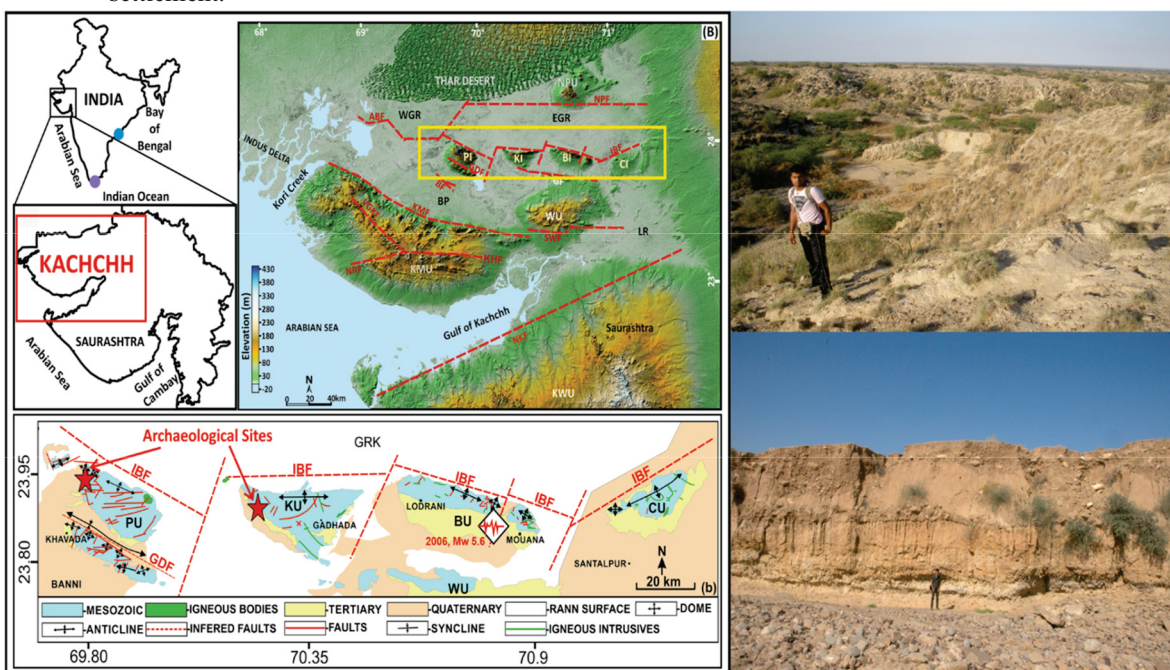


Figure 1: Map of the study area and exposed section

S. No.	Sample Name	Radiocarbon Age (BP)
1.	PB-2	19043±67
2.	PB- 18	18020±64
3.	PB- 25	9510±51
4	PB- 25	1563±27
5	KR- 5	15333±75
6	KR- 14	19706±68

Table: AMS dates of the samples from the Lithosection.

References:

- [1]. Resmi, M.R & Achyuthan, H , 2018 "The north-east monsoon variations since the Holocene: inferred from the paleo and active channels of the Palar River, southern Peninsular India", *The Holocene*. Vol. 28(6), 895-913
- [2]. Tyagi AK, Shukla AD, Bhushan R, Thakker PS, Thakkar MG, Juyal N (2012) Mid-Holocene sedimentation and landscape evolution in the western Great Rann of Kachchh, India. *Geomorphology* 151–152, 89–98

5.3.11**Cosmogenic nuclide studies on gravel spreads and aeolian sands in the Thar Desert, India**

R. K. Kaushal¹, S. Parida¹, P. V. Kumar², Pankaj K. Baghel², S. Chopra², S. Niedermann³, J. K. Pattanaik⁴, R.J. Wasson⁵, R.P. Dhir⁶, N. Chauhan¹ and A.K. Singhvi¹

¹AMOPH Division, Physical Research Laboratory Ahmedabad -380009, India

²National Geochronology Facility, Inter University Accelerator Centre, New Delhi -110067, India

³Deutsches GeoForschungsZentrum, Telegrafenberg, D-14473 Potsdam, Germany

⁴Department of Geology, Central University of Punjab, Ghudda, Badal Road, Bathinda - 151401, Punjab, India

⁵College of Science and Engineering, James Cook University, Cairns, 4232, Australia; Fenner School of Environment and Society, Australian National University, Canberra, 0200, Australia

⁶Central Arid Zone Research Institute, Pal Road, Jodhpur (deceased)

Cosmogenic nuclide analysis of sands and geomorphologically enigmatic gravel deposits from the Thar Desert is being explored to understand the long-term event chronology and the evolution of this desert¹. The study comprises conjunctive use of ¹⁰Be, ²⁶Al (measured at IUAC), ²¹Ne isotopes (measured at GFZ Potsdam) and Optically Stimulated Luminescence (measured at PRL, Ahmedabad).

The presence of fluvial gravels in the core of the Thar desert is enigmatic and their origin has been debated²⁻³. Largely devoid of matrix, these gravels are poorly sorted, subrounded to rounded pebbles of 1-80 cm size. Suggestions about their origin range from a fluvial transport from the Aravalli Ranges during the early Quaternary to the unroofing of conglomerates of Mesozoic age through weathering.

Major gravel occurrences at *Bhojka*, *Hamira*, *Jayal*, and *Solanki* were sampled. Initial ¹⁰Be measurements suggest exposure ages of 0.7 to 1.7 Ma. These ages are consistent with archaeological evidence of their being of pre-Acheulian age². A depth profile of ¹⁰Be at Bhojka suggests that the landscape was stable during most of the mid-late Quaternary and perhaps even longer. ²¹Ne data also suggest exposure ages of 1 to 1.2 Ma. While ²⁶Al results are still awaited from IUAC, a broad similarity of ¹⁰Be and ²¹Ne data suggests a simple unroofing history and the stability of the landscape for the past 1 Ma. Modelling of the concentrations of ¹⁰Be, ²⁶Al and ²¹Ne, should enable a first quantitative estimate of the antiquity of these gravels, the rates of their unroofing and the age of initiation of sand dynamism, here.

Also, ¹⁰Be data on aeolian sands suggest its potential for provenance studies and, in conjunction with ²⁶Al and ²¹Ne concentrations (data awaited) and OSL burial ages, will help model the long term antiquity of sands in the Thar⁴. Thar sands also contain a metamorphic mineral Berlinite. Its role as a sediment tracer and its impact on CRN/OSL measurements is being assessed.

This work was supported through a DST-SERB-YOCP grant, India. X-Ray diffraction measurements were carried out by Dr. J.K. Pattnaik, at the Central University of Punjab at Bathinda. This work has been accepted for presentation at the INQUA, Rome (abstract No. 2794 and EGU congresses, Vienna during 2023 (abstract No. EGU23-1016).

Publications from this study await completion of ²⁶Al measurements at IUAC.

We have submitted abstracts to the Annual meeting of the European Geosciences Union and the four yearly congress of the International Quaternary Union. These have been accepted for presentations and copies are enclosed.

References:

- [1] Granger, D.E., Kirchner, J.W. and Finkel, R. (1996). Spatially averaged long-term erosion rates measured from in situ-produced cosmogenic nuclides in alluvial sediment. *The Journal of Geology*, 104(3), pp.249-257.
- [2] Misra, V. N., Rajaguru, S. N., Agrawal, D. P., Thomas, P. K., Hussain, Z. and Dutta, P. S. (1980). Prehistoric palaeoenvironment of Jayal, western Rajasthan. *Man, and Environment*, 4:19–31.
- [3] Rajaguru, S.N., Mishra, S., and Ghate, S. (1996) A re-interpretation of gravel spreads in the Jaisalmer region, Thar Desert, India. *Journal of Arid Environments*, 32, 53–58
- [4] Vainer, S., Ben Dor, Y. & Matmon, A. (2018) Coupling cosmogenic nuclides and luminescence dating into a unified accumulation model of aeolian landforms age and dynamics: The case study of the Kalahari Erg. *Quaternary Geochronology*, 48, 33–144.

5.3.12 Impact of Quaternary climate change on long term denudation rate in Himalayan River basins

Amrutha K.¹, Jitendra Kumar Pattanaik¹

¹*Department of Geology, Central University of Punjab Bathinda, Punjab-151401, India.*

In the Himalayan region, River terraces have been widely studied for understanding the landscape evolution. Denudation rate is an important aspect in terms of landscape evolution and climate change. Spatial and temporal variation in the denudation rate is related to climate change, lithology, tectonic regime and microenvironment of a basin. Variation of sediment flux in the Himalayan Rivers is associated with tectonic and climatic changes. However, the casual correlation between climate and denudation rate is still under debate. Hence associating the chemical component of denudation with the past climatic changes might help in giving a less uncertain link between them, if any. Denudation rate of a mountain belt changes over time due to interplay between tectonics and erosional processes. Different proxies have been used to understand the extent to which denudation rate has responded to past climatic changes. Central Himalayan region has been studied to determine basin scale denudation rates using ^{10}Be in detrital quartz. This denudation rate is same as the sediment fluxes transported by the Ganga drainage system. Any variation in ^{10}Be signal in the upstream tributaries will affect the ^{10}Be signal of Himalayan Frontal River as the distance between these two are so less that the buffering of the signal rarely takes place (Lupker et al., 2012). Sediment from delta or floodplain will provide information about catchment area with a time lag and sometime it will be overprinted by the transportation history. To study this, samples have been collected from Uttarakhand (Srinagar, Gauchar and Pipalkoti). XRD facility of Inter University Accelerator Centre (IUAC)-New Delhi was used to analyse the mineralogy of both bulk and clay fraction. Illite, Kaolinite and vermiculite are the major clay minerals identified. Apart from that the Quartz fraction separated from the pebbles were chemically processed for AMS measurement. Total 38 samples were acid digested and their anion and cation column separation were carried out to separate the ^{10}Be and ^{26}Al for AMS analysis. This whole procedure was carried out in AMS chemistry lab, Geochronology group, IUAC, New Delhi. Apart from that, ^{14}C dating facility of IUAC has been utilized to date a sample collected from a sediment profile collected from Srinagar. However, the results show that the samples are modern in age.



Fig.1 (a) Samples ready for acid digestion

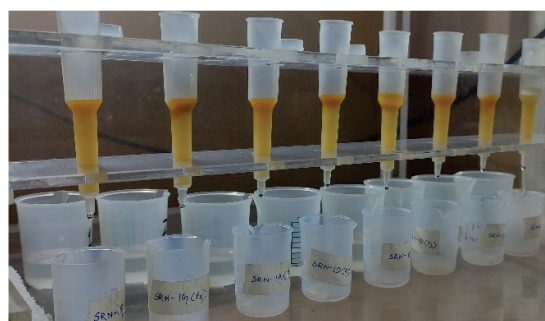


Fig.1 (b) Anion column separation of samples



Fig.1 (C) Cation column separation of samples

References:

- [1] Lupker, M., Blard, P. H., Lavé, J., France-Lanord, C., Leanni, L., Puchol, N., & Bourlès, D. Earth and Planetary Science Letters, (2012) 333.

5.3.13**Role of Indian Summer Monsoon and Westerlies on glacier variability in the Himalaya and East Africa during Late Quaternary: Review and new data.**

Kumar, Om^{1,2}, A.L. Ramanathan¹, Jostein Bakke³, B. S. Kotlia⁴, and J. P. Shrivastava², Pankaj Kumar⁵, Rajveer Sharma⁵, and Pramod Kumar

¹School of Environmental Sciences, Jawaharlal Nehru University (JNU), New Delhi, 110067, India

²Department of Geology, University of Delhi, Delhi, 110007, India

³Department of Earth Science and Bjerknes Centre for Climate Research, University of Bergen, Allègaten 41, 5007, Bergen, Norway

⁴Centre of Advanced Study in Geology, Kumaun University, Nainital, 263002, India

⁵Inter-University Accelerator centre, New Delhi-110067

Two atmospheric circulation patterns, the Indian Summer Monsoon (ISM) and mid-latitude Westerlies control precipitation and thus glacier variability in the Himalaya. However, the role of the ISM and westerlies in controlling climate and thus past glacier variability in the Himalaya is poorly understood because of the paucity of the ice core records. In this article, we present a new Holocene paleorecord disentangling the presence of the ISM and mid-latitude westerlies and their effect on glacier fluctuations during the Holocene. Our new record is based on high-resolution multi-proxy analyses ($\delta^{18}\text{O}$ porewater, deuterium-excess, grain size analysis, permeability, and environmental magnetism) of lake sediments retrieved from Chandratlal Lake, Western Himalaya. Our study provides new evidence that improves the current understanding of the forcing factor behind glacier advances and retreat in the Western Himalaya and identifies the 8.2 ka cold event using the aforementioned proxies. The results indicate that the ISM dominated precipitation $\sim 21\%$ of the time, whereas the mid-latitude westerlies dominated precipitation $\sim 79\%$ of the time during the last 11 ka cal BP. This is the first study that portrays the moisture sources by using the above proxies from the Himalayan region as an alternative of ice core records.

A total of 27 sediment cores were retrieved using piston corer under GLACINDIA project (2015) and a 235 cm long sediment core was selected for multi-proxy analysis at IUAC, New Delhi. Further, the sediment core was sub-sampled at a 1 cm interval to obtain high-resolution grain-size data and sand, silt, and clay particle sizes (%) ($n=235$) were determined using Laser Particle Size analyzer (Microtrac 3,500) at JNU, New Delhi. Eleven samples were analyzed for AMS ^{14}C dating by using 500KV pelletron at Inter-University Accelerator Center (IUAC), New Delhi and Department of Geology, Radiocarbon laboratory, Solvegatan, LUND, Sweden. Before analysis, the samples (~ 1 g each) were treated using Acid Base Acid (ABA) protocol. After removing carbonate, samples were neutralized by repeated washing with 18M Ω MiliQ water and subsequently treated with 0.5 N HCl, and then with 1 N HCl, and finally the samples were freeze-dried overnight before graphitization. The AMS ^{14}C radiocarbon dates were calibrated using calib 7.1

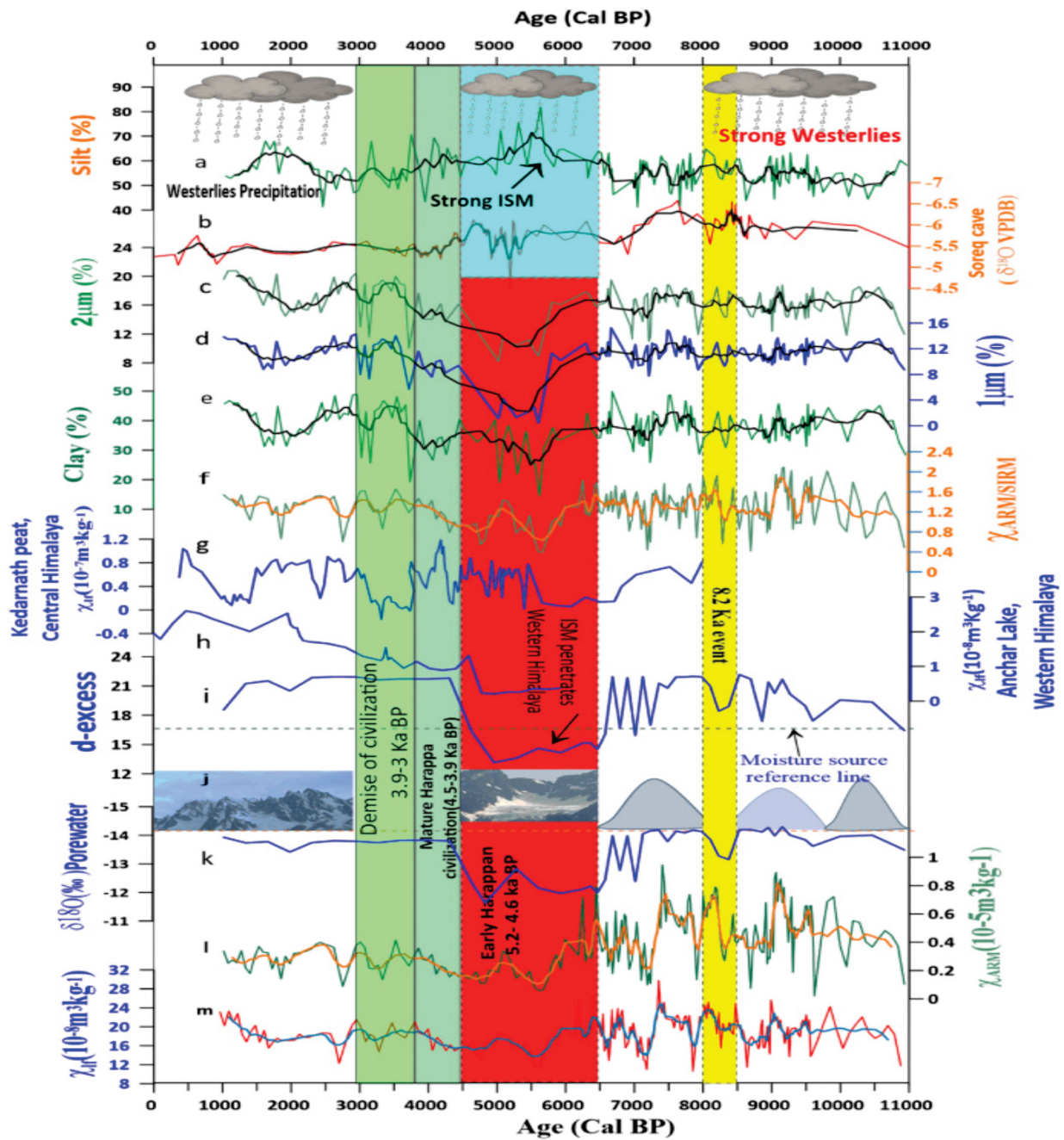


Fig. Comparison of Chandratral lake sediment results with other paleoclimate records from ISM and Westerlies dominated regions. (a) Percentage of silt; (b) westerlies representing $\delta^{18}\text{O}$ (‰) values from Soreq cave (c) percentage of dust particle size ($2\ \mu\text{m}$); (d) percentage of dust particle size ($1\ \mu\text{m}$); (e) percentage of clay, (f) $\chi_{\text{ARM/SIRM}}$; (g) magnetic susceptibility records from Kedarnath (h) χ_{IR} from Anchar lake (i) porewater d-excess parameter; (j) dashed line delineates sources of moisture (below 17 per mil reflects ISM) and Schematic diagram representing glacier fluctuations due to mid-latitude Westerlies and ISM precipitation; (k) porewater $\delta^{18}\text{O}$ (‰) value from Chandratral lake (present study); (l) χ_{ARM} ($10^{-5}\ \text{m}^3\ \text{kg}^{-1}$) and (m) magnetic susceptibility ($\chi_{\text{IR}}\ 10^{-8}\ \text{m}^3\ \text{kg}^{-1}$)

References

- [1] Kumar, O., Ramanathan, A. L., Bakke, J., Kotlia, B. S., & Shrivastava, J. P. (2020). Disentangling source of moisture driving glacier dynamics and identification of 8.2 ka event: evidence from pore water isotopes, Western Himalaya. *Scientific reports*, 10(1), 1-10.
- [2] Kumar, Om, A. L. Ramanathan, Jostein Bakke, B. S. Kotlia, J. P. Shrivastava, Pankaj Kumar, Rajveer Sharma, and Pramod Kumar. "Role of Indian Summer Monsoon and Westerlies on glacier variability in the Himalaya and East Africa during Late Quaternary: Review and new data." *Earth-Science Reviews* 212 (2021): 103431.
- [3] Shamurailatpam, Monica Sharma, Om Kumar, and A. L. Ramanathan. "Testing the reliable proxies to understand the mid-Holocene climate variability records from Chandratral lake, Western Himalayas." *Quaternary International* 599 (2021): 55-61.

5.4 Atomic and molecular physics

5.4.1 Exploring Three Body Fragmentation of Acetylene Trication

Jatin Yadav¹, C.P. Safvan², Pragma Bhatt², Pooja Kumari¹, Jasmeet Singh³ and Jyoti Rajput¹

¹Department of Physics and Astrophysics, University of Delhi, Delhi 110007, India.

²Inter-University Accelerator Center, Aruna Asaf Ali Marg, New Delhi 110067, India.

³Department of Physics, Keshav Mahavidyalaya, University of Delhi, Delhi 110034, India.

Three body fragmentation of $[C_2H_2]^{3+}$ into (H^+, C^+, CH^+) and (H^+, H^+, C_2^+) fragments formed in interaction of neutral acetylene with a slow highly charged ion (Xe^{9+} having velocity ≈ 0.5 a.u.) is studied using the technique of Recoil Ion Momentum Spectroscopy (RIMS). The experiment was conducted at the Low Energy Ion Beam Facility (LEIBF) of Inter-University Accelerator Centre (IUAC), New Delhi.

For the breakup of $[C_2H_2]^{3+}$ into (H^+, C^+, CH^+) fragments, three different dissociation pathways are observed, namely concerted breakup in acetylene configuration, concerted breakup in vinylidene configuration and a sequential breakup via $[C_2H]^{2+}$ intermediate molecular ion. For the breakup of $[C_2H_2]^{3+}$ into (H^+, H^+, C_2^+) , only concerted mode of breakup is observed.

For the breakup of $[C_2H_2]^{3+}$ into (H^+, C^+, CH^+) fragments, two Newton diagrams are plotted as a function of kinetic energy release of unimolecular breakup of molecular intermediate $[C_2H]^{2+}$ [see figure 1]. From these diagrams, concerted breakup from acetylene and vinylidene configuration and a sequential breakup via $[C_2H]^{2+}$ intermediate molecular ion are clearly visible. The contributions from vinylidene configuration is a clear evidence of H-migration in triply charged acetylene. For details see reference [1].

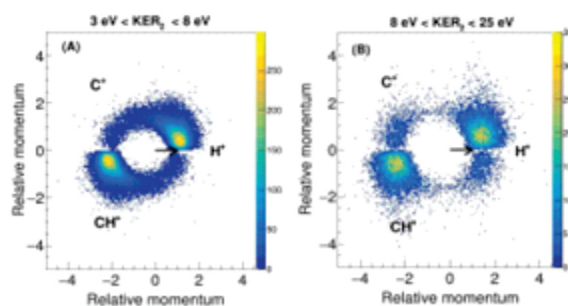


Figure 1. (A) and (B) shows Newton diagrams for breakup of $[C_2H_2]^{3+}$ into (H^+, C^+, CH^+) . The two diagrams are separated on the basis of kinetic energy release of unimolecular breakup of $[C_2H]^{2+}$ intermediate ion [1].

The *ab-initio* calculations of the potential energy surface (PES) for the lowest electronic state of $[C_2H]^{2+}$ are performed [2]. The PES shows two dissociation pathways, one along the C–C stretch coordinate and another along the C–H stretch coordinate with potential barriers of ≈ 0.6 eV and ≈ 2.7 eV respectively. This indicates that it is easier for this electronic state to dissociate via the C–C stretch by tunnelling. The measured KER for the unimolecular breakup of $[C_2H]^{2+}$ along the C–C stretch is in good agreement with the *ab-initio* calculations indicating that the lowest electronic state of $[C_2H]^{2+}$ is populated in our experiment.

For the breakup of $[C_2H_2]^{3+}$ into (H^+, H^+, C_2^+) , only concerted mode of breakup is observed [2] through the asymmetric and symmetric stretch of the C–H coordinate of the $[C_2H_2]^{3+}$ molecular ion.

References:

- [1] J Yadav, C P Safvan, P Bhatt, P Kumari, A Kumar and J Rajput, J. Chem. Phys. (Comm.) 156 (2022) 141101.
- [2] J Yadav, C P Safvan, P Bhatt, P Kumari, J Singh and J Rajput, J. Chem. Phys. 158 (2023) 074302

5.4.2 Measurements of the Line Resolved M-shell X-ray Production Cross Sections for ^{70}Yb , ^{79}Au and ^{81}Tl by N^{q+} Ion Beam

Balwinder Singh¹, Shehla^{2,3}, Anil Kumar¹, Deepak Swami⁴, Ajay Kumar⁵ and Sanjiv Puri^{1#}

¹Department of Physics, Punjabi University, Patiala, Punjab, India

²Department of Physics, Chandigarh University, Gharuan, Mohali-140413, Punjab, India

³Department of Physics, Govt Mohindra College, Patiala, India

⁴Inter University Accelerator Centre, New Delhi, Delhi 110067, India

⁵Nuclear Physics Division, Bhabha Atomic Research Centre, Trombay, Mumbai 400 085, India

Accurate knowledge of the X-ray production (XRP) cross sections and relative intensities for different elements at various incident ion energies are important for ion-beam applications including material modification by ion-implantation and the quantitative elemental analysis of different types of samples employing proton induced X-ray emission (PIXE) technique. Besides, such data is useful for testing the theories governing the ion-atom collisions. The cross sections for production of Mk ($k=M\xi$, $M\alpha\beta$, $M\gamma$, $Mm1$) X-rays of $_{70}\text{Yb}$, $_{79}\text{Au}$ and $_{81}\text{Tl}$ induced by 1.75 MeV and 1.5 MeV nitrogen ions have been measured. These measurements were performed at the atomic physics beam line of LEIBF, IUAC, New Delhi. The targets used in present work were prepared at IUAC by using vacuum deposition technique. The thickness of these targets were obtained by performing RBS measurements and the thickness of these targets were found to be $\sim 30 \mu\text{g}/\text{cm}^2$. The photopeak areas in the M X-ray spectra of different elements have been determined using ORIGIN 6.0. The measured Mk XRP cross sections have been compared with the theoretical values calculated using the nitrogen ionization cross sections based on the ECUSAR and ECPSSR model [1], the X-ray emission rates based on Dirac-Hartree-Slater (DHS) model [2], fluorescence yields and Coster-Kronig (CK) transition probabilities based on Dirac-Hartree-Slater (DHS) model [3]. The fluorescence and CK yields available in literature pertained to the single vacancy states only. Multiple vacancies in the target atom arising from the charged particle induced ionization are expected to change the atomic parameters namely the fluorescence yields and the CK yields, which in turn may alter the X-ray production cross sections. In the present work, available values of the fluorescence and CK yields [3], were corrected for multiple ionization using a model prescribed by Lapicki et al. [4] and these modified values were used, in turn, to calculate the Mk XRP cross sections. The data analysis is still under process, however, some initial results obtained have been presented in International/National Symposia/Conferences.

Reference:

- [1]. Z. Liu, S. Cipolla, *Comput. Phys. Commun.* 97, 315 (1996), 176, 157 (2007); 180, 1716 (2009); 182, 2439 (2011)
- [2]. S. Puri, *At. Data Nucl. Data Tables* 93, 730 (2007)
- [3]. Y. Chauhan, S. Puri, *At. Data Nucl. Data Tables* 94, 38 (2008)
- [4]. G. Lapicki, R. Mehta, J. L. Duggan, P. Kocur, J. Price, and F. D. McDaniel, *Physical Review A* 34, 3813 (1986).

5.4.3 Study of charge state distribution for Si projectile with carbon target

D.K. Swami^{1,3*}, Sarvesh Kumar², S. Ojha¹ and R.K. Karn³

¹*Inter University Accelerator Centre, New Delhi-110067*

²*Chemical Sciences Division, Lawrence Berkeley National Laboratory, Berkeley, California 94720, United States*

³*Jam. Co-operative College, Kolhan University, Chaibasa, Jharkhand*

The study focused on the charge state distribution of Si projectiles with initial charge states ranging from 4 to 10+ and energies between 1.78 and 3.93 MeV/u after passing through a carbon foil with a thickness of $10 \mu\text{g}/\text{cm}^2$. The aim of the study was to determine the relevant parameters of the charge state distribution such as mean charge state, distribution width, and asymmetric parameter, and compare them with the predictions of the Fermi gas model [1] and ETACHA4[2]. The results of the study showed a significant difference between the experimental results and the theoretical calculations, with the theoretical calculations overestimating the experimental results. This overestimation was attributed to the non-radiative electron capture taking place at the exit surface in the influence of wake and dynamic screening effect. Charge state fractions are important parameters that are used in various applications [4], such as detecting superheavy ions and solving problems in laboratory and astrophysical plasma. Therefore, studies like this are important for understanding the behavior of charged particles in matter and improving the accuracy of theoretical models. This study concludes that the non-radiative electron capture at the exit surface of the target is very important and it needs to be included in the theoretical calculations.

Dosimetric Aspects of Calcium Based Phosphate MaterialsChand Sansar¹, Mehra Rohit¹, Chopra Vibha², Sen Debashish³¹*Department of Physics, Dr. B. R. Ambedkar National Institute of Technology Jalandhar, Punjab, India.*²*PG Department of Physics and Electronics, DAV College Amritsar, Punjab, India.*³*Health Physics Lab, Inter University Accelerator Centre, Aruna Asaf Ali Marg, New Delhi, India*

The research work is devoted to study the calcium based phosphate materials for thermoluminescence dosimetric applications. Till now literature regarding the search work has been completed. Further, some calcium based phosphate materials have been synthesized using wet chemical method such as $\text{Ca}_{(10-x)}\text{K}(\text{PO}_4)_7:\text{Dy}_x$ (CKP), $\text{Ca}_{(1-x)}\text{Zn}_2(\text{PO}_4)_2:\text{Dy}_x$ (CZP), $\text{Li}_{1-x}\text{CaPO}_4:\text{Eu}_x$ (LCP), $\text{NaCa}_{1-x}\text{PO}_4:\text{Dy}_x$ (NCP). These materials have been prepared with activators such as Dy and Eu with doping concentration varying from ($x=0.00, 0.01, 0.03, 0.05, 0.07, 0.09$) to study the variation of doping concentration of activators. Effect of doping conc. on TL properties has been studied and the best doping conc. has been optimized for the prepared phosphors which is 5 mol% for the first three phosphors and 1 mol % for the rest as the best TL response is recorded for these hence the further studies were carried out using this concentration. To find out the TL response and TL linearity at different doses the above prepared samples were subjected to gamma ray irradiation using gamma chamber available at IUAC New Delhi from 10Gy- 12kGy dose. The effect of heating rates on TL properties has been investigated and 5 °C/s heating rate is the optimized heating rate since the well behaving TL glow curve is observed with this heating rate of TLD reader. Annealing conditions (pre, post) have been optimized for the prepared phosphors to be used in radiation dosimetry which lie in the range of 200-400 °C with duration of 30 minutes – 60 minutes. TL linearity has been investigated of these materials in which CKP shows linear response form 10Gy-2kGy, NCP: 10Gy-1500Gy, LCP: 10Gy-3kGy, CZP: 5Gy-1kGy respectively. TL properties of all the samples have been studied by Harshaw TLD-300 reader. Reusability study of these materials have been studied after post annealing and exposing to some gamma doses. CKP, and NCP showed good reproducibility where the same study is being carried out for CZP and LCP. Batch to batch homogeneity studied have been carried out for CKP, CZP and same is under investigation for LCP and NCP. TO assess the suitability of the materials for ion beam dosimetry they have been exposed to 80 MeV C^{6+} beam and 100 MeV O beam with different fluences at 1 pA current. The effect of the ion beams on TL properties is being analysed and is NCP and LCP show a very good response towards 80 MeV C beam and 100 MeV oxygen beam as the response as the TL response is linear from 1×10^{10} - 3.3×10^{11} ion/cm² however the data corresponding to the other materials is being analysed which are expected to show good response. The effect of ion beam irradiation on TL properties of other compounds are being investigated to check their suitability as energy independent dosimeter. Most of the experimental work has been done at Health Physics Lab IUAC, New Delhi. The formation of the compound and phase identification for $\text{Ca}_{10}\text{K}(\text{PO}_4)_7:\text{Dy}$ and $\text{CaZn}_2(\text{PO}_4)_2:\text{Dy}$, LCP and NCP has been done by XRD available at Dr. B. R. Ambedkar National institute of Technology Jalandhar. The samples are studied using other characterization techniques like XRD, TEM, FE-SEM etc. available at NIT Jalandhar and IUAC New Delhi. Moreover till now the studies are being done with gamma irradiation and ion beams of high energy. To check the energy independency the materials, they may be irradiated with low energy to propagate this research and to find the suitability of these materials for ion beam dosimetry using C and O ion species.

References:

- [1] C. B. Palan, K. A. Koparkar, N. S. Bajaj, A. Soni, S. K. Omanwar, *Research on Chemical Intermediates* 42 (2016) 7637.
- [2] L. Guan, C. Liu, X. Li, G. Jia, Q. Guo, Z. Yang, G. Fu, *Materials Research Bulletin* 46 (2011), 1496.
- [3] C. Furetta, *Handbook of thermoluminescence*. World Scientific Publishing Singapore 2010.
- [4] K. N. Shinde, S. J. Dhoble, *Radiation protection dosimetry* 152(2012), 463.